Investigation of novel filtered multi-carrier waveforms in the context of massive MIMO systems

Fatima Hamdar

COLLEGES SCIENCES
BRETAGNE POUR L'INGENIEUR
LOIRE ET LE NUMERIQUE

IMT Atlantique
Bretagne-Pays de la Loire
École Mines-Télécom

THESE DE DOCTORAT DE

L'ÉCOLE NATIONALE SUPERIEURE
MINES-TELECOM ATLANTIQUE BRETAGNE PAYS DE LA LOIRE –
IMT ATLANTIQUE

ECOLE DOCTORALE N° 648
Sciences pour l'Ingénieur et le Numérique
Spécialité : Télécommunication

Par

Fatima HAMDAR

Étude de nouvelles formes d'ondes multiporteuses filtrées dans le contexte des systèmes MIMO massifs

Thèse présentée et soutenue à IMT Atlantique à Brest, le 23 Octobre 2023
Unité de recherche : Lab-STICC
Thèse N° : 2023IMTA0368

Rapporteurs avant soutenance :

Iyad Dayoub	Professeur des Universités, Université Polytechnique Hauts-de-France
Youssef Nasser	HDR, Directeur du secteur d'activité 5G/6G, Greenerwave

Composition du Jury :

Président :	Laurent Ros	Professeur des Universités, Grenoble INP
Examinateurs :	Iyad Dayoub	Professeur des Universités, Université Polytechnique Hauts-de-France
	Youssef Nasser	HDR, Directeur du secteur d'activité 5G/6G, Greenerwave
	Joumana Farah-Francis	Professeur, INSA Rennes
	Alain Mourad	Directeur du Future Wireless Europe, InterDigital Research and Innovation
Dir. de thèse :	Amer Baghdadi	Professeur, IMT Atlantique
Co-dir. de thèse :	Charbel Abdel Nour	Professeur, IMT Atlantique
Encadrant :	Jérémy Nadal	Ingénieur de recherche, ANFR

Acknowledgments

Foremost among my expressions of gratitude are reserved for my esteemed supervisors, Amer Baghdadi, Charbel Abdel Nour, and Jeremy Nadal, whose unwavering guidance played an instrumental role throughout the entirety of my Ph.D. journey. A heartfelt acknowledgment extends specifically to Charbel Abdel Nour and Jeremy Nadal, whose meticulous guidance and profound insights led me through the intricate landscape of research, providing invaluable expertise at every step.

I extend my appreciation to all those who contributed to my education, recognizing the profound impact of even the smallest lessons. In the labyrinth of life's challenges, I am grateful to every individual who supported and encouraged me, serving as a beacon of strength during the most arduous moments.

A poignant note of gratitude is directed towards my father, whose steadfast support and encouragement accompanied me throughout my entire life. His untimely passing during the first year of my Ph.D. adds a poignant layer to this acknowledgment, as I recognize the profound influence he had on my academic journey.

Lastly, but certainly not least, I express deep gratitude to my cherished family, whose unwavering support and boundless love have been the cornerstone of my perseverance.

Contents

List of Figures

List of Tables

List of Abbreviations

3GPP	Third generation partnership project
4G	Fourth generation
5G	Fifth generation
6G	Sixth generation
AWGN	Additive White Gaussian noise
AFB	Analysis Filter Bank
ACLR	Adjacent Carrier Leakage Ratio
ACI	Adjacent Channel Interference
APM	Amplitude Phase Modulation
BS	Base station
BER	Bit-Error Rate
CCDF	Complementary Cumulative Distribution Function
CIR	Channel Impulse Response
CSI	Channel State Information
CP	Cylic Prefix
CPE	Common Phase Error
CR	Coding Rate
CAVs	Connected Autonomous Vehicles
CE	Channel Estimation
DFT	Discrete Fourier Transform
DAC	Digital-to-Analog Converter
DC	Diversity Combining
DD	Delay-Doppler
DCT4	Discrete Cosine Transform type-IV
eMBB	Enhanced Mobile Broadband
eUMBB	Enhanced Ultra-Mobile Broadband

FFT	fast Fourier transform
FMT	Filtered multitone modulation
FBMC/OQAM	Filter Bank Multi-Carrier with OQAM
FTN	Faster-Than-Nyquist
FDC	Frequency Domain Compensation
FS	*Frequency Spread*
FEC	Forward Error Correction
HARQ	Hybrid Automatic Repeat-Request
HC-MCM	High Compaction Multi-Carrier Modulation
IoT	Internet-of-Things
IFFT	Inverse Fast Fourier transform
ISI	Inter-Symbol Interference
IDCT4	Inverse Discrete Cosine Transform type-IV
IAM	Interference Approximation Method
ISFFT	Inverse Symplectic Finite Fourier Transform
INI	Inter-Numerology Interference
KPI	key performance indicator
LoS	Line-of-sight
LTE	Long-term evolution
L_{CP}	CP length
LDPC	Low-Density Parity Check Code
LS	Least Squares
LRx	Linear Receivers
LMMSE	Linear Minimum Mean Square Error
LSPs	Large-Scale Parameters
MBB	Mobile Broadband
MMB4	Martin, Mirabassi, Bellange
MCO	Modulation Code Overlapping
MMC	Massive Machine Communication
mMTC	Massive machine-type communications
MIMO	Multiple-input multiple-output
mMIMO	massive MIMO
MU-MIMO	Multi-user MIMO
MT	Mobile terminal

ML	Maximum Likelihood
MP	Message Passing
NLoS	Non-LoS
NR	New Radio
NLRx	Non-Linear Receivers
OFDM	Orthogonal Frequency Division Multiplexing
OOBPL	Out-Of-Band-Power Leakage
OQAM	Offset Quadrature Amplitude Modulation
QuaDRiGa	Quasi Deterministic Radio Channel Generator
PAPR	Peak-to-Average Power Ratio
Pe	Probability of Error
PER	Packet Error Rate
PF	Prototype Filter
PS	Pilot Structure
PDP	Power Delay Profile
QoS	Quality of service
QMF1	Quadrature Mirror Filter 1
RMa	Rural macrocell
Rx	Receiver
RRC	root-raised-cosine
SC-FDE	Single-Carrier with Frequency-Domain Equalization
SE	Spectral efficiency
SINR	Signal-to-interference-plus-noise ratio
SIR	signal-to-intereference ratio
SNR	Signal-to-noise ratio
SR	sum-rate
SIC	Successive Interference Cancellation
SFFT	Symplectic Finite Fourier Transform
SCM	Spatial Channel Model
TDL-B	Tapped Delay Line B
Tx	Transmitter
TO	Timing Offset
TF	Time-Frequency
TFL1	Time Frequency Localization 1

TTI	Time Transmission Interval
UE	User equipment
UL	Uplink
Uma	Urban macrocell
URLLC	Ultra-reliable low-latency communications
UFMC	Universal Filtered Multi-Carrier
V2X	Vehicle-to-Anything
V2V	Vehicle-to-Vehicle
V2I	Vehicle-to-Infrastructure
XPR	Cross-Polarization Ratio
ZC	Zadoff-Chu

Résumé long

La cinquième génération (5G) de réseaux mobiles est le standard de communication cellulaire spécifiquement conçue pour prendre en charge une pluralité de services soumis à des contraintes diverses et variées. Malgré les avancés technologiques de la 5G, il y a une demande toujours aussi croissante en terme de données transmises, avec l'émergence de nouvelles applications et de nouveaux services sans fil. De ce fait, la sixième génération (6G) de réseaux mobiles devra fournir des débits de données encore plus élevés tout en garantissant une latence plus faible et une connectivité améliorée pour une gamme d'appareils de plus en plus diversifiée. Avec des prévisions estimant que la quantité de trafic sans fil sera 10 000 fois plus élevé, la 6G devra prendre en charge des réseaux de plus grande capacité pour répondre au nombre massif d'appareils qui auront besoin de se connecter. En outre, de nouveaux services tels que la télémédecine, les véhicules autonomes et les applications de ville intelligente nécessiteront des niveaux de fiabilité, de disponibilité et de sécurité sans précédent. Ces dernières tendances en matière de communications sans fil poussent la 5G à ses limites, la rendant incapable de gérer efficacement le trafic attendu à l'avenir. Par conséquent, la 6G, actuellement en cours de pré-normalisation, devra proposée une solution efficace pour satisfaire ces tendances émergentes. Cette nouvelle génération devra prendre en charge de nouveaux services tout en améliorant les performances des services conventionnels fournis par la 5G, notamment en augmentant les débits de données, la capacité et la couverture réseau.

Le service *enhanced Massive Machine Communication* (eMMC) est attendu pour les applications de type internet des objets en 6G. Ce service est conçu pour répondre aux situations où un grand nombre de capteurs doivent accéder au réseau sans fil. Le principal défi du service eMMC est d'assurer une durée de vie de la batterie plus longue qu'en 5G pour les appareils à faible consommation d'énergie. D'autres applications émergentes nécessitent des communications à faible latence et à haute fiabilité, telles que l'internet tactile, l'automatisation des usines et la surveillance des signes vitaux. Pour prendre en charge ces applications, le service *Enhanced Mission Critical Communication* (eMCC) est envisagé. Dans le domaine de la 5G, un service notable concerne les communications véhiculaires, connu sous le nom de service V2X (Vehicle-to-Anything). Cela correspond à des communications entre plusieurs véhicules, ou entre des véhicules et l'infrastructure. Alors que nous entrons dans l'ère de la 6G, les systèmes de communication véhiculaires devront évoluer, offrant des services V2X plus avancés avec des exigences de plus en plus élevées. Cela implique un temps de latence extrêmement faible (0,01 ms) et un débit élevé, ainsi qu'une grande fiabilité ($99,999999\%$).

Pour exploiter tout le potentiel des services mentionnés, la 6G devra répondre à des indicateurs de performance rigoureux, ce qui nécessitera l'exploration de nouvelles technologies, allant de la couche applicative à la couche physique. Cependant, la forme d'onde actuelle *Orthogonal Frequency Division Multiplexing* (OFDM), introduite dans la 4G et maintenue dans la 5G, pourrait ne pas suffire à satisfaire ces exigences strictes. En effet, la coexistence de tous les nouveaux services, en plus de ceux existant, dans la même bande de fréquences est compromise par l'importante fuite de puissance hors bande de l'OFDM. En outre, l'OFDM nécessite une synchronisation temporelle et fréquentielle stricte avec la station de base (BS) pour chaque utilisateur, ce qui entraîne une augmentation substantielle de signaux de synchronisation. Par conséquent, la latence et la consommation d'énergie sont considérablement affectées.

Dans ce contexte, plusieurs formes d'onde ont été étudiées en tant que candidats potentiels pour la 5G et maintenant la 6G. Il s'agit notamment :

1. Filter Bank Multi-Carrier with Offset Quadrature Amplitude (FBMC/OQAM),
2. Universal-Filtered Orthogonal Frequency-Division Multiplexing (UF-OFDM),
3. Filtered-Orthogonal Frequency-Division Multiplexing (F-OFDM),
4. Orthogonal Time Frequency Space (OTFS).

Ces formes d'ondes ont pour point commun d'introduire un filtrage comme moyen de remédier aux inconvénients identifiés de l'OFDM. Cette opération de filtrage réduit considérablement la fuite de puissance hors bande, améliorant ainsi la capacité de coexistence des services et atténuant les contraintes de synchronisation. Dans ce travail de thèse, nous avons considéré les modulations FBMC/OQAM. Une description technique de ces formes d'ondes est donnée dans la suite de ce résumé.

La forme d'onde FBMC/OQAM et les avancées récentes

Pour la forme d'onde FBMC, un banc de filtres appliquant un filtre prototype (PF) est introduit pour donner une forme d'impulsion efficace au signal transmis sur chaque sous-porteuse. Ce banc de filtres joue un rôle important dans le contrôle de la puissance d'émission transportée par les lobes secondaires de la réponse en fréquence du PF. Il permet en outre une plus grande flexibilité dans la gestion de la fuite de puissance hors bande au prix d'une complexité matérielle accrue du côté de l'émetteur et du récepteur. Il s'agit d'une différence majeure par rapport à l'OFDM qui utilise des des impulsions rectangulaires. L'absence de *Cyclic prefix* (CP) est une autre différence par rapport à l'OFDM qui peut conduire à une amélioration de l'efficacité spectrale (SE), mais demande d'utiliser des techniques de réception plus complexe à implémenter.

Selon le théorème de Balian-low, il est impossible d'atteindre simultanément les trois caractéristiques suivantes, quel que soit le système de communications considéré :

1. L'orthogonalité dans le domaine des nombres complexes.

2. La localisation en temps et en fréquence (filtrage).

3. L'efficacité spectrale maximale.

En ce qui concerne l'OFDM, l'orthogonalité complexe est obtenue au sacrifice de la seconde propriété qui affecte la localisation fréquentielle et, par conséquent, provoque une fuite de puissance hors bande élevée. De plus, l'OFDM réduit également son efficacité spectrale (troisième propriété) pour éviter l'interférence entre symboles causée par les canaux multi-trajets, grâce à l'utilisation d'un préfixe cyclique. Afin de rétablir la deuxième propriété, les modulations en banc de filtres appliquent un filtrage par sous-porteuse. De ce fait, l'efficacité spectrale ou l'orthogonalité dans le domaine des nombres complexes doit être abandonnée selon le théorème de Balian-low.

Traditionnellement, deux types distincts d'implémentation émetteurs-récepteurs FBMC avec différents niveaux de complexité calculatoire et de performance ont été proposés dans la littérature : le *Polyphase Network* (PPN) et le *Frequency Spread* (FS). Le premier est généralement utilisé du côté de l'émetteur en raison de sa faible complexité. D'autre part, l'implémentation FS est principalement adoptée du côté du récepteur à cause de son processus d'égalisation peu complexe.

Les symboles FBMC transmis se chevauchent dans le temps, de sorte que le signal FBMC ne soit pas constitué de symboles de blocs successifs et séparés comme pour l'OFDM. Chaque symbole FBMC, composé de L échantillons, transporte jusqu'à M sous-porteuses filtrées. Le nombre de symboles se chevauchant est défini par le facteur de chevauchement K, qui est le ratio entre la longueur du filtre prototype L et le nombre total de sous-porteuses M.

Pour assurer l'orthogonalité dans le domaine des nombres réels, le traitement OQAM est introduit. Tout d'abord, les composantes réelles et imaginaires du signal QAM sont séparées. Après la rotation de phase, la composante imaginaire est retardée de la moitié de la durée d'un symbole FBMC. Cette opération est suivie d'un transformé de fourier discrète inverse (IFFT) de taille M. Un traitement PPN est ensuite réalisé, où le bloc d'échantillons en sortie de la IFFT est répliqué $K-1$ fois. Ensuite, une opération de fenêtrage est appliquée en utilisant la réponse impulsionnelle du PF ayant une longueur de $L = KM$. Enfin, les composantes résultantes sont additionnées pour fournir le signal d'émission.

Côté récepteur, les deux types d'implémentations (PPN et FS) appliquent des opérations inversées par rapport à celles effectuées par l'émetteur. Pour l'implémentation basée sur le PPN, les opérations doivent être effectuées dans l'ordre suivant: PPN, FFT de taille M, et démappeur OQAM. Le récepteur FS-FBMC commence par applique une FFT de taille KM sur le signal reçu contenant le symbole FBMC à démoduler, ce qui augmente sa complexité. Pour utiliser un égaliseur à faible complexité basé sur les sous-porteuses du côté du récepteur, l'étape de filtrage est déplacée dans le domaine des fréquences. Enfin, les symboles *Pulse-Amplitude-Modulation* (PAM) à récupérer sont obtenus en extrayant la partie réelle du signal à rotation de phase en quadrature et sous-échantillonné.

Grâce à la méthode de l'OQAM, la FBMC présente désormais les caractéristiques suivantes:

1. orthogonalité dans le domaine réel,
2. une localisation temporelle et fréquentielle améliorée par rapport à l'OFDM, grâce au filtrage par sous-porteuse,
3. offre une meilleure efficacité spectrale que l'OFDM, car aucun préfixe cyclique n'est transmis.

Outre ces avantages, la FBMC est plus résistante aux synchronisations temps/fréquence imparfaites en choisissant le filtre prototype approprié. Par conséquent, la FBMC/OQAM se positionne comme une technologie prometteuse pour divers services, renforçant la résilience des systèmes de communication face à différents types de déficiences. À titre d'exemple, la robustesse de la FBMC/OQAM face au décalage/étirement Doppler peut être exploitée pour prendre en charge le service V2X. De plus, la prise en charge efficace d'une synchronisation plus souple peut être envisagée avec la FBMC/OQAM pour les services eMMC, grâce à sa faible émission de puissance hors bande et sa résistance au décalage temporel.

Cependant, l'introduction de l'OQAM n'est pas sans conséquence. En effet, cela complexifie l'utilisation des techniques d'estimation de canal et des technologies *massive Multiple-Input Multiple-Output* mMIMO faisant intervenir un large nombre d'antennes au niveau des stations de base.

Objectifs de la thèse et contributions

Bien que l'OFDM ait été la technologie de pointe au cours des dernières décennies, elle présente plusieurs inconvénients qui limitent son efficacité dans certains scénarios. D'autre part, des projets de recherche ont identifié les formes d'ondes multiporteuses filtrées comme des technologies de couches physiques prometteuses pour la prochaine génération de réseaux mobiles. Parmi ces techniques, la FBMC/OQAM a été considérée comme la forme d'onde la plus prometteuse en raison de son confinement supérieur du spectre, de sa capacité à supporter une synchronisation imparfaite dans les réseaux denses avec des communications *Device-to-Device* (D2D) et des communications asynchrones entre machines, et de sa robustesse dans les scénarios de grande mobilité tels que les communications entre véhicules.

Au cours des dernières années, l'équipe de recherche d'IMT Atlantique a réalisé des progrès significatifs dans le développement et de dépôts de brevets sur des contributions innovantes liées à la FBMC, tant du côté de l'émetteur que du récepteur. Du côté de l'émetteur, un nouveau filtre prototype court a été proposé pour la FBMC, et permet une reconstruction presque parfaite du signal tout en ayant la même taille qu'un symbole OFDM. Combiné à d'autres techniques de réception originales, ce filtre devient un avantage majeur pour la plupart des scénarios de communication mentionnés ci-dessus, permettant en outre de réduire considérablement la complexité du matériel et la consommation d'énergie des émetteurs. Du côté du récepteur, une

nouvelle technique de réception FBMC adaptée aux filtres courts a également été proposée. Elle implique l'utilisation d'un égaliseur dans le domaine temporel basé sur l'algorithme Overlap-Save (OS), qui permet d'effectuer des opérations de convolution rapides, avant la démodulation FBMC. Il a été démontré que l'égaliseur dans le domaine temporel et le récepteur FBMC peuvent être regroupés en une seule structure en raison de la localisation en fréquence du filtre, ce qui réduit considérablement la complexité calculatoire. Le récepteur qui en résulte améliore considérablement la robustesse contre les canaux doublement dispersifs quand des filtres courts sont utilisés, et supporte les communications asynchrones pour ces même filtres. Un autre schéma OS-FBMC dans lequel les symboles FBMC sont transmis et démodulés par bloc dans le domaine des fréquences a été dérivé, ce qui dimininue encore plus la complexité.

Cependant, il reste encore quelques aspects importants à résoudre. Certaines techniques utilisées par l'OFDM ne peuvent pas être directement appliquées à la FBMC en raison du schéma OQAM, comme la structure des pilotes (PS) pour l'estimation du canal (CE), les techniques d'estimation conventionnelles utilisées pour l'OFDM, ainsi que la compatibilité avec la technologie mMIMO qui utilise un grand nombre d'antennes au niveau de la BS. Cette dernière est une technologie essentielle pour la prochaine génération de réseaux de données sans fil. Elle offre des avantages substantiels en termes de fiabilité, de données et de SE. Il est donc essentiel de trouver des solutions appropriées à ces problèmes techniques pour que la FBMC devienne une solution technologique mature et utilisable dans les futurs systèmes de communication.

Dans ce contexte, l'objectif principal de cette thèse est de proposer des solutions aux défis mentionnés ci-dessus pour les formes d'ondes multi-porteuses filtrées pour les systèmes utilisant la technologie mMIMO. Plusieurs objectifs ont été considérés :

1. L'extension aux systèmes mMIMO des progrès récents susmentionnés proposés, en particulier l'utilisation de l'algorithme OS couplé à un filtre prototype court afin de réduire la latence et la complexité de l'émetteur-récepteur.

2. Support de la synchronisation relaxée, des communications asynchrones et de la résilience contre les différents types d'interférences pour les systèmes mMIMO.

3. Développement d'un PS qui permet la mise en oeuvre de techniques OFDM conventionnelles d'estimation de canal pour les systèmes FBMC.

4. Exploiter la robustesse aux interférences de la FBMC/OQAM lorsqu'elle est associée aux récepteurs avancés, en proposant de nouvelles techniques de transmission efficaces en termes d'utilisation du spectre.

Structure du manuscrit et résumé des chapitres

Le manuscrit de thèse est composé de cinq chapitres, qui sont résumés dans les paragraphes suivants.

Chapitre 1 : Introduction

Le premier chapitre présente le contexte général de ce travail et introduit les bases des contributions développées dans les sections suivantes. Il décrit ensuite les objectifs de la thèse et fournit une liste complète des contributions apportées, suivie de résumés concis de chaque chapitre et d'une liste de publications.

Chapitre 2 : Formes d'onde pour au-delà de la 5G et après-OFDM

Ce deuxième chapitre présente le contexte scientifique de base pour appréhender les contributions présentées dans les chapitres suivants. Le chapitre commence par une brève introduction à l'OFDM, qui est couramment utilisé dans le service eMBB conventionnel de la 5G. Il explique ensuite les contraintes spécifiques des différents scénarios de la 6G, tels que l'eMMC, le MCC et les communications V2X. Le chapitre souligne les limites de la modulation OFDM pour répondre à ces contraintes. Ensuite, le chapitre fournit une description technique de la FBMC/OQAM, qui est la forme d'onde étudiée dans cette thèse. En outre, un bref aperçu d'autres formes d'onde prometteuses est présenté. Ce chapitre présente les avantages de l'utilisation de PF courts pour la FBMC/OQAM, tels que la prise en charge des communications à faible latence, la faible complexité de calcul et l'efficacité énergétique élevée. Il présente également les inconvénients associés, notamment une diminution de la robustesse aux canaux à trajets multiples avec un long étalement des retards et des dégradations de performances dues à de long décalage temporel. En outre, le chapitre présente les récepteurs FBMC/OQAM pertinents dans la littérature qui étudient ces questions. Enfin, le chapitre identifie les défis en suspens qui empêchent actuellement l'adoption à plus grande échelle de la FBMC/OQAM.

Chapitre 3 : Nouvelle technique de transmission pour formes d'ondes multiporteuses

Un élément crucial des réseaux de communication cellulaire est l'efficacité spectrale (SE) atteignable. En effet, motivée par la croissance continue du trafic de données mobiles dans les réseaux sans fil, l'amélioration de l'efficacité spectrale a représenté l'un des principaux objectifs du 3GPP sur plusieurs générations de normes en réseaux mobiles.
Dans ce contexte, un nouveau schéma de transmission appelé *Modulation Code Overlapping* (MCO) est proposé dans ce chapitre. La première section commence par présenter les solutions pertinentes présentées dans la littérature pour l'amélioration de la SE. Dans une seconde section, la technique MCO est présentée. Il est basé sur le chevauchement intentionnel des sous-porteuses des utilisateurs adjacents, ce qui permet d'augmenter le débit de données et l'efficacité spectrale du système. Cela se fait au prix d'un niveau de puissance élevé en interférences. Pour résoudre ce problème, nous proposons d'optimiser conjointement le taux de codage, la quantité de sous-

bandes superposées et l'ordre de modulation. Enfin, une dernière section est dédiée à l'analyse des performances de la technique MCO pour différentes dégradations du canal, y compris les décalages multi-trajets et temporels. Contrairement aux travaux antérieurs, nous avons effectué des simulations à l'aide d'un modèle de canal réaliste généré par QuaDRiGa afin de valider le système proposé. Les résultats révèlent que le récepteur FBMC-OS surpasse l'OFDM sur le modèle de canal spécifié, permettant d'obtenir un gain en SE remarquable de 66%. Cependant, dans certaines applications 6G, le gain en SE obtenu en employant l'approche MCO proposée peut ne pas être suffisant. Par conséquent, dans le chapitre suivant, nous étendons les récepteurs FBMC-OS aux systèmes mMIMO afin d'exploiter pleinement le potentiel cette technologie multi-antennes pour obtenir un gain en SE encore plus élevé.

Chapitre 4 : Récepteurs OS-FBMC pour les systèmes mMIMO

L'utilisation de systèmes mMIMO, caractérisés par un large nombre d'antennes déployés sur les station de bases desservant de nombreux utilisateurs simultanément, est une solution prometteuse pour augmenter plus significativement l'efficacité spectrale. Bien que l'OFDM ait été largement adopté dans la littérature pour l'étude des systèmes multi-utilisateur (MU) mMIMO, cette forme d'onde est très sensible aux déficiences provoquées par une synchronisation imparfaite. Or, les gains significatifs en performance des systèmes couplant OFDM et MU-mMIMO sont obtenus pour des situations où tous les utilisateurs sont parfaitement synchronisés. Pour des procédures de synchronisation relaxées et asynchrones, les performances sont significative dégradées à moins d'annuler les interférences résultants entre utilisateurs, antennes et sous-porteuses ce qui augmente massivement la complexité du récepteur OFDM. En revanche, FBMC/OQAM est reconnue pour être résiliant aux synchronisation imparfaite, en particulier suites aux avancés récentes sur les techniques de réception. Dans ce chapitre, nous étendons ces progrès récents sur les récepteurs FBMC au contexte des systèmes MU-mMIMO, afin de profiter pleinement de l'avantage de ces deux technologies.

La premier partie de ce chapitre présente les émetteurs-récepteurs multiporteurs de la littérature pour le MIMO massif ainsi que leurs inconvénients. Ensuite, de nouveaux récepteurs FBMC basés sur l'algorithme OS sont proposés, suivis d'une étude analytique en présence de différentes dégradations du canal. La dérivation analytique proposée du SINR réduit considérablement le temps de calcul nécessaire à la sélection des paramètres du récepteur OS lors de la recherche du meilleur compromis performance/complexité adapté à l'application envisagée. Il est démontré que l'OS-FBMC améliore de manière significative les performances en taux d'erreur binaire sur des canaux à trajets multiples, par rapport à l'OFDM. En outre, le récepteur proposé supporte les communications asynchrones en plus d'accroître la robustesse contre les décalages de fréquence dans le contexte des systèmes MU-mMIMO.

Chapitre 5 : Nouvelles structures pilotes et technique d'estimation du canal associée pour les systèmes FBMC/OQAM mono- et multi-utilisateurs

La précision de l'estimation du canal (CE) joue un rôle crucial pour pleinement profiter des gains apporté par la technologie mMIMO, comme l'amélioration du SE et de la résilience face aux perturbations provoqués par des conditions de propagation canal difficiles. Contrairement à l'OFDM, le FBMC/OQAM ne présente qu'une orthogonalité dans le champ des nombre réels. Par conséquence, les signaux reçues, incluant les pilotes, souffrent d'interférences intrinsèques, ce qui rend les techniques de CE plus contraignante à concevoir pour FBMC.
Ainsi, dans ce chapitre, nous proposons une nouvelle structure de pilote (PS) ainsi qu'une technique de CE associée pour les systèmes FBMC/OQAM pour le cas d'une transmission avec un seul utilisateur. Contrairement aux méthodes existantes, le modèle proposé n'impose pas que l'intervalle en temps entre les symboles soit beaucoup plus long que le délai d'étalement maximal du canal. Nous avons ensuite étendu ces contributions aux systèmes MU-mMIMO, dans lesquels les pilotes des différents utilisateurs sont entrelacés en fréquence par un simple décalage circulaire sans qu'il soit nécessaire d'utiliser des symboles de garde entre eux. Il en résulte une forte réduction du nombre de signaux de préambules transmis, particulièrement lorsque le nombre d'utilisateurs est conséquent. De ce fait, la méthode proposée améliore considérablement le SE par rapport aux solutions disponibles dans la littérature qui nécessitent un grand nombre de bande de gardes pour séparer les pilotes des différents utilisateurs, tout en offrant la meilleure performance réalisable connue à ce jour si la complexité n'est pas une contrainte.

Chapitre 6 : Conclusions et travaux futurs

FBMC/OQAM offre des avantages significatifs par rapport à l'OFDM, tels qu'une fuite de puissance hors bande plus faible et une meilleure résistance aux erreurs de synchronisation. Cependant, l'ajout d'un étage de filtrage complique l'adoption de certaines techniques supportées par l'OFDM, telles que l'estimation de canal et l'implémentation de la technologie mMIMO. Grâce aux nouveaux algorithmes proposés dans ce manuscrit, la FBMC/OQAM peut être facilement couplé à la technologie mMIMO et surpasse en performance l'OFDM pour différentes dégradations due au canal de propagation. De plus, l'efficacité spectrale peut être encore améliorée grâce à la technique MCO proposée dans cette thèse, ouvrant ainsi la voie à des systèmes de communication mobile plus efficaces.

Des pistes d'améliorations peuvent être envisagées pour la suite des travaux de cette thèse. Ces dernières années, l'équipe de recherche à IMT Atlantique a développé une plateforme capable de simuler des scénarios 5G avec des récepteurs FBMC conventionnel de type PPN et FS. Une amélioration possible consiste donc à concevoir et à implémenter des architectures matérielles optimisées pour les récepteurs FBMC de cette plateforme. De plus, la plateforme ne prend en

charge que la communication SISO. Étant donné que les techniques mMIMO sont largement adoptées dans la 5G, une amélioration significative de la plateforme impliquerait l'intégration de la prise en charge de la technologie mMIMO avec les récepteurs proposés dans ce manuscrit. Cela impliquerait principalement de modifier la plateforme RF actuelle, qui n'intègre qu'une seule antenne pour l'émission et une pour la réception.

Enfin, la procédure MCO proposée a été initialement conçue pour les transmissions SISO. Étendre la procédure MCO au contexte des systèmes mMIMO permettrait d'augmenter davantage l'efficacité spectrale des systèmes de communication.

Chapter 1

Introduction

1.1 Next generation communication networks and services

The Fifth Generation (5G) New Radio (NR) is the first cellular network standard that was specifically designed to support multi-service communication, comprising services with diverse and varying requirements. It introduces service classes such as Ultra-Reliable Low-Latency Communication (URLLC) and Machine-Type Communication (MTC) alongside enhanced Mobile BroadBand (eMBB) to cater to the different communication needs of users. Despite the perceived step forward thanks to the introduction of 5G, with the ever-growing demand for data and the emergence of new wireless applications and services, it is expected that the Sixth Generation (6G) mobile networks will need to deliver even higher data rates, lower latency, and improved connectivity for an increasingly diverse range of devices. With predictions of up to $10,000$ times increase in wireless traffic [1, 2], 6G will need to support higher capacity networks to accommodate the massive number of devices that will need to connect. Furthermore, new services such as telemedicine, autonomous vehicles, and smart city applications will require unprecedented levels of reliability, availability, and security. These latest trends in wireless communications are pushing the 5G to its limits, making it unable to efficiently handle the expected traffic in the future. As a result, the 6G of wireless communication networks, currently in the process of pre-standardization, is expected to offer an efficient solution to these emerging trends. This new generation is anticipated to support emerging services while also enhancing the capabilities of the conventional eMBB service provided by 5G, including higher data rates, capacity, and coverage [2]. This new service in 6G is referred to as enhanced Ultra-Mobile Broadband (eUMBB).

The enhanced Massive Machine Communication (eMMC) is a new service expected for Internet-of-things (IoT) applications in 6G. It represents a revolutionary advancement over the Massive Machine Communication (MMC) service in 5G, to cope with the anticipated massive connectivity requirements that can reach 10^7 devices/km^2 [3], while prioritizing power consumption and Spectral Efficiency (SE) besides low hardware cost [3]. Similar to MMC, this service is designed to cater to situations where a large number of sensors and actors need to access the wireless network, but each device requires a relatively low data rate. The transmission of data

is sporadic and involves small packets per connection. Unlike the eUMBB service, the main challenge for the eMMC service is to ensure extended battery life compared to that in 5G for low power devices. The objective is to achieve a battery life that can last for a week or even longer [4]. This necessitates reducing energy consumption by minimizing signaling overhead and optimizing hardware implementation.

Other emerging applications require low latency communications with high reliability, such as tactile Internet, factory automation, and monitoring of vital signs. These types of applications impose a constraining set of technical requirements to ensure that data is transmitted quickly and accurately. In order to support such applications, the Mission Critical Communication (MCC) service has been introduced in the 5G known as URLLC in 3rd Generation Partner Project (3GPP) terminology. In 6G wireless networks, the evolution of URLLC services to Enhanced Ultra Reliable Low Latency Communications (eURLLC) is expected. It aims to achieve end-to-end latency, and reliability requirements of 0.01 ms, and 99.99999%, respectively [5] [6]. This envisioned target service of 6G networks has the potential to revolutionize various aspects of our lives, such as self-driving vehicles and tele-surgeries [7].

In the realm of 5G, a notable service revolves around vehicular-based communications known as Vehicle-to-Anything (V2X) service [8]. It corresponds to communications between two vehicles Vehicle-to-Vehicle (V2V), or between a vehicle and the infrastructure Vehicle-to-Infrastructure (V2I). As we move into the 6G era, vehicular communication systems are expected to evolve, offering more advanced V2X services with increasingly demanding requirements. This entails extremely low latency (0.01ms) and high throughput along with high reliability (99.999999%), with the aim of accommodating a wide range of potential applications associated with future vehicles, including autonomous and intelligent vehicles. Furthermore, the transportation industry is a critical sector for 6G, with Connected Autonomous Vehicles (CAVs) being one of its most demanding areas due to the various required service qualities [9]. Initially, autonomous and connected vehicles were developed independently but combining them in CAVs is expected to address their inherent limitations and to help solve transportation challenges. CAVs have many promising applications, such as smart intersections, cooperative perception, and cooperated platooning, which can significantly enhance road safety, fuel/battery consumption, and congestion. To harness the complete capabilities of CAVs, 6G needs to meet the aforementioned more stringent connectivity Key Performance Indicators (KPIs) along with extremely massive instant access anytime and anywhere, a concept referred to as Grant Free (GF) [2].

To unleash the full potential of the aforementioned services, 6G would have to meet the corresponding stringent KPIs, thereby resorting to the exploration of novel methods, spanning from the application to the physical layer. However, the current Orthogonal Frequency Division Multiplexing (OFDM) waveform, introduced in 4G and kept in 5G, may not be sufficient to satisfy these stringent demands. Despite its robustness against multipath channels thanks to its Cyclic Prefix (CP), its orthogonality in both the time and frequency domains, its efficiency in supporting numerous Multiple-Input Multiple-Output (MIMO) techniques [10], like

spatial multiplexing and MIMO diversity scheme employing Alamouti code [11], its simple one-tap equalizer and implementation through Fast Fourier Transform (FFT), OFDM may not be versatile enough to support all demanding constraints.

However, the coexistence of the above services within the same frequency band, as envisioned in 6G, is jeopardized by the high Out-Of-Band-Power Leakage (OOBPL) associated with OFDM. Moreover, OFDM requires fine time and frequency synchronization with the Base Station (BS) for each user, leading to a substantial increase in signaling overhead. As a result, both latency and energy consumption are significantly affected.

In this context, various waveforms have been explored as potential candidates for 5G and now 6G. These include Filter Bank Multi-Carrier with Offset Quadrature Amplitude modulation (FBMC/OQAM), Universal-Filtered Orthogonal Frequency-Division Multiplexing (UF-OFDM), Filtered-Orthogonal Frequency-Division Multiplexing (F-OFDM), and Orthogonal Time Frequency Space (OTFS). They introduce filtering as means to address the identified drawbacks of OFDM. The filtering operation is carried out in the digital domain before transmitting the baseband discrete signal to the Digital to Analogue Converter (DAC). This filtering step significantly reduces the OOBPL, thereby enhancing the service coexistence capability and mitigating the synchronization constraints.

The primary distinction between these waveforms is based on the filtering operation type, which could be applied per subcarrier or per group of subcarriers (subband), and the orthogonality property. For example, FBMC/OQAM uses per subcarrier filtering while maintaining orthogonality in the real field. UF-OFDM and F-OFDM both use subband filtering, but the latter is not orthogonal.

1.2 Objectives of the thesis

While OFDM has been the state-of-the-art technology for the past few decades, it has several drawbacks that limit its efficiency in certain scenarios. On the other hand, recent research projects have identified filtered multi-carrier waveforms as next-generation enabling technologies at the physical layer. Among these techniques, FBMC/OQAM was considered as the most promising waveform during the drive for 5G. It was preferred over OFDM, which is currently the state-of-the-art technology, thanks to its superior spectrum confinement, ability to withstand imperfect synchronization in dense networks with Device-to-Device (D2D) and asynchronous machine communications, and its robustness in high-mobility scenarios such as vehicular communications.

Over the past few years, the research team at IMT Atlantique has made significant progress in developing and patenting innovative contributions related to FBMC at both the transmitter and receiver sides [12,13]. At the transmitter side, a novel short Prototype Filter (PF) for FBMC that enables near-perfect reconstruction while having the same size as one OFDM symbol has been proposed. When combined with other original receiver techniques, it becomes a major enabler for most of the communication scenarios mentioned above, while also significantly reducing hardware

complexity and energy consumption. At the receiver side, a novel FBMC receiver technique that is suitable for short filters has been also proposed [13]. It involves using a time-domain equalizer based on the Overlap-Save (OS) algorithm, which allows for fast convolution operations, before the FBMC demodulation. It has been demonstrated that the time-domain equalizer and the FBMC receiver can be merged into a single structure due to the frequency localization of the filter, significantly reducing computational complexity. An alternative FBMC-OS scheme where FBMC symbols are transmitted by block and demodulated all at once in the frequency domain has been derived, further reducing complexity and enabling efficient Alamouti-based MIMO support. The resulting receiver greatly improves robustness against doubly dispersive channels for short filters and supports asynchronous communications.

Yet, there are still some important issues that need to be resolved. Some techniques used for OFDM cannot be directly applied to FBMC due to the OQAM scheme, such as Pilot Structure (PS) for Channel Estimation (CE), along with conventional estimation techniques used for OFDM, added to the compatibility with massive Multiple-Input Multiple-Output (mMIMO). The latter with a large number of antennas at the BS is a critical technology for the next generation of wireless data networks [14, 15]. It offers substantial benefits in terms of reliability, data rates, and SE/energy efficiency. Therefore, it is crucial to find appropriate solutions for these technical issues if FBMC is to be used for certain services in future communication systems.

In this context, the main goal of this thesis is to propose solutions to the above-mentioned challenges for filtered multi-carrier waveforms targeting mMIMO systems. Several objectives were considered:

- Extension to mMIMO of the methods proposed in [13] that involve the use of the Overlap-Save algorithm, specifically by utilizing a short prototype filter to reduce latency and the complexity of the transceiver.
- Support of relaxed synchronization, asynchronous communications, and resilience against different interference types.
- Development of a PS that enables the implementation of conventional OFDM CE techniques for FBMC systems.
- Leveraging the robustness to interference of FBMC/OQAM when associated with the advanced receivers in new Bandwidth (BW) efficient transmission techniques.

1.3 Thesis contribution

In pursuit of these objectives, this PhD thesis has proposed several novel contributions:

- A novel transmission technique for multi-carrier systems is proposed for Single-Input-Single-Output (SISO) transmissions. It is based on partially overlapping adjacent subbands by overlapping a portion of the corresponding subcarriers. A procedure is then proposed to compensate for the overlapping-induced interference while enhancing the SE.

Employing the OS-FBMC and the OFDM receivers, the proposed technique achieves new tradeoff levels between error rates and SE.

- The OS-based FBMC receivers with short filters are extended to the context of Multi-User (MU)-mMIMO systems. We investigate their advantages in comparison to OFDM under different channel impairments. Signal-to-Interference Ratio (SIR) expressions are derived analytically under several channel impairments such as Timing Offset (TO) and Carrier Frequency Offset (CFO). Furthermore, we conducted an asymptotic study on the performance of FBMC augmented with the proposed receivers in the context of mMIMO systems.

- A novel spectrally efficient PS for improving CE in mMIMO-FBMC/OQAM is proposed. It is based on interleaving users' pilots in frequency by introducing a circular shift. In addition to improved performance, the proposed pilot structure reduces the training overhead while reducing the complexity by enabling the employment of conventional OFDM CE techniques, particularly the Least Squares (LS) method in the context of Single-User (SU) and MU scenarios.

1.4 Manuscript Organization

The rest of this dissertation is organized as follows:

Chapter 2 provides a detailed explanation of the emerging services forseen in 6G. It is shown that the current OFDM technology may not be sufficient to support all of these services. Therefore, alternative waveforms have been explored and some of these, such as FBMC/OQAM, are described. This is followed by discussing the motivations for employing short PFs with FBMC/OQAM. Specifically, the challenges associated with FBMC/OQAM are highlighted and how can short PFs provide a suitable solution. Then, relevant state-of-the-art equalizer techniques such as the time domain equalizer in [16] and the OS equalizer [13] are introduced. This chapter ends by discussing the open issues for FBMC/OQAM which is still hindering it from a wide adoption.

Chapter 3 starts by reviewing the existing SE enhancement techniques in the literature. Then, a novel transmission technique called Modulation Code Overlapping (MCO) is proposed. The proposed method is flexible since it can achieve new tradeoff levels between error rates and SE. Finally, to illustrate the benefits of the proposed contribution, several channel impairments are considered such as TO, and multipath channel condition. It is shown that, FBMC augmented by the OS receiver outperforms OFDM. In particular, the FBMC transceiver offers up to 66% higher SE gain compared to OFDM. Although the proposed MCO approach enhances the SE for SISO systems, but some 6G applications demand even higher levels, and mMIMO may be a promising solution for that. Therefore, the extension of the OS-based receivers to the

context of mMIMO systems is tackled in the next chapter.

Chapter 4 reviews the relevant receivers in mMIMO literature. Then, the OS-based FBMC receivers are extended to mMIMO systems. Finally, several performance metrics are evaluated and compared to illustrate the benefits of the proposed contribution. In this regard, several channel impairments are considered such as TO, CFO, adjacent interference, asynchronous transmissions and multipath channel conditions. Performance results are compared with mMIMO OFDM and FBMC/OQAM receivers. Simulation and analytical results reveal the superiority of the proposed receivers to those in mMIMO literature. So far, the Channel State Information (CSI) is assumed to be perfectly estimated at the receiver side. However, the potential of mMIMO technology highly relies on the accuracy of the CE. To this end, CE issue is addressed in the next chapter.

Chapter 5 provides general overview on the CE techniques for FBMC/OQAM systems found in the literature. Then, a novel PS design is proposed. The main idea is to interleave the users' pilots in frequency domain by applying a simple circular shift. The proposed PS enables the employment of conventional CE methods used for OFDM by eliminating the noise correlation and intrinsic interference. Moreover, it improves the SE by eliminating the Guard Band (GB)s between users' pilots. To exemplify the benefits of the proposed PS over those in the literature, several channel metrics are considered, such as, Normalized Mean Square Error (NMSE) and Sum-Rate (SR). Simulation results reveal how the proposed method outperforms state-of-the-art techniques while enhancing the SE.

Chapter 6 summarizes the work presented in this dissertation and discusses some interesting directions for future research in the scope of this dissertation.

1.5 List of publications

1.5.1 Patent

1. Hamdar, F., Nadal, J., Abdel Nour, C., and Baghdadi, A., "Multiuser FBMC/OQAM Systems: Pilot Structure and Channel Estimation Technique for Improved Spectral Efficiency", Patent application 2023.

1.5.2 Journal publications

1. Hamdar, F., Nadal, J., Abdel Nour, C., and Baghdadi, A., "Overlap-Save FBMC receivers in the context of massive MIMO" (submitted).

2. Hamdar, F., Gussen, C., Nadal, J., Abdel Nour, C., and Baghdadi, A., "FBMC/OQAM Transceiver for Future Wireless Communication Systems: Inherent Potentials, Recent

advances, Research Challenges", IEEE Open Journal of Vehicular Technology, 2023 (accepted).

3. Hamdar, F., Nadal, J., Abdel Nour, C., and Baghdadi, A., "Multiuser FBMC/OQAM Systems: Pilot Structure and Channel Estimation Technique for Improved Spectral Efficiency" (ready to be submitted).

1.5.3 Conference publications

1. Hamdar, F., Nadal, J., Abdel Nour, C., and Baghdadi, A., "Overlap-Save FBMC receivers for massive MIMO systems under channel impairments" in IEEE 94th Veh. Tech. Conf. (VTC2022- Spring), 2022.

2. Hamdar, F., Nadal, J., Abdel Nour, C., and Baghdadi, A., "Novel transmission technique based on intentional overlapping for spectral efficiency enhancement in multicarrier systems" in IEEE PIMRC Conf., 2023 (accepted).

Chapter 2

Beyond 5G and post-OFDM waveform candidates

The development of 6G mobile network technologies is being driven by the complex demands of emerging mobile applications, such as digital twins and extended reality, which require capabilities beyond what 5G can offer. Although 6G is still in its conceptualization stage, some of the top vendors have released initial proposals for technology-based KPIs for 6G, which include achieving a peak data rate of 1 Tb/s, radio latency of 0.01 ms [5], a maximum of one outage per million, 10 times greater energy efficiency, a battery life of 20 years [17], and a connection density of 10^7 devices per square km compared to 5G [18]. It is important to note that these requirements are not necessarily expected to be fulfilled by a single device. To unleash the full potential of the emerging applications, 6G needs to fulfill the aforementioned more stringent KPIs.

Waveform design is an important technology component, and the OFDM waveform, which is used in 5G, has some drawbacks in terms of spectrum usage and its ability to handle synchronization errors. To address these limitations and meet the 6G requirements, researchers have conducted various studies to develop new waveforms. These new candidates, known as post-OFDM waveforms, use multicarrier modulation with a specific filtering scheme applied on top of the OFDM basis.

The chapter starts by providing a brief introduction to OFDM, which is commonly used in conventional eMBB service in 5G. It then explains the specific demands of various scenarios in 6G, such as eMMC, MCC, and V2X communications. The chapter highlights the limitations of OFDM modulation in addressing these requirements. Next, the chapter provides a technical description of FBMC/OQAM, which is the waveform addressed in this thesis. Additionally, a brief overview of other promising waveform candidates is given. The chapter discusses the advantages of using short PFs for FBMC/OQAM, as well as the associated drawbacks. Furthermore, the chapter presents relevant FBMC/OQAM receivers in the literature that address these issues. Finally, the chapter identifies the outstanding challenges that are currently preventing the wider adoption of FBMC/OQAM waveform.

2.1 Beyond 5G scenarios and system constraints

The section discusses three primary 6G communication scenarios, namely, (1) enhanced Massive Machine Communications, (2) Mission-Critical communications, and (3) Vehicular-to-Anything communications. The KPIs of the aforementioned 6G scenarios will be much more stringent than those considered for 5G and include a diverse set of novel metrics not considered before. This section gives a concise overview of these scenarios and also provides some background on the utilization of OFDM in traditional eMBB services in 5G.

2.1.1 Enhanced mobile broadband service and OFDM in 5G

The scenario known as Mobile Broadband (MBB) communications pertains to the conventional mobile Internet access service, which was introduced for the first time in 1991 as part of the second generation mobile networks (2G). With the advent of the third (3G), fourth (4G), and 5G generations, higher speeds were established. In the 6G, this scenario is referred to as eUMBB, which expands upon the conventional eMBB in 5G by improving data rates, capacity, and coverage. This scenario is typically utilized for activities such as multimedia streaming, voice-over-IP, internet browsing, videoconferencing, file downloads, and so on.

OFDM is the foundation of 5G downlink radio transmission, where data is transmitted through a large number of parallel narrow-band subcarriers. The use of relatively narrowband subcarriers in combination with a CP makes OFDM transmission robust to time dispersion on the radio channel without requiring advanced and potentially complex receiver-side channel equalization. For the uplink, where the available transmission power is significantly lower than for the downlink, Single-Carrier Orthogonal Frequency-Division Multiplexing (SC-OFDM) is used. This transmission mode is based on Discrete Fourier Transform (DFT)-precoded OFDM and has a smaller Peak-to-Average Power Ratio (PAPR) than conventional OFDM, thus enabling less complex terminals and the use of low cost amplifiers.

OFDM modulation

OFDM was first suggested by Weinstein and Ebert in 1971 [19], and since then it has been extensively employed in wireless communication systems [20]. Some examples of these systems include the Digital Video Broadcasting-Terrestrial standard, the IEEE 802.11 standard (Wi-Fi), 4G/LTE and the 5G standards. OFDM is a multi-carrier modulation technique that partitions the available BW into numerous narrow-bands known as subcarriers.

The subcarriers in OFDM are modulated by complex valued symbols obtained from a conventional digital modulation scheme such as Quadrature Amplitude Modulation (QAM), which carry the data to be transmitted. Each transmitted subcarrier creates a cardinal sine function spectrum with side lobes that result in overlapping spectra between subcarriers in the frequency domain. The subcarriers are evenly spaced such that the peaks of individual subcarriers align with the nulls of other subcarriers, with subcarrier frequency spacing denoted by ΔF. This orthogonality allows for the symbols to be received without interference in both time and frequency

Frequency range	μ	$\Delta F = 2^{\mu}.15$ kHz	$N_{subframe}^{slots}$	$N_{slots}^{symbols}$
FR1	0	15	1	14
	1	30	2	14
	2	60	4	12 or 14
FR2	3	120	8	14
	4	240	16	14

Table 2.1: Multi-numerology parameters in 5G

domains.

To implement an OFDM transmitter, an Inverse Fast Fourier Transform (IFFT) is used with a size of N, where N represents the total number of subcarriers that can be transmitted. A subset of these subcarriers is selected to carry N_C QAM symbols for transmission, and these subcarriers are known as the allocated subcarriers. The N_C QAM symbols are fed to the corresponding input of the IFFT, while the remaining subcarriers are set to zero. After the IFFT is performed, a time domain signal consisting of N samples is obtained. A CP of length L_{CP} is then inserted before the first samples by copying the last L_{CP} samples of the obtained time domain signal. The resulting time domain signal is composed of $L_{CP} + N$ samples, representing the OFDM symbol. These steps are repeated for each OFDM symbol to be transmitted.

Multi-numerology is a key technology in 5G networks that enables them to handle various applications and services, such as low-latency or high-bandwidth communications. It achieves this by providing flexibility in the choice of the OFDM waveform parameters, which can be adapted to the propagation environment. These parameters primarily depend on the selected frequency range, where 5G networks operate on two different frequency bands: sub-6 GHz (FR1) and Millimeter-Wave (mmWave) (FR2).

Sub-6 GHz operates within a frequency range of 410 MHz to 6 GHz, while mmWave operates above 24 GHz. Although mmWave provides high bandwidth capacity, its coverage is limited due to the high frequency and low penetration through obstacles. Among the configurable parameters, the CP length and the subcarrier spacing ΔF are crucial. The latter can be selected from a set of values, such as $\{15^{\mu} \mid \mu = 0, 1, .., 4\}$ kHz, as defined in the standard [21].

This flexibility in parameter selection offers a more adaptable frame structure that can be customized according to the chosen numerology as shown in Figure 2.1. The 5G frame structure comprises 10 subframes, each lasting 1 ms. The number of slots in each subframe ($N_{subframe}^{slots}$) and the number of symbols per slot ($N_{slot}^{symbols}$) depend on the selected numerology. Table 2.1 presents the specific values of these parameters for each numerology.

To transmit an OFDM symbol, each sample is sent at a sampling frequency F_s, which allows us to determine the duration of one OFDM symbol, given by $T = (N + LCP)/F_s$ seconds where F_s is measured in Hz. The subcarrier frequency spacing ΔF, which determines the BW used, is given by $\Delta f = F_s/N$ Hz. Thus, for a given number of subcarriers N_C, the total BW used is $N_C \Delta f$ Hz.

In 5G, the choice of parameters depends on the selected numerology and BW. Table 2.2 presents the 5G set of parameters for the first numerology ($\mu = 0$) $\Delta f = 15$ kHz. Unlike

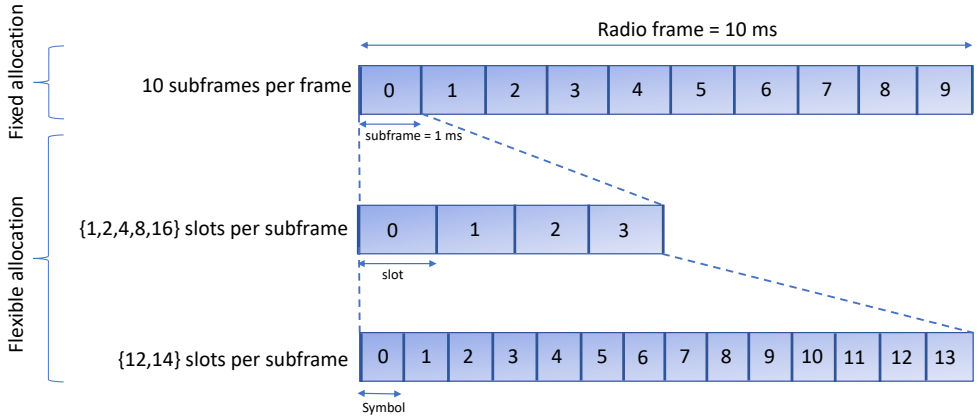

Figure 2.1: 5G frame structure.

4G/LTE, where the minimum size of an RB covers 12 consecutive subcarriers over a subframe duration, 5G RBs are defined only by the same BW definition; their duration is not fixed, as shown in Table 2.1.

From Table 2.2, we determine the effective BW in 5G using the expression $N_c\Delta f = 12N_{RB}\Delta f$, where N_{RB} is the number of allocated RBs. However, the BW configuration only specifies the OFDM parameters to be used for transmission within the available BW. Due to the introduction of a GB to limit out-of-band radiation, the effective BW obtained is always less than the available BW in 5G. For instance, when the 5 MHz BW configuration is used, a maximum of 25 Resource Blocks (RBs) (i.e. 300 subcarriers) are allocated, and since the subcarriers are spaced by $\Delta F = 15$ kHz, the resulting effective BW is 4.5 MHz.

After the OFDM symbol is generated, the resulting baseband signal is sent to the Radio Frequency (RF) interface, which consists of several components. First, the digital baseband signal is converted to the analog domain using a DAC. Then, an analog filter is used to minimize the OOBPL. Next, a High Power Amplifier (HPA) is employed to amplify the power of the signal. A frequency mixer is used to shift the baseband signal to the desired carrier frequency. Finally, the signal is converted into radio waves by the antenna.

The radio waves are transmitted through the channel, but the ideal propagation scenario is only achievable in Line of Sight (LoS) conditions where the signal travels directly from the transmitter antenna to the receiver antenna. However, in practical wireless communications, the channel environment is more complicated and involves the reflection or diffraction of the signal by various obstacles, such as buildings, trees, and vehicles. This results in the creation of multiple paths, each with its own propagation delay, amplitude, and phase distortion. Therefore, if we denote the transmitted OFDM signal as s, the channel impulse response as h, and the delay spread as τ (which is the difference between the arrival time of the earliest and latest significant multipath components), then the signal received at a specific time t, denoted by $r(t)$, is the sum

BW configuration (MHz)	5	10	15	20
Fs (MHz)	7.68	15.36	23.04	30.72
IFFT size M	512	1024	1536	2048
Number of available RB	25	52	79	106
CP length	36	72	108	144
Effective bandwidth (MHz)	4.5	9.37	14.22	19.08

Table 2.2: 5G set of parameters for some available configurations considering the first numerology (μ = 15 kHz)

of the signals carried by each of these paths as shown below:

$$r(t) = \int_0^{\tau} h(\tau)s(t-\tau)d\tau \tag{2.1}$$

Following the RF interface, the received signal r, represented by $r(k)$ in the discrete domain (where k represents the sample number), can be expressed as the convolution of the transmitted signal s with the channel impulse response h as follows

$$r(k) = \sum_{l=0}^{L_{DS}-1} h\left(lT_s\right) s\left((k-l)T_s\right) + w(k), \tag{2.2}$$

where $T_s = 1/F_s$ is the sampling time, and L_{DS} is τ in samples. A noise term w is added due to the imperfection of electronic components and residual RF interferences. The multipath channel may introduce Inter-Symbol Interference (ISI), however, the CP acts as a guard interval and helps to avoid ISI if τ is shorter than the CP duration. The CP also facilitates equalization since it converts the linear convolution introduced by the channel at the FFT input to a circular convolution. The received OFDM symbol is demodulated by applying the dual operation of the transmitter, which involves removing the CP and applying a FFT of size N. Therefore, with H being the frequency response of the channel, S the transmitted QAM symbols, and the W the noise term, the symbols at the output of the FFT module can be expressed mathematically as follows:

$$Y(m) = H(m)S(m) + W(m) \tag{2.3}$$

Finally, the equalized symbols $\hat{S}(m)$ are obtained by using a simple per-subcarrier equalizer applied on the received signal Y as follows:

$$\hat{S}(m) = C(m)Y(m) \tag{2.4}$$

with $C(m)$ being the equalizer coefficient at subcarrier m. One way to express $C(m)$ is $1/H(m)$ when using the Zero-Forcing (ZF) equalizer. Another option is to use the coefficients of the Minimum Mean Square Error (MMSE) equalizer, which aims to reduce the squared mean of the noise-induced errors. In this case, we have:

$$C(m) = \frac{H^*(m)}{\|H(m)\|^2 + \eta} \tag{2.5}$$

where $\|H(m)\|^2 = H(m)H^*(m)$ represents the absolute value of $H(m)$, and η is defined as the reciprocal of the Signal-to-Noise Ratio (SNR) when using an Additive White Gaussian Noise (AWGN). However, computing the coefficients of the MMSE equalizer involves estimating the SNR beforehand, which introduces additional complexity and may lead to approximation errors that could hinder its effectiveness.

OFDM has several attractive features that make it a viable solution for the eUMBB scenario. These include its orthogonality in both time and frequency domains, which enables it to be highly robust against multipath channel conditions, as well as its ease of implementation using FFT and its ability to apply per-subcarrier equalization.

However, with the emergence of multiple new services and requirements in the beyond 5G and 6G systems, will OFDM be capable of effectively addressing all the challenges that arise?

2.1.2 Massive machine communications

MMC can be regarded as a component of MTC [22]. Its corresponding 3GPP term is massive MTC (mMTC). It pertains to the deployment of a large number of sensors or actors throughout a landscape, all requiring access to a wireless network. This scenario is commonly known as IoT.

Smart metering, natural ecosystem monitoring, remote maintenance/control, and remote diagnostics are some typical use cases for MMC. It is commonly assumed that communication in MMC is primarily unidirectional, with uplink communication being the dominant mode [23]. The transmission is sporadic and involves relatively small packets per connection, resulting in a low required data rate of around 1 kb/s to 10 kb/s per device. However, the user density in MMC is much higher than what is typically assumed for eUMBB services. In this regard, it is estimated that the number of connected devices in 6G will grow three-fold compared to the current generation [23]. Such a massive number of devices needing to communicate within a single cell goes beyond 5G system capability [24]. Additionally, sensors in MMC have limited hardware resources and must operate on long battery life [17], so the complexity and energy consumption of hardware implementation for modulation techniques must be kept to a minimum.

To minimize energy consumption in the scenario of MMC involving a large number of devices, it is important to minimize the signaling overhead introduced by the synchronization procedure. Therefore, the ideal transmission scheme for MMC should follow these steps to minimize energy consumption:

1. The sensor/UE wakes up from sleep mode.
2. It transmits the data to the BS.
3. It returns to sleep mode.

Achieving this ideal transmission scheme is difficult in practice since it requires support for asynchronous communications where there is no prior synchronization with the BS. This means that the relative delays between the received user signals are random and can be higher than the symbol duration, making it unsuitable for OFDM modulation which relies on strict

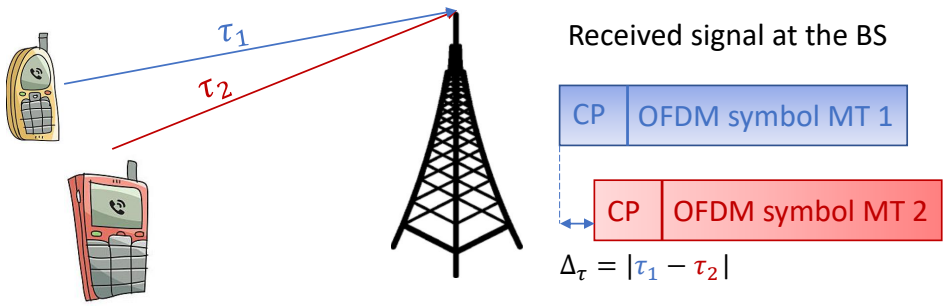

Figure 2.2: Example of MCC service.

orthogonality between users. An alternative solution is synchronizing each sensor with the BS using downlink reference signals. However, since each user is located at different distances from the BS, they can have different propagation delays. This results in the received signals sharing the same time base overlapping at the BS, leading to time misalignment and potential interference across all users. Figure 2.2 illustrates an example where two devices, identified as UE1 and UE2, transmit an OFDM signal through their corresponding channels with propagation delays of τ_1 and τ_2, respectively. The use of a CP allows the received data of each device to be perfectly recovered if the TO between devices $\Delta\tau$ is lower than the CP duration T_{CP}, which occurs when $T_{CP} > |\tau_1 - \tau_2|$. To achieve this, a circular shift operation must be applied to the OFDM symbol for each device. This operation is efficiently implemented after the FFT, in the frequency domain, using a simple Linear Phase Rotation (LPR) operation.

However, if $\Delta\tau > T_{CP}$, the processing window at the BS for some devices will not be aligned with the OFDM symbol (including CP) for demodulation. This means that part of the next (or previous) OFDM symbol will be included in the processing window. Therefore, devices with a TO higher than the CP duration will suffer from severe performance loss because the processing window at the BS will not be aligned with the OFDM symbol for demodulation. As a result, orthogonality is lost, and devices occupying adjacent subcarriers introduce Inter-User Interference (IUI), even if they are perfectly synchronized.

In 5G, the Timing Advance (TA) mechanism is used to solve this issue. The BS estimates the relative propagation delay of each device and transmits this information back to the corresponding device. At the next uplink transmission, each device applies a delay such that all the signals received by the BS are correctly aligned in time. Since the TA mechanism involves a feedback transmission, it corresponds to a closed-loop synchronization technique.

The main problem with the TA mechanism is the significant amount of required signaling, especially when a device is in motion and the TA value needs to be updated. This results in increased power consumption due to the frequent re-transmission of TA values through the downlink channel. As a result, a less strict synchronization approach is necessary for MMC.

Open-loop synchronization is a technique where each device is synchronized in time with the BS without any feedback information transmitted to the device. Therefore, the relative TO between devices must be estimated and compensated for at the BS.

One possible approach to estimate the TO value, is to use CE techniques to evaluate

the Channel Impulse Response (CIR) between the BS and each device, and then estimate the corresponding propagation delay. The BS can then apply a common TO correction for all received signals, based on the estimated propagation delays. This approach can reduce the signaling overhead associated with the TA mechanism since it does not require any feedback information from the devices.

However, open-loop synchronization has its own challenges. For example, the accuracy of the TO correction depends on the accuracy of the CE, which can be affected by various factors such as fading and interference. In addition, since the compensation of TO is applied at the receiver, it can introduce additional processing delay, which can affect the overall system latency.

An alternative possible approach to deal with the TO issue in OFDM is to increase the duration of the CP through multi-numerology so that it can accommodate any propagation delay. However, in a multi-user uplink scenario, users face different channels, hence experience different effects of frequency selectivity. Therefore, the user suffering the most from selectivity determines the required target CP length for all users sharing the same received OFDM symbol slot. However, this yields a SE loss since the other users do not require such a long CP length. Furthermore, any attempt to adapt the CP length to each user's channel condition leads to interference and performance degradation for the subset of users suffering from longer delay spread channels. Therefore, a compromise between interference-limited performance and SE needs to be set for OFDM. Thus, alternative modulation techniques may need to be considered to support open-loop synchronization while maintaining high data rates and energy efficiency.

2.1.3 Mission critical communications

MCC is a type of MTC that requires wireless connectivity with very low latency and high reliability for transmitting sensor and actor messages between communication partners [25]. The 3GPP term for this is URLLC. In the context of 6G, eURLLC refers to the evolution of concepts already present in the definition of URLLC in 5G. MCC is used in various applications such as factory automation, vital sign monitoring, and safety and security applications like video surveillance.

The flexibility offered by the multi-numerology in 5G copes with such applications that require ultra-low-latency. In contrast to 4G, where the latency, related to the Time Transmission Interval (TTI), is fixed at 1 ms [26], 5G introduces the use of specific numerology for each unitary signal, enabling variable latency ranging from 1 to 0.125 ms. This flexibility allows for the transmission of composite signals comprising multiple unitary ones sharing contiguous sub-bands within a common band, as depicted in Figure 2.3.

Looking ahead to 6G, the expected latency is 100 times less than that in 5G, reaching 0.01 ms for specific applications [5]. However, the minimum achievable latency in 5G is still 0.125 ms, without considering propagation delay, hardware latency, and re-transmission mechanisms. Consequently, the overall end-to-end communication latency in 5G is higher than 0.01 ms [5], making it difficult to fulfill the MCC latency requirement in 6G. As a result, 5G cannot support time-critical applications which require instantaneous communication with negligible

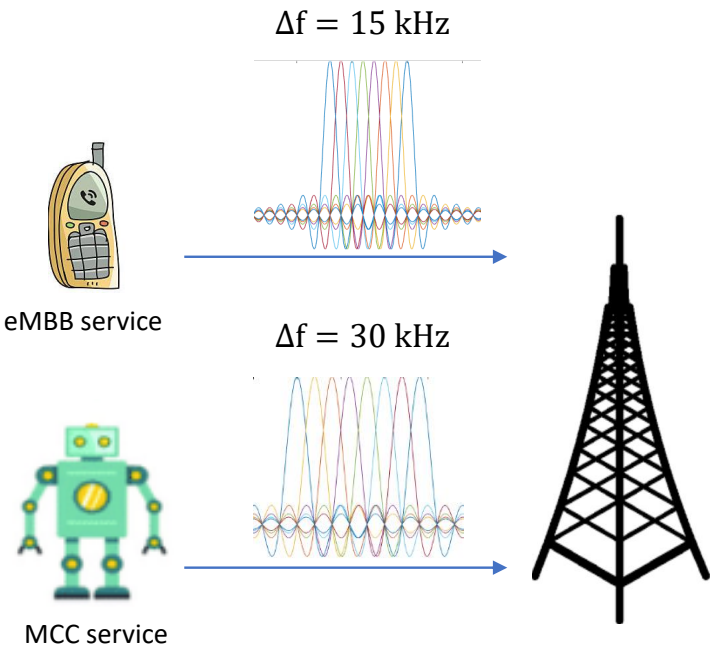

Figure 2.3: Example of different services employing distinct numerology.

latency such as autonomous driving or real-time healthcare assistance, as their required delay falls below 0.1 ms.

In addition to the aforementioned considerations, multi-numerology signals suffer from Inter-Numerology Interference (INI) due to the loss of orthogonality between neighboring signals that do not share the same numerology. The issue of INI in multi-numerology OFDM-based systems has been extensively studied, and various techniques have been proposed to reduce INI [27, 28]. One of the most common techniques involves inserting GBs between sub-bands at the cost of SE [29]. For instance, reference [30] shows that up to 300 kHz of guard-band (20 subcarriers) must be inserted between two users to obtain a Packet Error Rate (PER) of 10^{-9}. This corresponds to the case where one user has a typical subcarrier spacing of ΔF = 15 kHz, while the second has ΔF = 60 kHz, both using a convolution Forward Error Correction (FEC) code with 1/2 Coding Rate (CR) and a 64-QAM constellation. An alternative solution to address the SE issue, data subcarriers can be inserted within the GB, with their indices chosen according to a limited increase of INI [31]. Other methods include the windowed-OFDM scheme to mitigate INI along with an iterative algorithm at the receiver side to cancel remaining interference, or pre-equalization at the transmitter side when the transmitted data is known [27] at the cost of high complexity. Furthermore, the authors in [32] propose power scheduling or scheduling managed by machine learning algorithms to reduce INI. Unfortunately, all of the aforementioned techniques present some drawbacks, they either suffer from high complexity or SE loss and are only based on OFDM systems. Therefore, alternative modulation techniques may be required to support mixed-numerology systems for low-latency communications for 6G MCC.

2.1.4 Vehicular-to-anything communication

The V2X service refers to communications between two vehicles, also known as V2V, or between a vehicle and infrastructure, also known as V2I. V2X is part of intelligent transportation systems and includes use-cases with high-speed nodes [33]. V2V communications provides several benefits, including reducing traffic accidents, improving traffic efficiency, and enabling new applications [34]. The technical requirements for V2X are often combined with those of other 6G services, such as MCC and eUMBB. Composite services are created by combining more than one core service, such as pay-as-you-drive, which combines V2X with MCC, and infotainment [35], which combines V2X with eUMBB.

The 5G-NR V2X system provides improved performance and advanced services compared to 4G/LTE, but this is achieved by investing more in spectral and hardware resources while maintaining the underlying mechanisms and system architectures of 4G/LTE-based V2X [36]. As the number of autonomous vehicles increases, there will be a surge in communications devices and digital applications to enable intelligent autonomous vehicles, as well as emerging services ranging from 3-D displays to immersive entertainment, which will pose new communication challenges to the V2X network [6, 36]. All of these advances are expected to push the capacity limits of existing wireless networks, requiring a significant paradigm shift towards more versatile and diversified network approaches.

The upcoming 6G wireless communications network aims to combine terrestrial and non-terrestrial communication networks and is expected to enable genuinely intelligent and ubiquitous V2X systems with enhanced reliability, security, extremely high data rates, and adaptive learning capabilities. Furthermore, the 6G wireless communication network is envisioned to provide ultra-reliable high-rate V2X communications in high-mobility environments, where connected vehicles and high-speed trains are moving at speeds of 1000 km/h or even higher [37, 38]. However, such high speeds are not supported by the current 5G standard, where the mobility limit is considered to be 500 km/h [39]. Consequently, high speeds can cause a significantly reduced channel coherence time, resulting in rapidly time-varying vehicular channel fading coefficients. While OFDM is commonly used for high-rate transmissions in 4G/LTE and 5G NR, it is sensitive to the Doppler effect, which can hinder multicarrier orthogonality and increase Inter-Carrier Interference (ICI) and ISI. Consequently, the complexity of the OFDM receiver is greatly increased to cope with such challenges. Moreover, the orthogonality between users is compromised since the amplitude peaks and the zeros of the cardinal sine pulse conveyed by each subcarrier are frequency-shifted. Again, novel advanced multicarrier waveforms are required to cope with these scenario-specific drawbacks in 6G V2X communications.

2.1.5 5G Quadriga channel

The Quasi Deterministic Radio Channel Generator (QuaDRiGa) [40] is a simulation platform that is recommended by the 3GPP standardization organization for use in 5G-and-beyond wireless communication systems. It is a complete geometry-based 3D stochastic channel model that extends the WINNER II/WINNER+ [41] and 3GPP-3D models and incorporates many features

included in the Spatial Channel Model (SCM) and WINNER channel models, as well as some novel modeling approaches.

The modeling approaches used in QuaDRiGa provide features that make the multilink tracking of users accurate and qualitative in changing environments. To obtain different channels, QuaDRiGa randomly determines channel parameters, such as the delay/angle spread and Cross-Polarization Ratio (XPR), based on real-world measurements extracted from statistical distributions.

QuaDRiGa is capable of supporting arbitrary carrier frequencies from 0.45 to 100 GHz with up to 1 GHz radio frequency bandwidth. The simulation platform allows for the continuous time evolution of channel parameters, such as time delay, power, angle, shadow fading, and the Ricean K-factor through the positions of the scattering clusters and users.

When it comes to user mobility, the user track is divided into multiple segments, and the length of each segment is linked to the decorrelation distances of the Large-Scale Parameters (LSPs). In each segment, a scenario (e.g., LoS or Non Line of Sight (NLOS)) is assigned, the LSPs vary steadily, and the Wide-Sense Stationary (WSS) condition is satisfied. The segments are then combined into a continuous channel. The spatially correlated modeling of LSPs in the LoS and NLOS scenarios is determined by the Sum-Of-Sinusoids (SOS) approach to simulate a Gaussian random process to ensure the spatial consistency of Small-Scale Parameters (SSPs).

Procedure to generate channel coefficients and delays

The input variables such as network layout, terminal trajectories, antenna patterns, and the propagation scenario are required for generating the channel coefficients and delays. The Mobile Terminal (MT) trajectory is split into segments. A segment can be seen as an interval in which the LSPs do not change considerably. Hence, after the computation of the LSPs for each MT, the channel traces are generated independently for each segment following the summarized procedure below:

1. Determination of the initial delay and path angles of each Multi-Path Component (MPC) for each MT separately.
2. Definition of the power for each MPC.
3. Application of the K-factor, delay spread, and angular spreads. The channel coefficients are then calculated by updating the initial characterization parameters.
4. Drifting of delays, angles, and phases over a short segment in case of mobility.
5. Computation of polarized channel coefficients using the Jones calculus [42]
6. Recalculation and application of the LSPs to the channel coefficient because the LSPs such as the K-factor will change with the movements of the user.

Finally, each segment of the user's trajectory is combined into a continuous channel. A smooth transition between segments is made through the birth-death procedure of clusters. More details of the QuaDRiGa modeling process can be found in [40].

2.2 Post-OFDM waveforms

In recent years, several waveforms have been studied as potential alternatives for OFDM in the context of 6G. These include FBMC/OQAM, UF-OFDM, F-OFDM, and OTFS. In this doctoral research, the focus has primarily been on investigating FBMC/OQAM, which involves adding a subcarrier filtering stage to OFDM. This section will provide a technical explanation of the FBMC/OQAM waveform, as well as an introduction to the few aforementioned promising waveforms under consideration.

2.2.1 UF-OFDM waveform

The initial name given to the UF-OFDM modulation was Universal Filtered Multi-Carrier (UFMC). This modulation technique separates complex information-carrying samples into multiple subbands, with each subband comprising Q subcarriers. These samples may originate from a QAM constellation. The number of subbands that can be used is limited to a maximum of $\lfloor N/Q \rfloor$, where N represents the total number of subcarriers and $\lfloor x \rfloor$ denotes the largest integer less than or equal to x. To suppress the secondary lobes of each subband, a filter of length L samples is used to independently filter each subband [43]. The filtered subbands are then combined to form the UF-OFDM symbol, which comprises $N + L - 1$ samples.

The operating principle of the UF-OFDM transmitter is depicted in Figure 2.4, which involves the following steps:

1. Complex information samples are mapped to their corresponding subcarrier indexes within each subband.

2. An IFFT of size N is conducted for each allocated subband.

3. A linear convolution operation is performed for each subband for the filtering stage.

4. All filtered subband signals are combined through a summation operation, producing a UF-OFDM symbol.

The aforementioned steps must be repeated for each UF-OFDM symbol. It is important to note that UF-OFDM symbols lack a CP [43], however, a slight data rate loss is observed due to the ramp-up and ramp-down transition of the subband filtering. Indeed, if the filter length is L, then $L - 1$ additional samples are added to the N time-domain samples carrying information. Typically, the filter length is designed to produce an equivalent data rate loss to the CP in OFDM, with $L = L_{CP} + 1$.

In contrast, the implementation of the UF-OFDM receiver differs from that of its transmitter [44] and comprises the following steps:

1. The $N + L - 1$ samples constituting the received UF-OFDM symbol are isolated.

2. $N - L + 1$ zeros are appended to the end of the isolated samples, yielding a signal of $2N$ samples.

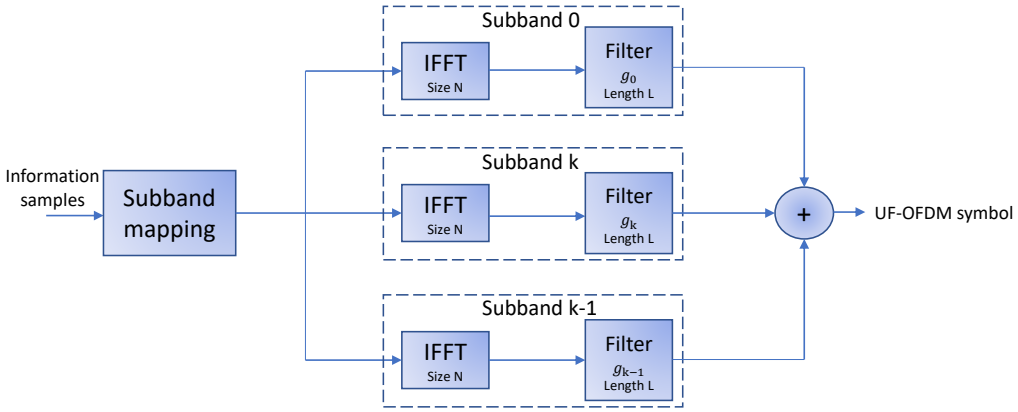

Figure 2.4: Illustration of UF-OFDM transmitter.

3. An FFT of size $2N$ is applied to the zero-padded signal to obtain the frequency domain signal.

4. The odd FFT output indexes are discarded (down-sampling by 2) to keep the even indexes where the main lobe of each transmitted subcarrier is concentrated.

The frequency-domain signal obtained in the previous step can be subjected to the same types of processing techniques as those used in OFDM, including equalization.

It is possible to apply a windowing operation to the time-domain samples between steps 2 and 3 prior to computing the FFT in UF-OFDM. Although this step is optional according to [44], it is highly recommended since it can improve the performance of the UF-OFDM receiver in case of relaxed synchronization as stated in [45]. Compared to the standard OFDM receiver, the UF-OFDM receiver requires a larger FFT size, which slightly increases its complexity. However, due to the fact that $N - L + 1$ input samples of the FFT are zero-valued and half of its outputs are discarded, there are redundant operations. In fact, it has been demonstrated in [33] that the FFT size can be reduced to N, the same size as used in the OFDM receiver, thus avoiding the need for zero-padding the $N + L - 1$ received UF-OFDM symbol samples. Indeed, rather than using zero-padding on the $N + L - 1$ samples of the received UF-OFDM symbol, the last $L - 1$ samples can be combined with the first $L - 1$ samples. If a windowing operation is to be employed, it should be done prior to this step. The resulting N samples can then be directly computed using a FFT of size N. As a result, the UF-OFDM receiver has nearly the same complexity as the OFDM receiver.

The primary drawback of the UF-OFDM waveform resides in its increased susceptibility to frequency selective fading. This is due to the use of subband filtering instead of per-subcarrier filtering. As a result, when a subcarrier in a subband experiences fading, the corresponding data symbol carried by that subcarrier is destroyed or potentially lost. Additionally, since the data symbols within the subband are filtered collectively, the filter also distorts the remaining data symbols in the same subband, leading to the occurrence of ISI.

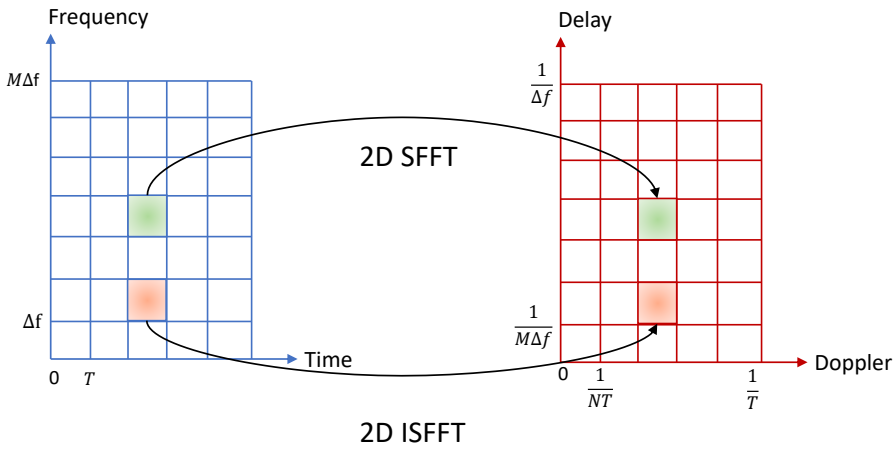

Figure 2.5: Transformation from TF to DD domain.

2.2.2 F-OFDM

F-OFDM, as described in [46], is a promising candidate waveform for beyond 5G. It employs subband filtering, similar to UF-OFDM, but there are some significant differences. First, F-OFDM incorporates a CP of length L_{CP}. Second, the subband filter length L exceeds the CP length. The impulse response coefficients of this filter are devised to concentrate most of the energy on L_{CP} samples to avoid severe ISI. Moreover, the filter is designed to have a flat frequency response over the supported subband bandwidth. The third difference is the use of a matched filter on the receiver side. F-OFDM has shown promising results in relaxed synchronization scenarios. Nevertheless, its complexity, particularly on the transmitter side, is an issue that needs to be addressed.

2.2.3 OTFS

OTFS modulation was proposed by Hadani et al. in WCNC'2017 [47] as a multiplexing scheme suited for doubly-selective channels. Unlike conventional modulation techniques such as OFDM, OTFS modulates information bits in the Delay-Doppler (DD) domain instead of the Time-Frequency (TF) domain. The key idea behind OTFS is to use a transformation that establishes a relationship between the wireless channel and the information symbols in the DD domain. This transformation is achieved using the Symplectic Finite Fourier Transform (SFFT) as shown in Figure 2.5. This enables OTFS to multiplex information symbols effectively in the DD domain using localized pulses as basis functions. This approach results in greater resilience to DD shifts caused by the channel.

Figure 2.6 portrays the block diagram of the OTFS transceiver. To transmit information bits $\boldsymbol{x}$, $M \times N$ classic Amplitude Phase Modulation (APM) symbols are used, where M represents the number of subcarriers, and N is the size of time slots. After operating the 2-D ISFFT, the DD $\boldsymbol{x}$ symbols are transformed to a 2-D TF symbols as follows

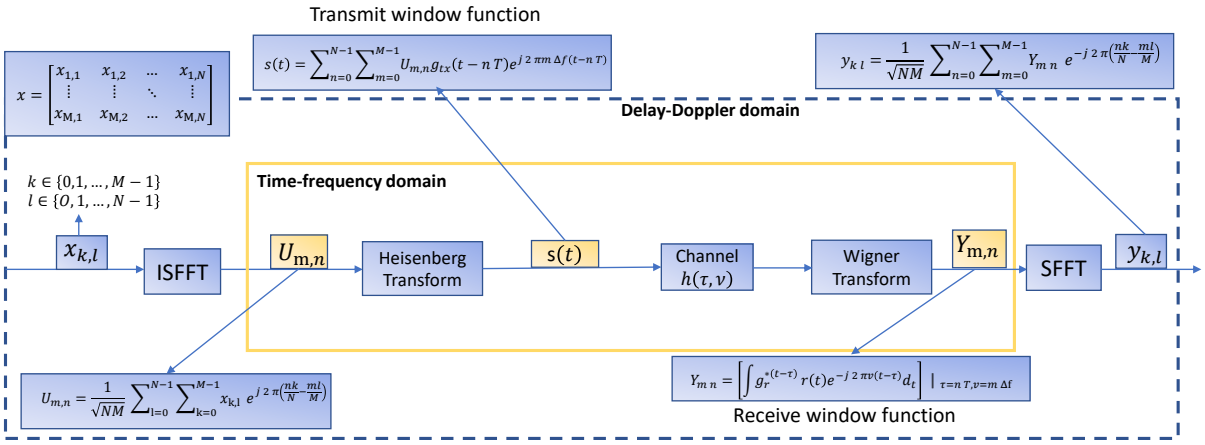

Figure 2.6: OTFS transceiver.

$$U_{mn} = \frac{1}{\sqrt{\mathrm{MN}}} \sum_{l=0}^{N-1} \sum_{k=0}^{M-1} x_{kl} e^{j2\pi\left(\frac{nk}{N} - \frac{ml}{M}\right)} \tag{2.6}$$

where $x_{k,l}$ is an element of $\boldsymbol{x}$.

Next, Heisenberg transform and a 2-D windowing are applied for the DD symbols as below

$$s(t) = \sum_{n=0}^{N-1} \sum_{m=0}^{M-1} U_{mn} g_{\mathrm{tx}}(t - nT) e^{j2\pi m\Delta f(t-nT)} \tag{2.7}$$

where g_{tx} is the impulse response of the transmit filter.

After that, the signal $s(t)$ will be transmitted over the time-variant channel as shown below

$$r(t) = \iint h(\tau, v) s(t - \tau) e^{j2\pi v(t-\tau)} d\tau dv \tag{2.8}$$

along with

$$h(\tau, v) = \sum_{i=1}^{P} h_i \delta(\tau - \tau_i) \delta(v - v_i) \tag{2.9}$$

where P is the total number of paths, τ_i and v_i are the path delay and Doppler shift of the i^{th} path.

At the receiver side, the Wigner transform is initially applied to the received signal, followed by SFFT for signal recovery as follows

$$Y_{mn} = \left[\int g^*_{\mathrm{rx}}(t - \tau) r(t) e^{-j2\pi v(t-\tau)} d_t \right] \Big|_{\tau = nT, v = m\Delta f} \tag{2.10}$$

$$y_{kl} = \frac{1}{\sqrt{NM}} \sum_{n=0}^{N-1} \sum_{m=0}^{M-1} Y_{mn} e^{-j2\pi\left(\frac{nk}{N} - \frac{ml}{M}\right)} \tag{2.11}$$

OTFS offers several advantages, such as managing high Doppler effects [48] and supporting

mMIMO [49, 50]. However, in the presence of a time-variant channel, OTFS experiences ISI and ICI, as mentioned in [51]. Moreover, the conventional data detection methods proposed for OTFS, including MMSE, Maximum Likelihood (ML), and Message Passing (MP) are known for their effectiveness in mitigating the impact of high Doppler effects, however, they suffer from high computational complexity due to the large size of the Delay-Doppler matrix [51].

In particular, traditional detectors designed for the classic OFDM system, which rely on single-tap frequency-domain channel equalization, may not be suitable for OTFS. A basic matched filter receiver, as described in [52], fails to adequately suppress interference caused by ISI and ICI in OTFS. Two types of receivers are commonly considered: Linear Receivers (LRx) and Non-Linear Receivers (NLRx). NLRx, like that in [53] and [54], offer performance close to ML but are computationally complex due to their iterative structure. On the other hand, LRx have simpler structures but exhibit relatively poorer performance compared to NLRx. Despite their linear processing requiring matrix inversion and multiplication, LRx still pose a computational burden on OTFS due to the large time-frequency grid size.

The Linear Minimum Mean Square Error (LMMSE) receiver is recognized for its interference cancellation capabilities [55, 56]. However, directly implementing the LMMSE receiver results in computational complexity on the order of $O(M^3N^3)$. Indeed, when M and N are in the order of hundreds, the complexity of the LMMSE receiver becomes excessively large.

Therefore, the current study items list for OTFS waveforms is still large and extensive research is needed to design detection schemes that offer less complexity while maintaining good performance.

2.2.4 FBMC/OQAM waveform

FBMC emerged as a candidate waveform to OFDM largely thanks to the results provided by the PHYDYAS project [57]. In FBMC waveform, a filter-bank applying a PF is introduced to effectively pulse-shape the transmitted signal over each subcarrier. It plays a significant role in controlling the amount of transmit power carried by the secondary pulse lobes. This provides greater flexibility for managing the OOBPL at the cost of added complexity at the transmitter and receiver sides. Also, this represents a major difference with respect to the rectangular pulse-shaping of OFDM [58]. The absence of a CP is another difference to OFDM that can lead to improved SE at the cost of more complex equalizer schemes.

Traditionally, two distinct FBMC transceiver implementation types with different levels of complexity and performance were proposed in the literature: Poly-Phase Network (PPN)-based [59] and *Frequency Spread* (FS)-based [60]. The first is usually employed at the transmitter side due to its lower complexity [61]. On the other hand, the FS implementation is mostly adopted at the receiver side thanks to its low-complexity equalization process [62, 63].

Fig. 2.7a depicts the PPN-based implementation. To support orthogonality in the real domain, OQAM processing is introduced [64]. First, the real and imaginary components of the QAM signal must be separated as shown in Fig. 2.7a. After phase rotation, the imaginary component is time delayed by half of the duration of a FBMC symbol. This is followed by

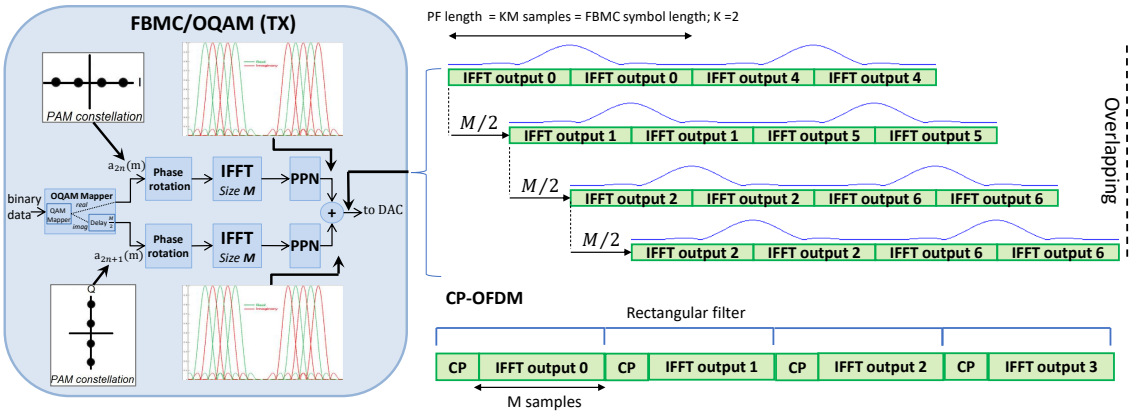

(a)

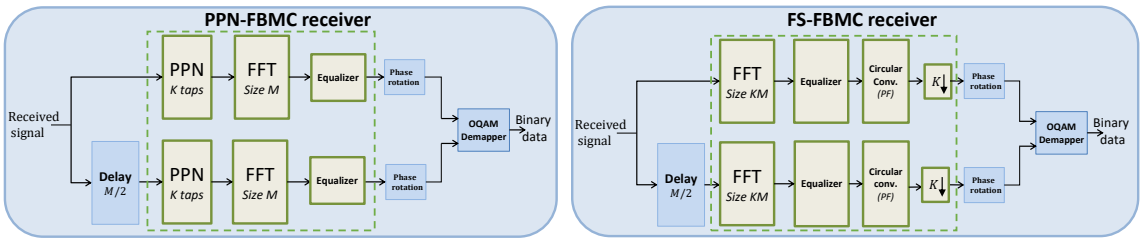

(b)

Figure 2.7: Overall original FBMC system illustration: (a) PPN-based FBMC transmitter implementation, (b) PPN and FS-based receiver implementations.

a size-M IFFT. A PPN processing is implemented next, where the IFFT output is replicated $K-1$ times, with K being the overlapping factor. After, a windowing operation is applied using the impulse response of the PF having a length of $L = KM$. Finally, the resulting components are summed up to provide the transmit signal. As shown in Fig. 2.7a, the transmitted FBMC symbols overlap in time, hence the FBMC signal is not made up of successive and separate block symbols.

To use a low-complexity subcarrier-based equalizer at the receiver side, the filtering stage was moved into the frequency domain for the FS implementation. As depicted in Fig. 2.7b, both receiver-side implementations apply dual operations with respect to the ones performed by the transmitter. For the PPN-based implementation, the operations must be performed in the following order: PPN, FFT of size M, and OQAM demapper. The FS-FBMC receiver first applies an FFT of size KM on the received signal containing the FBMC symbol to demodulate, comparatively increasing its complexity. This is followed by a filtering stage in the frequency domain. Finally, the recovered pulse amplitude modulated symbols are obtained by extracting the real part of the quadrature phase rotated and down-sampled signal.

The rest of the section provides a mathematical background of the PPN-FBMC transceiver

and the FS-FBMC receiver.

2.2.4.1 Poly-Phase Network-FBMC transceiver

If M is the total number of available subcarriers and $a_n(m)$ the Pulse-Amplitude Modulated (PAM) symbol at subcarrier index m and time slot n, then the baseband signal $s(k)$ can be mathematically expressed as follows:

$$s(k) = \sum_{n=-\infty}^{+\infty} g\left(k - n\frac{M}{2}\right) x_n(k) \tag{2.12}$$

$$x_n(k) = \sum_{m=0}^{M-1} (-1)^{nm} a_n(m) \phi_n(m) e^{i2\pi \frac{km}{M}} \tag{2.13}$$

where $\phi_n(m) = i^{n+m}$ is the quadrature phase rotation term to preserve the orthogonality in the real filed, g is the impulse response of the PF, with $g(l) = 0$ when $l \notin [0, L-1]$ and $L = KM$ where K is the overlapping factor.

The receiver-side implementation involves performing dual operations with respect to the transmitter. Consequently, if r represents the received signal, then the recovered PAM symbols $\hat{a_n}(m)$ can be expressed as follows:

$$u_n(m) = \sum_{l=0}^{K-1} g(k + lM) r\left(k + \frac{M}{2}(2l + n)\right) \tag{2.14}$$

$$U_n(m) = C_n(m) \sum_{k=0}^{M-1} u_n(m) e^{i2\pi \frac{km}{M}} \tag{2.15}$$

$$\hat{a}_n(m) = \Re\left(\phi_n^*(m) U_n(m)\right) \tag{2.16}$$

where the superscript '$*$' represents the complex conjugate operation, and $C_n(m)$ is the ZF equalizer coefficient used to compensate for the impairments introduced by the channel.

2.2.4.2 *Frequency Spread* receiver

As mentioned previously, the FS-FBMC implementation is typically performed at the receiver side thanks to its advantages in terms of complexity and equalization efficiency [62, 63]. The FS-FBMC receiver implementation illustrated in Figure 2.7b can be described mathematically as follows:

$$X_n(m) = C_n(m) \sum_{k=0}^{L-1} r\left(k + n\frac{M}{2}\right) e^{-i\frac{2\pi}{L}km} \tag{2.17}$$

$$Y_n(m) = \sum_{l=-\frac{L}{2}}^{\frac{L}{2}-1} G(l) X_n(m - l) \tag{2.18}$$

$$\hat{a}_n(m) = \Re\left(Y_n(Km) \phi_n^*(m)\right) \tag{2.19}$$

where G is the frequency response of the PF. The FS-FBMC implementation may initially appear complex. However, due to the frequency localization of the PF G, it contains many zero coefficients. As a result, the PF G can be truncated to have N_G coefficients and equation (2.18) becomes:

$$Y_n(m)(k) = \sum_{l=-\Delta}^{\Delta-1} G(l) X_n(m-l) \tag{2.20}$$

where $\Delta = (N_G - 1)/2$ with N_G being an odd number.

2.3 Limitations and recent advances of FBMC/OAM systems: Short PF design and equalizers

The overlapping factor K of the PF has a significant impact on the complexity of the FBMC transceiver. The most known PFs are the long Isotropic Orthogonal Transform Algorithm [65] [66] [67], and the long Martin, Mirabassi, Bellange (MMB4) PFs. The latter has an overlapping factor of $K = 4$ times larger than an OFDM symbol and is the most adopted in the literature [68] [69] [70] [71]. The MMB4 PF is highly localized in the frequency domain since the interference is limited to only one adjacent subcarrier. Nevertheless, it is highly advantageous to have K as low as possible, specifically when $K = 1$. This enables various benefits, including the support for short frame sizes that facilitate low-latency communication and the reduction of transmitter power consumption. On the other hand, there are limitations to using short PFs, and recent research advancements have been made to overcome these drawbacks [13]. The subsequent sections will provide further discussion on these topics. For clarity, filter configurations with $K > 1$ will be referred to as long filters, while filters with a duration equal to one OFDM symbol will be referred to as short filters.

2.3.1 Relevant short PFs

We present in this section some relevant short PFs including, the Time Frequency Localization 1 (TFL1), the Quadrature Mirror Filter 1 (QMF1), and the Near Perfect Reconstruction 1 (NPR1).

2.3.1.1 TFL1

The TFL1 PF is widely recognized as one of the prominent short PF designs in the literature [72]. It offers both time and frequency localization for FBMC modulation. It has already been successfully integrated into hardware platforms [73]. The analytical expression for the TFL1 PF [74] can be expressed as follows:

$$g(k) = \frac{\pi}{2}(1-x) + \gamma_0 t + 2t\left(t^2 - 1\right)\left(\beta_1 + 4\beta_2 t^2\right) \tag{2.21}$$

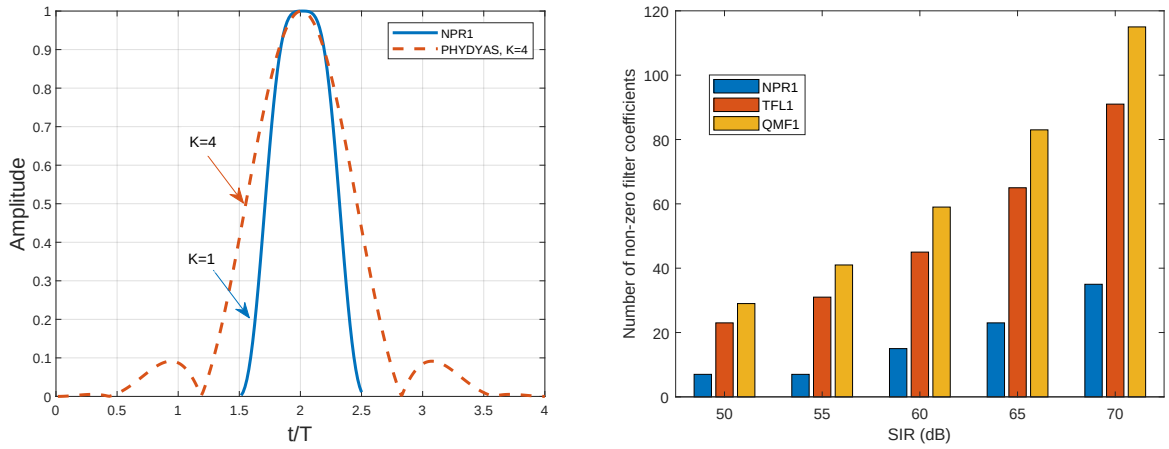

(a) (b)

Figure 2.8: Comparison of considered PFs: (a) impulse response, (b) truncation impact on near-perfect reconstruction property.

where $x = \frac{2k+1}{M}$ with $k \in [0, \frac{M}{2} - 1]$, $t = 2x - 1$ and

$$\gamma_0(k) = \frac{1}{X_0 + X_1 \frac{M}{2}}$$
$$\beta_1(k) = X_2 + \frac{1}{X_3 + X_4 \frac{M}{2}}$$
$$\beta_2(k) = X_5 + \frac{1}{X_6 + X_7 \frac{M}{2}},$$

2.3.1.2 QMF1

The QMF1 PF [75] was adapted for use in FBMC, resulting in a modified version known as Lapped-OFDM modulation [76]. Its corresponding analytical expression is:

$$g(k) = sin(\frac{\pi k}{M}) \tag{2.22}$$

2.3.1.3 NPR1

Lately, by inverting the time and frequency axes of the filter-bank impulse response of the MMB4 PF [57], the NPR1 short PF was proposed in [12] with a high time localization since the interference is limited to only adjacent FBMC symbols (see Fig. 2.8a). Its corresponding analytical expression is:

$$g(k) = \sqrt{1 - 2\sum_{l=0}^{2} P_g(l) \cos\left(\frac{2\pi k(2l+1)}{M}\right)}$$
$$P_g(0) = 0.564447 \tag{2.23}$$
$$P_g(1) = -0.066754$$
$$P_g(2) = 0.002300$$

The obtained SIR for the proposed NPR1 PF is 73 dB [12], which is of the same order of magnitude as for the MMB4 PF (70 dB) [57] corroborating the near-perfect reconstruction property of the NPR1 PF.

To improve the appeal of the short PF-based FBMC systems, the complexity of the FS receiver should be further reduced. Truncating the PF frequency response is one way to achieve this aim as discussed in Section 2.2.4.2. However, this aggravates the penalty of the non-perfect reconstruction at the receiver side, degrading performance. Therefore, a suitable compromise between complexity and performance should be targeted.

The 5G system error vector magnitude requirement for a reliable communication is 3.5% for a 256-QAM [21], which corresponds to a SIR of 30 dB. Therefore, each system block should achieve a larger SIR to adhere to the aforementioned overall system requirement. A residual SIR of 55 dB after truncation should be sufficient to avoid further degradation stemming from channel and hardware impairments. Fig. 2.8b evaluates the effect of the number of non-zero filter coefficients on the SIR for various short PFs. The NPR1 filter requires only 7 non-zero coefficients for a target SIR of 55 dB, as opposed to the 31 and 41 required coefficients by the other short PFs. Hence, the NPR1 filter offers a better compromise between complexity and performance. Furthermore, it shows improved robustness to CFOs and TOs [12]. Added to its comparatively reduced OOBPL [12], these advantages advocate for the use of the NPR1 PF.

2.3.2 Motivation for using short PF with FBMC

2.3.2.1 Efficient channel estimation

The introduction of OQAM for FBMC complicates the adoption of certain techniques supported by OFDM. We can mention here specific techniques related to CE: the use of scattered pilot patterns and the nature of the pilot values. Indeed, the transmitted pilots should be real-valued to prevent interference with the transmitted data. However, the received signal is still corrupted by imaginary-valued interference due to transmitted data on adjacent subcarriers.

To estimate the Channel Frequency Response (CFR), Successive Interference Cancellation (SIC) methods like those proposed in [77] can be used. This requires the introduction of iterative CE using FEC techniques. Hence, the resulting complexity is highly increased. Another approach, called the Interference Approximation Method (IAM), utilizes a block-type PS. IAM exploits the interference caused by adjacent data symbols and allows for power recovery, which improves estimation accuracy. However, IAM is susceptible to high PAPR and nonlinear distortions caused by HPAs. Nonetheless, IAM is applicable only in flat fading channels and may not perform well in other channel conditions.

In fact, FBMC can use complex-valued pilots. These latter should be shielded from interference. This can be done by keeping the neighboring FBMC subcarrier positions vacant or inactive at the cost of a data rate loss. However, for short PFs, where just one FBMC symbol is required as a guard interval to properly shield the pilots, the rate loss is negligible compared to long PFs. This makes short PFs more suitable than long PFs for CE techniques employing block-type PS.

2.3.2.2 Low computational complexity

Explained in Section 2.2.4.1, the PPN processing is heavily dependent upon the PF length since the applied processing involves the filtering stage. From the PPN processing, we can conclude that the windowing operation applies $2KM$ real multiplications per FBMC symbol, assuming that the impulse response of the PF is typically real-valued. Additionally, the summation operation requires $2KM$ real additions.

We recall that the overlapping factor of the PF is denoted as $K = L/M$. For long PFs, $K = 4$, while for short PFs, $K = 1$. Naturally, the computational complexity is significantly reduced for short PFs compared to long PFs. Specifically, the number of real multiplications is divided by 4. This lower computational complexity implies the potential for lower power consumption. Considering the FS implementation, an IFFT of size KM is required. Nonetheless, by utilizing a short PF, the IFFT size can be decreased to M, resulting in a significant reduction in complexity [78].

These general conclusions regarding the complexity analysis are also applicable at the receiver. However, no accurate complexity values can be put forward without considering other essential processing units such as the equalizer and without comparing the achieved performance of both short and long PFs under the relevant transmission scenario.

2.3.2.3 High energy efficiency

Multi-carrier modulations are typically susceptible to non-linear distortions due to their PAPR [79]. For instance, the distortion caused by the non-linearity of the HPA can degrade the Bit-Error Rate (BER) performance. To reduce the PAPR in OFDM systems, a precoder applying the DFT to QAM symbols can be used before their allocation to subcarriers. However, since orthogonality is restricted to the real domain for FBMC/OQAM, a different precoder is required. In this case, the Discrete Cosine Transform (DCT) can be employed. Nevertheless, other techniques are available [80, 81].

Fig. 2.9 depicts the Complementary Cumulative Distribution Function (CCDF) of OFDM and FBMC/OQAM signals with and without precoding. The choice of the PF has a negligible impact on the PAPR for FBMC/OQAM systems without precoding, as shown in the figure. However, compared to OFDM, the PAPR of the FBMC/OQAM signal is slightly increased due to the presence of a ramp-up and ramp-down at the beginning and end of the frame [82].

All precoded signals exhibit a significant reduction in PAPR compared to their non-precoded counterparts. However, the efficiency of the precoding technique in FBMC/OQAM depends on the choice of the PF. Employing a long PF results in a larger PAPR than a short one, even when the same precoder is used. This is because precoding techniques are typically applied to each FBMC symbol independently, while the FBMC symbols overlap before transmission through the channel and the number of overlapping symbols increases with the filter length. Since short PFs can achieve lower PAPR, higher power efficiency can be obtained when compared to long PFs.

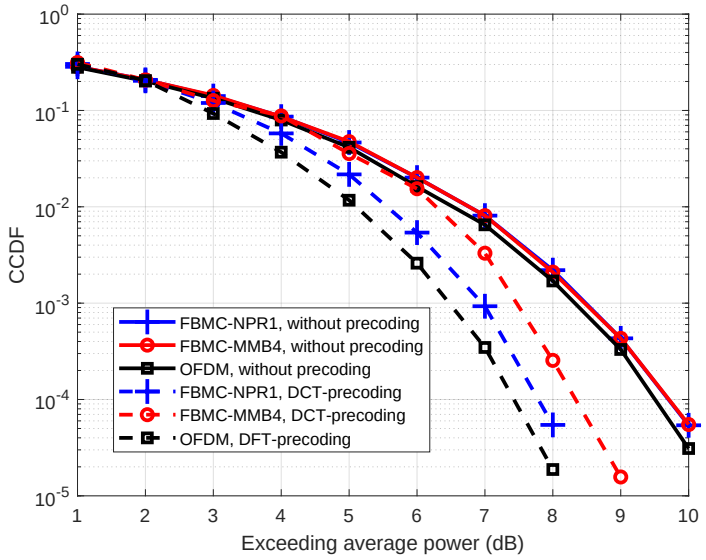

Figure 2.9: CCDF comparison between the considered receivers with and without precoding.

2.3.2.4 Support of short frame sizes for low-latency communication

One of the main challenges of using FBMC/OQAM with long PFs is the significant ramp-up and ramp-down at the beginning and end of each transmitted frame [46]. This poses a problem for FBMC/OQAM in supporting low-latency communications required in scenarios like MCC.

To address this concern, several solutions have been proposed in the literature. One simple approach is to truncate the PF impulse response for the first and last transmitted symbols [83]. This technique is easy to implement and does not incur additional complexity. However, truncating the impulse response can increase the OOBPL due to sharp transitions. To mitigate this, a windowing operation can be applied instead of hard truncation, smoothing the transition using coefficients obtained for instance from a raised-cosine function [84]. However, this technique compromises orthogonality and introduces interference, with higher interference levels as more filter coefficients are truncated.

Another technique proposed to reduce the filter transition is the transmission of virtual symbols [49]. These additional FBMC symbols are transmitted before the first and after the last symbols in a frame and do not contain any information. They are designed to suppress the ramp-up and ramp-down transitions of the PF. Subsequently, the first and last samples of the frame, which are nearly zero-valued, can be truncated or windowed. However, this technique increases complexity, requiring additional real addition and multiplication operations. Indeed, it was evaluated that at least 36% more real addition operations and 14% more real multiplication operations are required [85].

In conclusion, efficiently supporting short-frame sizes with long PFs remains an open issue. However, this is not the case for short PFs, since their duration is divided by 4 compared to long PFs with $K = 4$, resulting in reduced computational requirements in terms of real multiplication operations.

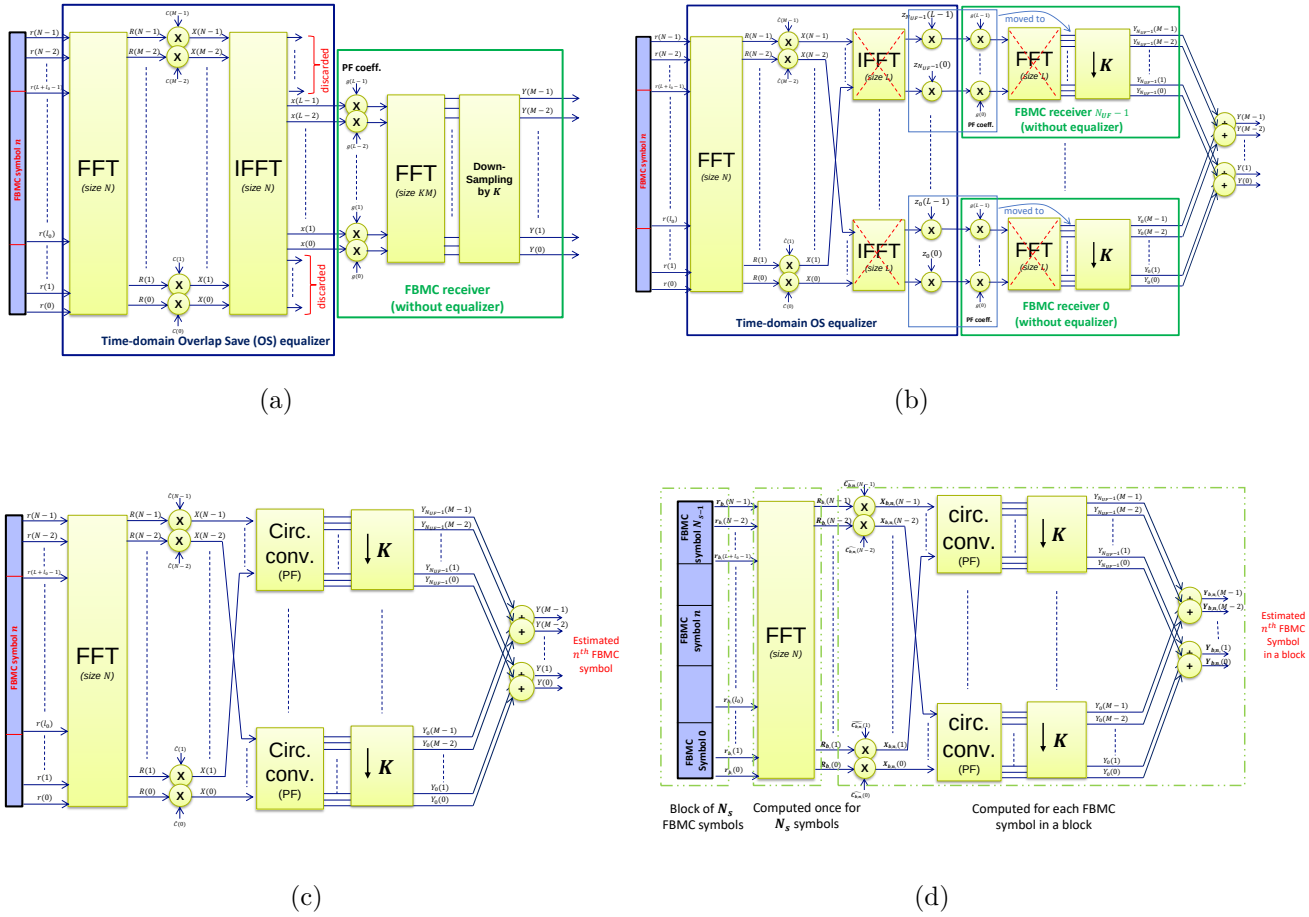

Figure 2.10: Next-generation overlap-save FBMC receiver development: (a) original FBMC receiver augmented with the time-domain equalizer [87], (b) Intermediate stage of the FBMC-OS receiver development (c) FBMC-OS receiver, (d) FBMC-OSB receiver.

2.3.2.5 Limitations of short PFs

Despite the aforementioned advantages, several open issues still need to be addressed. The first resides in lower robustness to TOs since, for long PFs, the signal information is replicated and transmitted during a longer period of time. The second is lower robustness to long delay spread channels [86]. In fact, system performance is highly dependent upon the ratio between the channel delay spread and the PF length [12]. Hence, long PFs offer improved robustness in this regard. However, these problems were tackled through advanced receiver techniques as shown in the next section.

2.3.3 Relevant FBMC receivers

Two main advantages motivate the introduction of advanced receiver techniques: improved robustness to long delay spread channels and TOs up to the support of asynchronous communications.

2.3.3.1 Time domain equalizer

Improved robustness is achieved by the introduction of a time-domain equalizer prior to the original FBMC receiver [87] as shown in Fig. 2.10a. Although system performance is improved compared to a conventional FS-FBMC receiver, the resulting complexity is prohibitive for practical applications due to the required computation of several FFT blocks. Nevertheless, when coupled with a short PF and a FS implementation, it is possible to significantly reduce its complexity [13]. The OS algorithm can be used to decompose and simplify the time-domain equalizer, efficiently performing fast convolution. This leads to the Overlap-Save FBMC receiver design, explained next.

2.3.3.2 Overlap-Save FBMC receivers

First, the IFFT of size N is decomposed by its decimation in time to obtain several IFFTs of size $L = KM$ followed by a radix-2 stage as shown in Fig. 2.10b. The number of IFFTs is equal to $N_{UF} = N/L$. Next, the summation of the selected radix-2 stage is moved after the FBMC receiver to obtain N_{UF} FBMC receivers before the final summation stage. In fact, the LPR terms of the radix-2 stage can be seen as a frequency shift and can be incorporated into the PF coefficients. Thus, both are shifted to the frequency domain after the FFT. As a result, the multiplications before FFT become circular convolutions. Hence, all IFFTs and FFTs of size L can be simplified as marked by the red-dotted lines. Fig. 2.10c shows the final structure of the FBMC-OS receiver for SISO transmissions, where the equalizer is directly integrated into the FBMC receiver, largely reducing complexity.

Despite this major step forward, the complexity of the proposed OS receiver is still dominated by the FFT size N. The latter depends on the up-sampling factor N_{UF} which provides a compromise between system performance and complexity. Indeed, the factor N_{UF} represents the number of FBMC symbols considered for processing only one FBMC symbol. As a means to achieve several trade-off levels between performance and complexity, it was proposed to flexibly modify the number of FBMC symbols N_s to be processed simultaneously by the receiver as shown in Fig. 2.10d. The newly introduced parameter N_s is related to the up-sampling factor N_{UF} as follows

$$N_{UF} = \frac{N_s + 1}{2}.$$

Indeed, an FFT of size $N = N_{UF}M$ is computed only once per block regardless of the value of N_s, which significantly reduces complexity. The rest, however, is computed for each FBMC symbol as depicted in Fig. 2.10d. This receiver type is denoted by Overlap-Save Block (OSB).

One of the most interesting results is that the FBMC-OS receiver can support asynchronous communications when short PFs are employed, while the OSB-FBMC receiver supports relaxed synchronization [13]. When facing multipath channel conditions with long delay spreads, it is shown that both FBMC-OS and FBMC-OSB receivers achieve similar BER performance compared to the FS-FBMC receiver with the MMB4 long PF while outperforming OFDM [13]. Considering the additional advantages brought by the proposed contributions in [13], the limi-

tations of FBMC with short PFs cited in section 2.3.2.5 were overcome.

2.4 Open issues

While considerable improvements were achieved by the aforementioned contributions, several research challenges and study item opportunities are still to be tackled when targeting 6G applications.

2.4.1 Increasing the spectral efficiency

The radio spectrum resource is of fundamental importance for wireless communications, especially since it is becoming scarce [88] [21]. In fact, future wireless networks are expected to face worsening congestion levels than nowadays [89]. Therefore, enhancing SE becomes crucial for the development of beyond 5G wireless communication systems. Multi-carrier systems, such as OFDM and FBMC/OQAM, divide the available frequency spectrum into multiple subcarriers to transmit data simultaneously. However, the efficient allocation of these subcarriers is essential to maximize the utilization of the limited spectrum resources. Improving SE in multi-carrier systems enables higher data rates, improved system capacity, and increased network throughput. This is particularly significant in modern wireless communication scenarios with the ever-increasing demand for high-speed data transmission. Furthermore, enhancing SE facilitates better coexistence and interference mitigation in MU environments, enabling multiple users to share the same frequency band while maintaining high-quality communication. Consequently, continuous research and development efforts focus on advancing modulation schemes and intelligent interference management techniques to enhance the SE of multi-carrier systems. These efforts aim to meet the growing demands of today's data-intensive applications.

2.4.2 Massive MIMO support

The 6G cellular network is expected to offer higher spectral and energy efficiencies with reduced latency, hence achieving an improved Quality of Service (QoS) compared to the 5G [90]. Fully exploiting mMIMO systems where the BS is equipped with a large number of antennas and serves several users simultaneously represents one of the promising solutions to address part of these requirements [14, 15]. Indeed, mMIMO is already considered as one of the main technologies for 5G networks since MU interference can be rendered relatively negligible by increasing the number of BS antennas [91].

In contrast to OFDM, the OQAM-based FBMC adopts real symbols since the orthogonality holds in the real field only [92]. The resulting intrinsic interference renders the association of FBMC with mMIMO systems challenging [93]. Hence, it is not always possible to extend the existing analysis of OFDM-based mMIMO systems to that of the mMIMO-FBMC systems. Thus the performance of FBMC-based mMIMO systems calls for a meticulous evaluation considering the chosen system parameters. Indeed, the prior art on FBMC-based mMIMO being still in its early stages, these systems require careful examination and investigation before drawing

definitive conclusions.

2.4.3 Improving the accuracy of channel estimation

To concretely achieve the promising advantages of mMIMO, accurate CE is necessary. Additionally, satisfying the constraints of future wireless networks in terms of reliability and latency calls for the use of precise CE techniques with minimal training overhead, particularly in MU situations. A salient drawback of FBMC/OQAM signals is that only real-field orthogonality can be kept, leading to the intrinsic imaginary interference being a barrier for high-performance CE. This advocates for devising specific sophisticated CE techniques devised for FBMC.

Existing CE methods proposed for FBMC primarily rely on the IAM introduced in [94], which assumes a flat gain approximation for the channel response over each subcarrier band. IAM is a frequency domain technique and requires the maximum channel delay spread to be significantly smaller than the symbol interval. Consequently, IAM produces inaccurate channel estimates when this condition is not met. To address this issue, time domain CE techniques were proposed in [95] [96]. In [95] and [97], authors propose time domain CE techniques that employ guard symbols to separate pilots from different users. However, this approach leads to a SE loss, which is undesirable when the number of users increases. An alternative time domain CE method for FBMC, as well as its extension to mMIMO channels, was proposed in [98] and further investigated in [96]. This method involves transmitting pilots for each user on all the subcarriers, with the users' pilots multiplexed in the code domain to enable sharing of the same time-frequency resources for CE. However, this solution requires a significant computational load at the receiver to demultiplex channel responses from different users based on their code sequences. Unfortunately, these prior solutions are either limited to frequency flat channels at the subcarrier level, require high complexity, or suffer from poor SE, especially in multi-user scenarios. In this regard, alternative PSs and CE approaches must be explored to address the aforementioned drawbacks.

2.5 Summary

This chapter represents an introduction to the scientific background related to the contributions presented in subsequent chapters of the PhD work. Initially, we discussed the principles of OFDM, which is commonly used in the conventional eMBB service of 5G. Subsequently, we delved into the specific new requirements anticipated in 6G scenarios, namely eMMC, MCC, and V2X communications. We highlighted the limitations of OFDM modulation in meeting these requirements. For eMMC, where the uplink is dominant, relaxation of the synchronization procedure is necessary to reduce signaling overhead. However, OFDM cannot accommodate such relaxed synchronization if the resulting TOs exceed the CP duration. In MCC, the use of mixed numerology can help reduce communication latency, but OFDM faces limitations due to its low spectral confinement, necessitating a large number of subcarriers as GBs to mitigate interference. In V2X, high mobility is a critical requirement, including vehicle speeds beyond

what OFDM in 5G can support. In this context, OFDM introduces significant ICI, compromising orthogonality between users. Consequently, alternative modulation techniques are required to efficiently overcome the specific limitations posed by these scenarios.

This was followed by a technical description of the FBMC/OQAM waveform in addition to a brief survey of other promising waveform candidates for beyond 5G. The chapter concluded with a detailed analysis aimed at highlighting the benefits of using short PFs for the FBMC/OQAM waveform including, support for low-latency communications, low computational complexity, high energy efficiency, and efficient block-based CE. However, the limitations associated with the use of short PFs were also summarized. Despite these limitations, recent advancements pertaining to the FBMC/OQAM waveform were discussed along with open issues. The subsequent chapters propose original contributions to overcome the remaining open issues.

Chapter 3

Novel transmission technique for multi-carrier waveforms

A crucial element of cellular communication networks is the achievable SE. Indeed, motivated by the continuous growth in mobile data traffic in wireless networks, improving SE has represented one of the key goals of the 3GPP along several generations of communication standards. In this context, a novel transmission scheme denoted as MCO is proposed in this chapter. The proposed scheme is based on intentionally overlapping the subcarriers of adjacent users considering two state-of-the-art waveforms: the OFDM and the FBMC/OQAM. We investigate the achievable SE improvement of the proposed transmission scheme in the presence and absence of TO impairments under the 5G QuaDRiGa channel.

The chapter starts by introducing the existing techniques for SE enhancement in the literature. Next, the novel transmission scheme is proposed. Finally, several performance metrics are evaluated and compared to illustrate the benefits of the proposed contribution.

3.1 Relevant SE enhancement techniques

In the literature, techniques known as "Partially Overlapping" (PO) have been introduced taking into account both the waveform and the network. A systematic model for PO is presented in [99], which demonstrates that the use of overlapped channels can improve spectrum utilization. In [100], the potential benefits of PO are studied, showing that it can lead to greater flexibility in resource allocation and result in up to a 100% increase in overall network capacity compared to conventional design. Additionally, [101] proposes channel allocation and link scheduling algorithms for partially overlapped channels at the MAC layer.

Besides of these approaches, the Nyquist pulse-shaping criterion emphasizes the orthogonality of signals to avoid ISI. However, applying this criterion sets major constraints since it requires a minimum distance to be respected between neighboring symbols in time and frequency, which reduces SE. To enhance SE while maintaining the orthogonality condition, one method is to increase the constellation order. However, high-order constellations are more susceptible to nonlinear effects. At this point, one can raise an important question: *For a given data rate, is it possible to reduce the minimum distance between neighboring symbols in time and frequency below the limits specified by the Nyquist criterion to increase the capacity?* In fact, loosening the orthogonality condition is a different technique to increase the SE of low-order modulations. These relevant existing methods for improving SE can be classified into two categories: non-overlapping and overlapping enhancement techniques. The rest of the section provides a background on these techniques.

3.1.1 Non-overlapping techniques

One of the well-known SE enhancement techniques that loosen the orthogonality condition is the Faster-Than-Nyquist (FTN) signaling approach [102, 103]. It reduces the spacing between two adjacent pulses in the time domain considerably below the Nyquist rate. Therefore, controlled ISI is introduced.

3.1.1.1 Faster than Nyquist signaling approach

The conventional technique of using Nyquist pulses to transmit data through a channel with a BW of $W = (1/2T)$ Hz is well-established and eliminates ISI. The received pulse train can be therefore expressed as follows:

$$u(t) = \sqrt{E} \sum_{n=N_1}^{N_2} a_n g(t - nT) \tag{3.1}$$

where n is the time index, a_n is the transmitted data on the n^{th} index, E is the energy of the data sequence, T is the symbol duration, along with the Nyquist pulse g given by

$$g(t) = \frac{\sin(\pi t/T)}{(\pi t/T)} \tag{3.2}$$

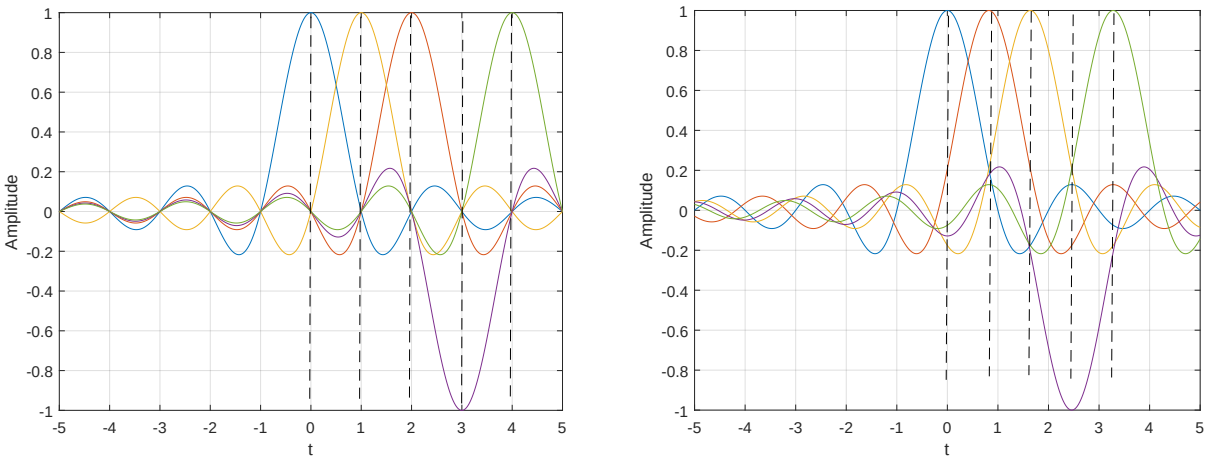

(a) Nyquist transmission (b) FTN transmission

Figure 3.1: Illustration of Nyquist and FTN transmission, with T = 1: (a) $\epsilon = 1$, (b) $\epsilon = 0.82$.

When dealing with AWGN with a two-sided spectral density of $N_0/2$, the optimal detector will have a Probability of Error (Pe) given as follows:

$$P_{\mathrm{e}} = Q\left(\frac{2\sqrt{E}}{\sqrt{2N_0}}\right) \tag{3.3}$$

along with

$$Q(x) = \frac{1}{\sqrt{2\pi}}\int_x^{\infty} e^{-v^2/2}dy = \frac{1}{2}\,\mathrm{erfc}\,\frac{x}{\sqrt{2}} \tag{3.4}$$

where erfc denotes the complementary error function.

Assume that (3.1) is transmitted and the achieved performance from (3.3) surpasses the target error rate of the system. One possibility to increase the SE would be to trade this improvement in error rate for SE. For instance, a Pe of 10^{-6} or 10^{-7} can be potentially achieved when a Pe of 10^{-5} would be sufficient. Therefore, is it possible to trade some of the extra achieved performance through transmitting the signal (which may have a lower error rate than necessary) for an increased data rate? To do this, FTN considers replacing the value of T with a smaller value $T' < T$ in equation (3.1), while keeping the transmitted power the same. Therefore, the FTN signalling which was proposed initially in [104] can be expressed as follows:

$$u(t) = \sqrt{E\epsilon}\sum_{n=-\infty}^{\infty} a_n g(t - n\epsilon T), \quad \text{with } 0 < \epsilon < 1 \tag{3.5}$$

where ϵ is the squeezing factor and $T' = \epsilon T$.

The difference between Nyquist ($\epsilon = 1$) and FTN transmission ($\epsilon = 0.82$) using sinc pulses with transmitted data {1,1,1,-1,1} is illustrated in Figure 3.1. ISI is not observed when ϵ is equal to 1. However, if we decrease ϵ to 0.82, we can observe the presence of ISI as depicted in Figure 3.1b. Since the symbol duration for FTN signaling is only $0.82T$, the data rate will be

approximately 1.22 times that of the Nyquist rate. This results in a 22% increase in data rate.

In fact, the introduced ISI in FTN systems must be effectively addressed to obtain such promising results and ensure good error performance. As a result, considerable effort has been devoted to developing advanced equalization and detection algorithms for the receiver side. For instance, a new M-algorithm has been proposed in [105], which uses low-complexity turbo equalization to handle severe ISI caused by coded FTN signaling. The resulting FTN turbo equalizer can provide up to 4 dB energy savings and 35% BW reduction compared to binary orthogonal signaling. However, it may not be applicable in all scenarios due to its limited performance under severe channel conditions.

A new method called l_∞-minimization has been proposed in [106] for recovering uncoded binary symbols in FTN signaling with a better trade-off between signal recovery accuracy and computational complexity than successive interference cancellation in [107]. However, it may not be practical for systems with higher-order modulation due to its high computational complexity. In [108], a multi-band architecture called block-SEFDM and an FFT-based soft detector have been analyzed for uncoded systems. However, it may also require complex hardware implementation, limiting their applicability in practical systems. The authors in [109] proposed a transmission technique that combines precoded FTN and OFDM with OQAM. Their approach, called sparse interference pre-cancellation, focuses on reducing interference caused by FTN signaling at the transmitter. To enhance receiver performance, they suggested additional improvements to the channel encoder, including modifications to the bit-to-symbol mapping and the mapping of symbols to time-frequency positions. Single-Carrier with Frequency-Domain Equalization (SC-FDE) using FTN signaling has been proposed for higher spectrum efficiency in [110]. However, its performance can be severely affected by deep fading and poor channel conditions, requiring additional techniques such as Diversity Combining (DC) Hybrid Automatic Repeat-Request (HARQ) [111]. Overall, while these techniques have shown promising results, their limitations and drawbacks need to be carefully considered before their implementation in practical FTN systems. Indeed, Nyquist's first criterion has been widely applied in traditional communication systems motivated by the limitations of hardware implementations caused by the complexity of the ISI cancellation algorithms.

3.1.2 Methods based on overlapping

In addition to the aforementioned approach, SE enhancement based on overlapping techniques has been studied in the literature. Relevant studies related to this approach include those in [112] and [113] which will be discussed next.

3.1.2.1 High compaction multi-carrier modulation

The authors in [113] proposed a multi-carrier transmission scheme called High Compaction Multi-Carrier Modulation (HC-MCM) to improve the SE of the OFDM waveform. HC-MCM is primarily characterized by modulation indices of $\Delta FT < 1$. It can easily attain a high transmission rate by arbitrarily overlapping the spectra of its subcarriers with a technique that involves

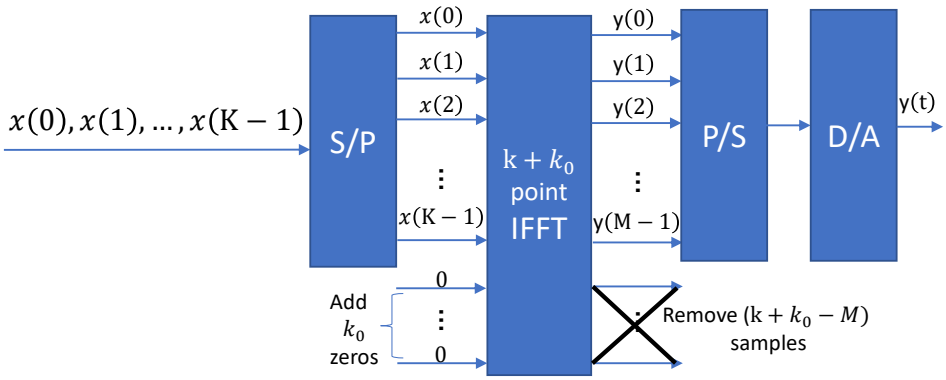

Figure 3.2: DFT-based HC-MCM transmitter.

truncating the transmitting signal with a rectangular window in the time domain. This is illustrated in Figure 3.2. To avoid frequency domain aliasing caused by the IFFT and interpolate samples in the time domain, K_0 zeros are padded to the subcarrier messages $x(k)$ at the input of the IFFT, and $(K+K_0-M)$ samples are removed from the IFFT output. When all IFFT samples are transmitted, the transmitter output $y(t)$ matches the OFDM waveform. In the HC-MCM, only a portion of the IFFT output samples (M out of $K+K_0$) are transmitted by truncating them with a rectangular window function in the time domain. As a result, the bandwidth of each subcarrier becomes larger than in the OFDM system, allowing the signal waveform corresponding to the spectrum illustrated in Figure 3.3 to be generated.

Figure 3.3b illustrates the spectrum of HC-MCM for a modulation index of $\Delta F \times T = 1/4$. The transmission rate for this case is the same as that of OFDM illustrated in Figure 3.3a because the bandwidth of each subcarrier is identical to that of OFDM, but the frequency spacing is smaller ($\Delta F = 1/4T$) than that of the OFDM. As a result, HC-MCM can achieve the same transmission rate as OFDM with a narrower bandwidth. Figure 3.3c shows another type of HC-MCM spectrum with the same modulation index as Figure 3.3b. In this case, the frequency spacing is the same as that in OFDM. However, the transmission rate can be increased by a factor of 4 compared to OFDM because each subcarrier has a larger bandwidth.

However, similarly to OFDM, the proposed multicarrier transmission scheme still suffers from a high OOBPL, hence requiring GBs that waste spectrum resources. Moreover, it reveals to be vulnerable to TO impairments which is expected to hinder its ability of managing/cancelling the overlapping-induced interference. Furthermore, the work in [113] was limited to the study of such a system under an AWGN channel, neglecting the effect of multipath.

3.1.2.2 Intentional-overlapping based on user-specific filters

As an alternative, the authors in [112] proposed a multicarrier transmission technique that incorporates partial overlap between adjacent symbols in both the time and frequency domains to take advantage of MU diversity and achieve higher SE. In fact, in MU scenarios, different users may have channels with varying degrees of dispersion in time and frequency. To ensure that all

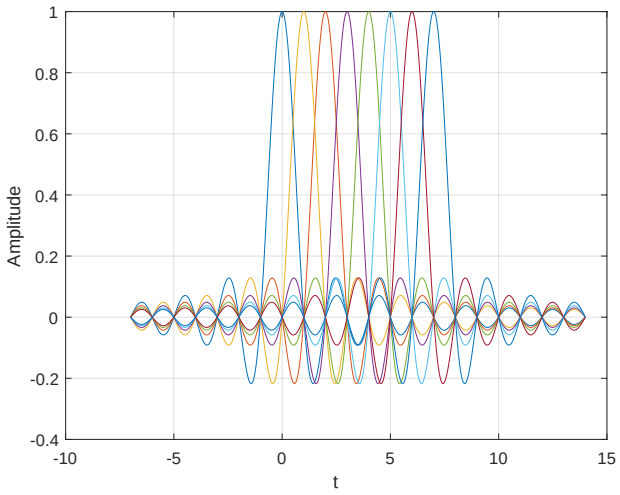

(a)

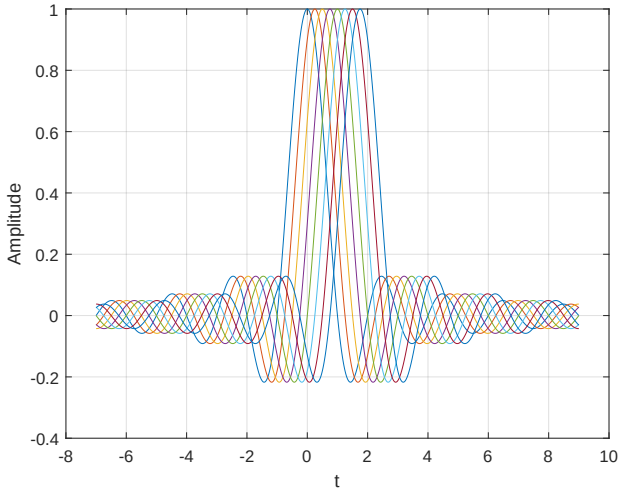

(b)

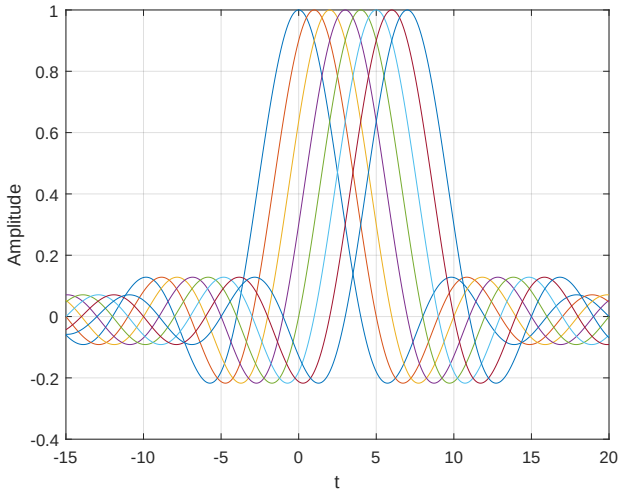

(c)

Figure 3.3: Illustration of signal spectra of OFDM and HC-MCMs: (a) OFDM ($\Delta F \times T = 1$); (b) HC-MCM, smaller ΔF compared to OFDM ($\Delta F \times T = 1/4$) and (c) HC-MCM, same ΔF as OFDM ($\Delta F \times T = 1/4$).

users have a desired SIR, conventional systems consider the user with the worst-case channel and design the entire system accordingly. However, this results in an over-designed system that unnecessarily protects users with low-dispersion channels. To address this issue, user-based precautions that involve pulse shape filtering are proposed. Therefore, rather than a fixed PF, the authors propose to employ user-specific filters to provide more flexibility in overlapping, which reduces the BW needed to achieve the same data rate. The Filtered Multitone Modulation (FMT) is employed with the Root-Raised-Cosine (RRC) filter. The parameter that makes the RRC filter specific to the user is its roll-off factor α which also determines its corresponding time–frequency characteristic.

The mathematical representation of the transmitted signal at the baseband, incorporating N subcarriers, can be expressed as follows:

$$x(t) = \sum_{m=-\infty}^{\infty} \sum_{k=0}^{N-1} X_{mk} g_{mk}(t) \tag{3.6}$$

where $p_{mk}(t)$ is the synthesis filter and X_{mk} is the complex symbol at the time index m and the frequency index k, along with

$$g_{mk}(t) = p_{mk}\left(t - m_{\tau_0}\right) e^{j2\pi k \nu_0 \tau_0} \tag{3.7}$$

Assuming linear time-varying wireless channel, the received signal is expressed as

$$y_i(t) = \int_{\tau} \int_{\nu} H_i(\tau, \nu) x(t-\tau) e^{j2\pi\nu t} \, \mathrm{d}\nu \mathrm{d}\tau \tag{3.8}$$

where $H_i(\tau, \nu)$ is the Fourier transform of the CIR of i^{th} user. The received symbol X_{nl} located at frequency bin l and time index n can be obtained by projecting the received signal on the analysis function $g'_{nl}(t)$ as follows:

$$\begin{aligned} \langle y_i(t), \dot{g}_{nl}(t) \rangle &\triangleq \int_t y_i(t) \dot{g}^*_{nl}(t) \mathrm{d}t \\ &= X_{nl} H_{nlnl} + \sum_{(m,k)\neq(n,l)} X_{mk} H_{nlmk} \end{aligned} \tag{3.9}$$

where

$$H_{nlmk} = \int_{\tau} \int_{\nu} H_i(\tau, \nu) \int_t g_{mk}(t-\tau) g^*_{nl}(t) e^{j2\pi\nu t} \, \mathrm{d}t \, \mathrm{d}\nu \mathrm{d}\tau \tag{3.10}$$

which captures the interference from the symbol (m, k) to the desired symbol (n, l).

The SIR can be expressed as $\gamma_i = \sigma^2_{\mathrm{S},i} / \sigma^2_{\mathrm{I},i}$, where

$$\sigma^2_{\mathrm{S},i} = \int_{\tau} \int_{\nu} S_i(\tau, \nu) |A(\tau, \nu)|^2 \, \mathrm{d}\nu \mathrm{d}\tau \tag{3.11}$$

and

$$\sigma^2_{\mathrm{I},i} = \sum_{(m,k)\neq(0,0)} \int_{\tau} \int_{\nu} S_i(\tau, \nu) \left|A\left(m\tau_0 + \tau, k\nu_0 + \nu\right)\right|^2 \, \mathrm{d}\nu \mathrm{d}\tau \tag{3.12}$$

along with

$$A(\phi,\psi) \triangleq e^{-j2\pi\rho} \int_{-\infty}^{\infty} p_{m,k}(t-\phi)p_{rx}^{*}(t)e^{j2\pi\psi t}\ \mathrm{d}t \tag{3.13}$$

with $\rho = k\nu_0\tau$ [114].
Note that the SIR is a function of not only ν_0,τ_0, and $H_i(\tau,\nu)$ but also Λ, where $\Lambda = [\alpha_1,\alpha_2,\ldots,\alpha_M]^T$ and $\Gamma = [\gamma_1,\gamma_2,\ldots,\gamma_M]^T$ being the vectors for the users-specific roll-off factors and corresponding SIRs. Hence, the authors maximize the SIR of the user in the worst case by finding optimum roll-off factors for a given time interval and frequency spacing. This translates mathematically as follows:

$$\Lambda = \arg\max\{\min(\Gamma)\} \tag{3.14}$$

The authors, however, simply considered an exponentially decaying channel in their simulations. Therefore, the results may differ over more realistic channels. Moreover, the FMT modulation is less BW efficient than other filtered multicarrier waveforms due to the roll-off factor of the pulse-shaping filter. For all these reasons, considering other filtered multicarrier waveforms to address these drawbacks reveals to be interesting in order to achieve the highest SE gain.

3.2 The proposed MCO transmission technique

3.2.1 Description of the proposed overlapping scheme

We consider a scenario where U users transmit data on different adjacent frequency bands (or sub-bands). We propose to partially overlap adjacent sub-bands by fully overlapping a portion of the corresponding subcarriers. This results in two possible types of overlap: two-sided (2S) or one-sided (1S) overlap as shown in Figures 3.4a and 3.4b respectively. Therefore, if OL denotes the number of overlapped subcarriers per user, and SB the number of subcarriers allocated for each user, then the SE gain $\boldsymbol{G_{SE}}$ thanks to the overlap is

$$\boldsymbol{G_{SE_{OL}}} = \frac{OL}{SB}, \quad OL \in [\![0,...,SB]\!] \tag{3.15}$$

It is crucial to select the appropriate scheme that results in a lower level of interference in order to improve system performance. The overlap between adjacent data symbols located at frequency bin p and time q can be used to calculate the induced interference $J_n(m)$ for the data symbol at symbol n and frequency bin m. In fact, by taking the weighted sum of the neighboring overlapped data symbols, denoted as $d_{n+q}(m+p)$ with the weights given by the ambiguity function of the PF, denoted as $A_g(\tau,\mu)$, we can compute

$$J_n(m) = \sum_{(p,q)\in\Omega^*} d_{n+q}(m+p)A_g(-\frac{qM}{2},\frac{p}{M}) \tag{3.16}$$

along with

$$A_g(\tau,\mu) = \int_{-\infty}^{+\infty} g_t(t+\tau/2)g_r^{*}(t-\tau/2)e^{i2\pi\mu t}dt \tag{3.17}$$

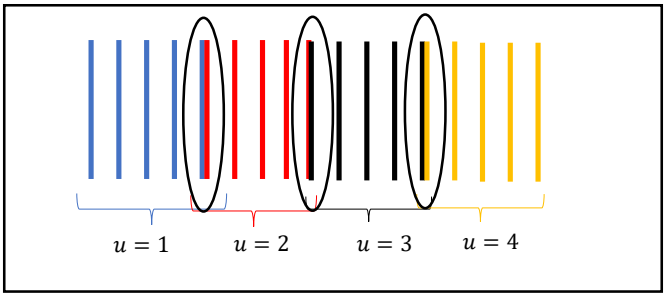

(a) Two-sided (2S) overlapping

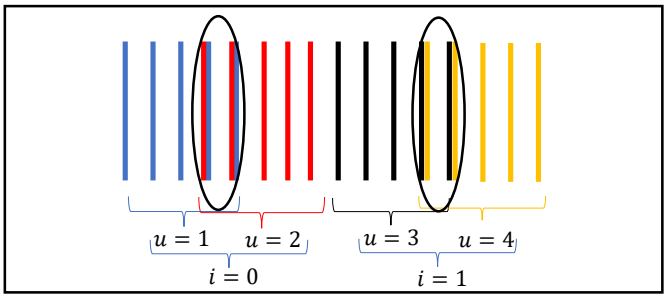

(b) One-sided (1S) overlapping

Figure 3.4: Illustration of the proposed overlapping transmission schemes with $OL = 2$.

where g_t and g_r are the transmit and receive PFs respectively, $\Omega = [\![-\infty, +\infty]\!][\![-\frac{M}{2}, \frac{M}{2}]\!]$, and $\Omega^* = \Omega \backslash (0,0)$.

Note that,

$$d_n(m) = \begin{cases} 1, & m \in \Omega_c \\ 0, & \text{otherwise} \end{cases}$$

where Ω_c is Ω_1 for the 1S scheme (Figure 3.4b) and Ω_2 for the 2S scheme (Figure 3.4a), with

$$\Omega_1 = [\![0, ..., OL - 1]\!]$$

$$\Omega_2 = [\![0, ..., \tfrac{OL}{2} - 1]\!] \cup [\![M - \tfrac{OL}{2}, ..., M - 1]\!]$$

Therefore, the interference power σ^2 induced from overlapping by OL subcarriers can be computed as follows:

$$\begin{aligned} \sigma^2 &= E[J_n(m)^2] \\ &= \sum_{(p,q)\in\Omega^*} A_g(-\frac{qM}{2}, \frac{p}{M})^2 \end{aligned} \tag{3.18}$$

where $m - p \in \Omega_c$

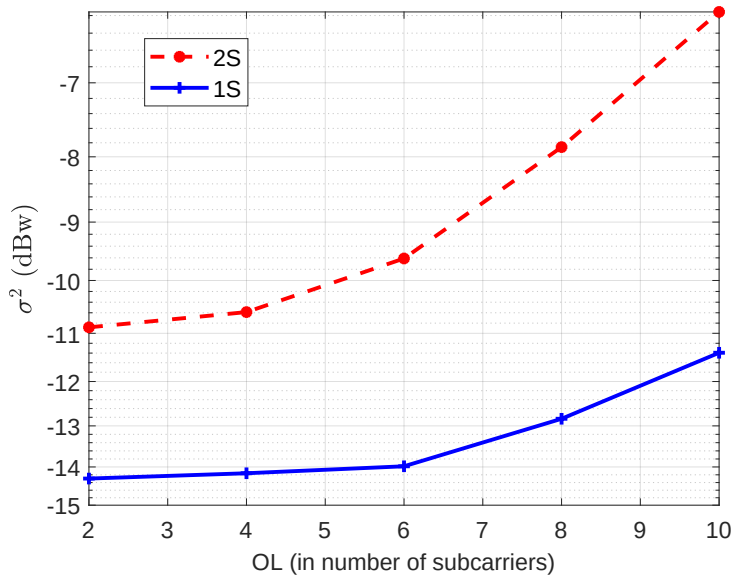

Figure 3.5: Interference power comparison of the proposed one-sided and double-sided transmission schemes with CR = 1.

Hence, using (3.18) and by employing the NPR1 short PF [12], we compare in Figure 3.5 the interference power versus OL of the two proposed overlapping transmission schemes with CR = 1. Since the NPR1 PF is highly localized in time, the interference is limited to only adjacent FBMC symbols. Therefore, $\Omega = [\![-1, 1]\!][\![-\frac{M}{2}, \frac{M}{2}]\!]$. Both schemes display an increase in interference level with OL, while the 2S overlapping suffers from a higher level of interference than the 1S. Consequently, we chose the 1S scheme for the rest of the study. In this case, the set of overlapped users is indexed by i. Therefore, the FBMC/OQAM transmit signal $s(k)$ in (4.2) will be modified as follows:

$$\boldsymbol{s}(k) = \sum_{u=1}^{U} \sum_{n=-\infty}^{\infty} \sum_{m \in \mathcal{F}_u} a_n(m - f_u) g_{m,n}(k) \tag{3.19}$$

along with

$$\mathcal{F}_u = \{f_u, ..., f_u + SB - 1\}$$

$$f_{u+1} - f_u = \begin{cases} 1 + SB + OL, & \text{if } i_{u+1} - i_u = 0 \\ SB, & \text{otherwise} \end{cases}$$

where f_u is the u^{th} user starting subcarrier index, and i_u is the solution set index of the u^{th} user.

Similarly, the OFDM transmit signal $\boldsymbol{s}(k)$ considering the proposed overlapping transmission scheme can be expressed mathematically as shown below

$$\boldsymbol{s}(k) = \sum_{u=1}^{U} \sum_{n=-\infty}^{\infty} \sum_{m \in \mathcal{F}_u} a_n(m - f_u) e^{j2\pi \frac{(k - L_{CP})m}{M}} \tag{3.20}$$

where $a_n(m)$ are the complex user's transmitted symbols on the m^{th} subcarrier within the n^{th} OFDM symbol, and L_{CP} is the cyclic prefix length.

3.2.2 Proposed MCO procedure for SE enhancement

OFDM is vulnerable to Adjacent Channel Interference (ACI) due to its low frequency localization, necessitating the introduction of guard bands. The added guard bands reduce the data rate and, therefore, the SE. Thanks to the introduced filtering stage, FBMC/OQAM is more robust against ACI. Therefore, overlapping-induced interference management can be more efficient with the FBMC/OQAM waveform by exploiting its inherent advantage. The introduction of channel coding can help combat interference. In what follows, we propose a step-by-step MCO procedure for SE enhancement.

1. *Selection of best tuple*

   If CR_{OL} is the coding rate relevant to OL, and K the modulation order, the tuple (CR^*, K^*, OL^*) should be chosen such that the ratio of the energy per bit to the spectral noise density $\frac{Eb}{N0}$ is minimized for a target SE α as

   $$(CR^*_{OL}, K^*, OL^*) = \underset{SE=\alpha}{\operatorname{argmin}}(\frac{Eb}{N0}(CR_{OL}, K, OL)). \tag{3.21}$$

2. *Coding rate optimization*

   The CR^*_{OL} of the selected combination is optimized to maximize the SE for a target BER $= \beta$ at $\frac{Eb}{N0} = \gamma$. Target β and γ values are issued from the non-overlapping case ($OL = 0$). This translates mathematically as follows:

   $$CR^{'}_{OL} = \underset{BER=\beta, \frac{Eb}{N0}=\gamma}{\operatorname{argmax}} (SE(CR_0, K, 0)). \tag{3.22}$$

3. *Spectral efficiency gain*

   Eventually, the SE gain corresponding to the selected combination can be computed as follows:

   $$\boldsymbol{G_{SE_{OL}}} = \frac{CR^{'}_{OL} - CR^*_{OL}}{CR^*_{OL}}. \tag{3.23}$$

3.3 Application example

We first describe our simulation setup. Then, the performance of the FBMC-OS receiver using the NPR1 short PF is compared to OFDM considering the proposed MCO transmission scheme. In our simulations, the CSI is assumed to be perfectly estimated at the receiver side. Furthermore, the number of non-truncated filter coefficients is set to $N_G = 7$ for a SIR of 55 dB [12]. The total number of users is $U = 4$ where the transmit powers of all transmissions are equal and normalized to 0 dBW. For the FBMC-OS receiver, N_{UF} is set to 4 leading to the FBMC-OS$_4$

Parameters	**Value**
Carrier frequency	3.5 GHz
Cyclic prefix	36
Channel model	TDL-B
Channel type	NLOS
Total number of subcarriers	512 subcarriers
Sub-band size per user	128 subcarriers
Number of UE	4
BS height	25 m
Interleaver type	Short-random
Modulation schemes	16QAM, 64QAM

Table 3.1: SISO simulation parameters

receiver notation. This choice represents a good compromise between system performance and complexity.

At the receiver, one reference set of overlapped users was processed to simplify the performance analysis and to reduce the simulation time. In Figures 3.4a and 3.4b, the set centered on user $u = 2$ or $u = 3$ can be considered a reference.

3.3.1 Simulation setup

The Tapped Delay Line B (TDL-B) multipath 3GPP channel model is used for our simulations considering a delay spread τ of 1μs. Chosen parameters follow the 5G standard [21]. The 5G New Radio Low-Density Parity Check Code (LDPC) is used in our simulations [115] with base graph 1. A short-random interleaver is considered rather than a long one since the interference pattern is well-defined, allowing for lower latency. Simulation parameters are summarized in Table 3.1.

3.3.2 Selection of the best tuple

We consider now (3.21) for selecting the best tuple of (CR^*, K^*, OL^*) leading to the highest SE gain. We plot in Figure 3.6 the required $\frac{Eb}{N0}$ versus OL for different tuples achieving the same SE with the FBMC-OS$_4$ and OFDM receivers and a target BER of 10^{-4}.

To achieve a target SE gain, we consider $K = 4, 16$, and 64. For $K = 4$, the target SE is not achievable by any tuple, since the CR cannot exceed 1. On the other hand, the target BER is not achievable by any tuple when $K = 64$, and therefore its corresponding curve is not shown in the figure. Therefore, we provide an in-depth analysis for $K = 16$. Regarding the FBMC-OS$_4$ receiver, $\frac{Eb}{N0}$ initially increases with OL. After $OL = 4$, it decreases until reaching a minimum value of 15.8 dB at $OL = 24$ and $CR = 1/2$. The performance starts to degrade after $OL = 24$, showing that the maximum value of OL for exhibiting the best performance is 24 subcarriers. Similar interpretation can be made when considering the OFDM receiver, where $\frac{Eb}{N0}$ starts increasing with OL until $OL = 16$, and then reaches a minimum value of 17 dB at

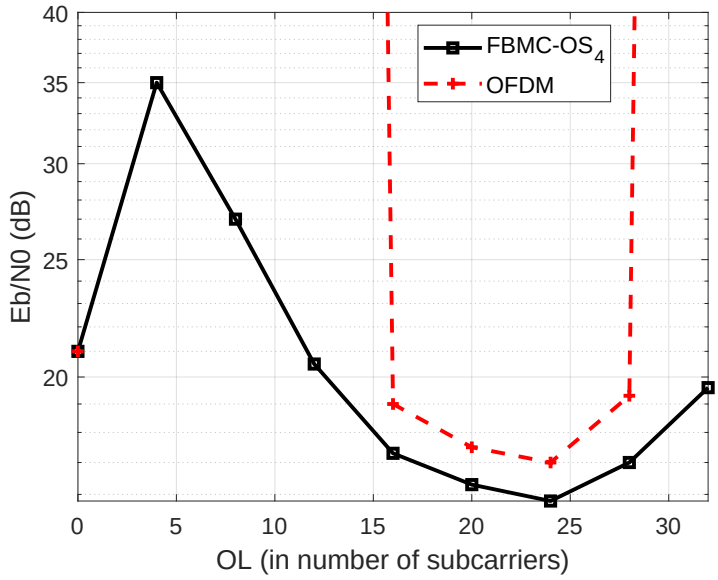

Figure 3.6: $Eb/N0$ vs OL of the considered receivers over the TDL-B 5G QuaDRiGa channel for a target BER of 10^{-4}.

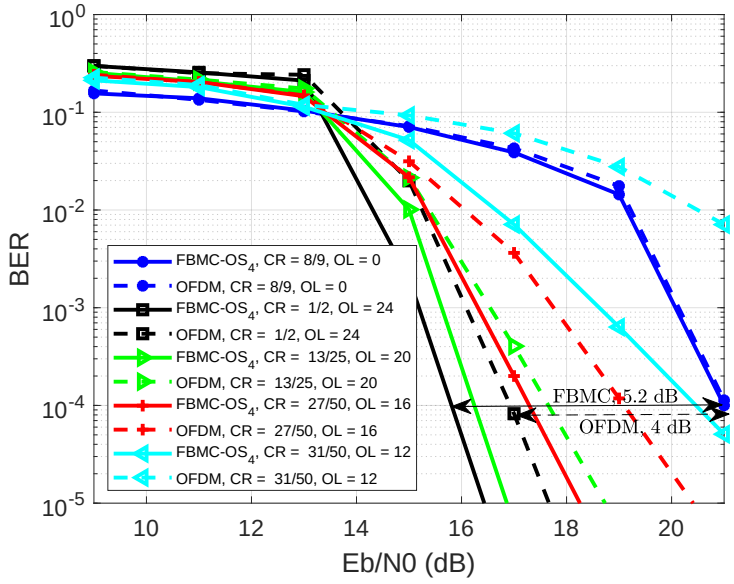

Figure 3.7: BER performance comparison of the OS_4-FBMC and OFDM receivers over the TDL-B 5G QuaDRiGa channel with different tuples achieving the same SE.

$OL = 24$ and $CR = 1/2$. Note that FBMC can attain lower values of $\frac{Eb}{N0}$ than OFDM for the same value of OL thanks to its inherent capabilities to combat interference. To summarize, the tuple $(CR^*, K^*, OL^*) = (1/2, 16, 24)$ is selected for the rest of the work.

3.3.3 Simulation results over the 5G multipath channel

In order to provide a more detailed understanding of the efficiency of the proposed approach, we also compare in Figure 4.3 the BER performance as a function of the $Eb/N0$ of both the OFDM and FBMC-OS_4 waveforms for the considered scenario. Several combinations of CR_{OL}

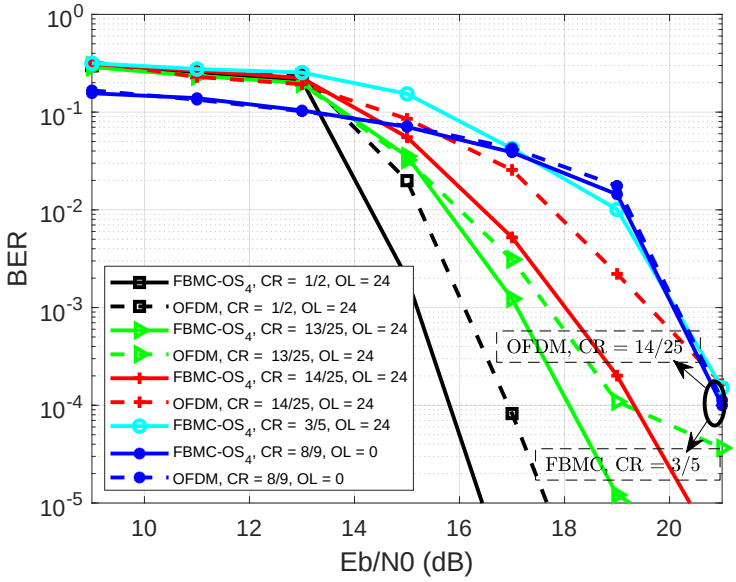

Figure 3.8: SE improvement capability for the proposed transmission technique for the OFDM and FBMC-OS$_4$ receiver over the TDL-B 5G QuaDRiGa channel, with $OL = 24$.

and OL (in number of subcarriers) are considered targeting the same SE with $K^* = 16$.

When the subcarriers do not overlap (i.e., $OL = 0$) and a CR of 8/9 is used, both waveforms exhibit the worst BER performance. Increasing the amount of overlap between subcarriers results in a higher degree of interference, making it necessary to reduce the CR while maintaining the same SE. This, in turn, leads to a significant improvement in BER performance, as illustrated in the same figure for various combinations of OL values, specifically 12, 16, 20, and 24. In particular, overlapping by 24 subcarriers yields the best performance, providing a gain of approximately 5.2 and 4 dB in $Eb/N0$ for FBMC and OFDM, respectively. This finding confirms the conclusions drawn in Section 3.3.2 from Figure 3.6.

3.3.4 Spectral efficiency gain

We use (3.22) to evaluate the SE gain of the best overlapping case of $OL = 24$ relative to the non-overlapping scenario. Figure 3.8 depicts the BER performance for $OL = 24$ with increasing CR_{24} values. We determine the SE gain once the BER performance of both scenarios is nearly identical for a target $\frac{Eb}{N0}$ ($\gamma = 21$ dB). As shown in Figure 3.8, the curve corresponding to the non-overlapping scenario intersects with the one corresponding to the overlapping scenario at $CR'_{24} = 3/5$ for FBMC/OQAM and 14/25 for OFDM, resulting in a 20% and 12% SE gain for FBMC/OQAM and OFDM, respectively. Therefore, FBMC/OQAM augmented with the FBMC-OS receiver provides superior performance and a higher SE gain compared to OFDM.

An alternative and simple method to improve the SE could be to increase the modulation order. Therefore, we compare in Figure 3.9 the BER performance with equal SEs of 64QAM with non-overlapping subcarriers (i.e., $OL = 0$) and $CR = 16/27$ to that of 16QAM with $CR = 8/9$. As depicted in the figure, 64QAM performs similarly to 16QAM for a target BER of 10^{-4}, confirming the efficiency of our proposed transmission scheme to improve the SE.

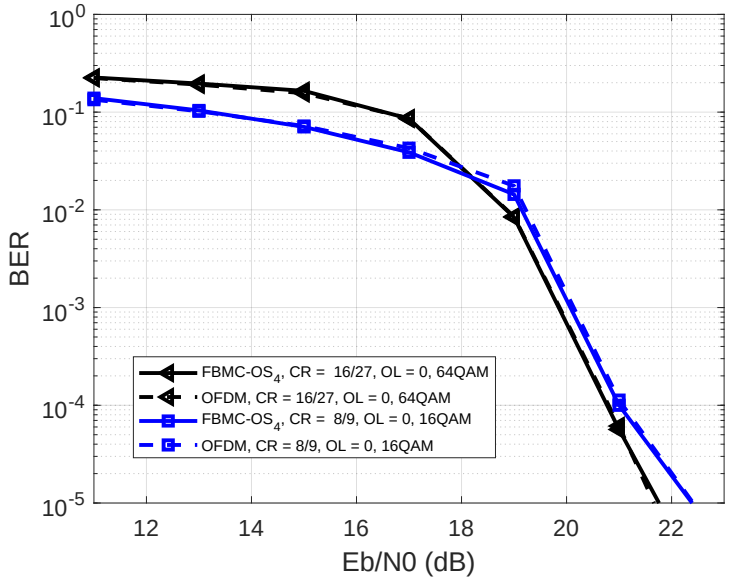

Figure 3.9: BER performance comparison of the OFDM and FBMC-OS_4 receiver over the TDL-B 5G QuaDRiGa fading channel, with 16QAM and 64QAM modulation schemes, and same SE.

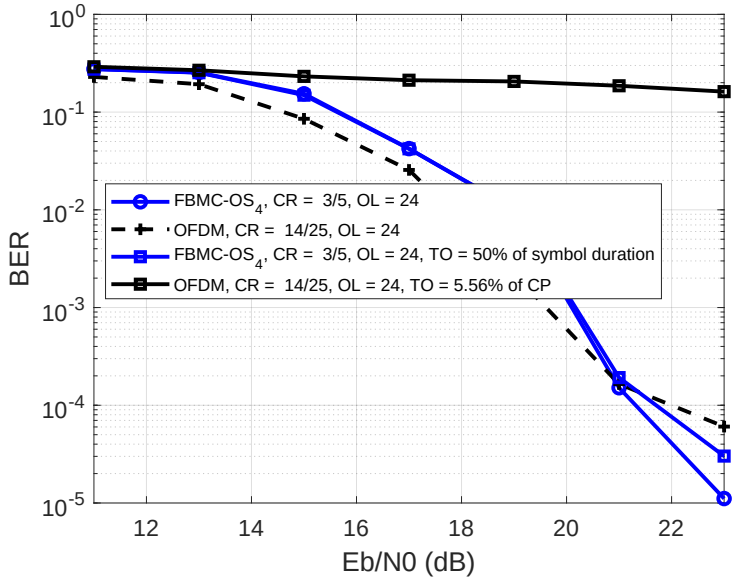

Figure 3.10: BER performance comparison of the FBMC-OS_4 and OFDM receivers over the TDL-B 5G QuaDRiGa fading channel in the presence of TOs, with $OL = 24$.

3.3.5 Effect of timing offsets

TO impairments occur when the transmitter and receiver windows are not aligned in time. It is always the case in practice due to the channel-induced propagation delay. Therefore, it is important to investigate the robustness in terms of BER performance of the proposed transmission technique and the two considered waveforms in the presence of TO impairments. Corresponding results are plotted in Figure 3.10. Without overlapping, OFDM exhibits a high vulnerability to TO impairments since it cannot support any TO value larger than half of its cyclic prefix

duration. This vulnerability is worsened by overlapping. Indeed, considering the case that corresponds to the highest SE gain (i.e., $OL = 24$ with CR = 14/25) for OFDM, a TO that corresponds only to 5.56% of the CP duration was enough to severely degrade the performance, leading to an irreducible error floor as depicted in Figure 3.10. On the contrary, FBMC augmented by the OS receiver can support asynchronous communications as demonstrated in [13]. Thus, applying a much larger TO value that corresponds to 50% of the symbol duration shows the same BER performance down to the target BER of 10^{-4} with a slight performance degradation for lower error rates ($Eb/N0 > 21$ dB). This slight performance degradation is brought on by the introduced change in the interference pattern due to TO impairments. This can be, at least partly, compensated for by a suitable design of the interleaver located between the waveform and the outer channel code.

3.4 Summary

In this chapter, we proposed a novel transmission scheme denoted by MCO for SE enhancement considering the OFDM and FBMC/OQAM waveforms. The proposed MCO scheme intentionally overlaps the subcarriers of adjacent users, which allows for a higher data rate and improved system efficiency. This comes at the cost of a high level of interference. To address this issue, we propose to compile and optimize jointly the coding rate, the amount of overlapped subbands, and the modulation order. Unlike prior works, to validate the proposed scheme, we conducted simulations using a realistic channel model generated by QuaDRiGa. Therefore, while relying on simulations, we have obtained the following results:

1. The FBMC transceiver outperforms OFDM over the TDL-B 5G QuaDRiGa channel while confirming the targeted SE improvement by the proposal.

2. FBMC augmented by the OS_4 receiver offers up to 66% higher SE gain compared to OFDM.

3. The FBMC/OQAM waveform with the OS_4 receiver exhibits higher robustness against TO compared to OFDM. With a TO reaching 50% of the symbol duration, the FBMC/OQAM waveform with the OS_4 receiver outperforms the OFDM receiver even if it only undergoes a TO of 5.56%.

Consequently, augmented by the OS-based receiver, the FBMC/OQAM waveform proves to be a promising challenger for OFDM in future communication systems. However, in some 6G applications, the SE gain obtained by employing the proposed MCO approach may not be sufficient. Therefore, in the next chapter, we extend the FBMC-OS receivers to mMIMO systems to fully exploit the potential of mMIMO technology for achieving even higher SE gain.

Chapter 4

Overlap-save FBMC receivers for mMIMO systems

While the techniques explored in the previous chapter enhance SE, the achieved improvement may not be enough for some 6G applications. To address this concern, exploiting large-scale MIMO systems, which involve equipping the BS with numerous antennas and serving multiple users simultaneously, represents a promising solution [14, 15]. Due to its simplicity, robustness to multipath channels and adoption in multiple standards, OFDM was first associated with mMIMO [91] in the context of 5G systems. Despite the aforementioned advantages, it is well known that OFDM is highly sensitive to CFOs since the latter leads to ICI [116, 117]. Furthermore, the receiver needs to be finely synchronized in time to avoid TO impairments. However, in some 6G-Internet of Things (IoT) applications, the signaling overhead due to hand-shaking in the synchronization procedure, and for setting up the transmission must be minimized. This is a key requirement prior to serving a large number of energy-constrained connected devices. As potential solutions, relaxed synchronization and asynchronous communications were considered [118]. Unfortunately, supporting the aforementioned scenarios with OFDM is a challenging task since it degrades the performance and increases receiver complexity.

FBMC/OQAM is one of the main waveforms that has been investigated in recent years as an alternative to OFDM in the context of 5G. During the last years, several innovative contributions were proposed at the transmitter and receiver sides related to FBMC/OQAM [12, 13]. At the transmitter side, a novel short PF for FBMC allowing for near perfect reconstruction and having the same size as one OFDM symbol was proposed. At the receiver side, a novel FBMC receiver technique suitable for short filters was proposed [13]. For that, a time-domain equalizer based on OS algorithm (for fast convolution operation) is employed before the FBMC demodulation. It was shown that both the time-domain equalizer and the FBMC receiver can be merged in a unique structure due to the frequency localization of the filter, greatly reducing the computational complexity. An alternative FBMC-OS scheme is derived, where FBMC symbols are transmitted by block and demodulated all at once in the frequency domain, which further reduces the complexity and enables efficient Alamouti-based MIMO support. The resulting receiver largely improves the robustness against doubly dispersive channels for short filters and

enables the support of asynchronous communications. The extension of these proposals and their advantages to MU-mMIMO is not straightforward and therefore is tackled in this chapter. The chapter presents in addition an in-depth analysis of the robustness against CFOs, TOs and multi-path channel impairments of the proposed FBMC receivers in the context of MU-mMIMO systems. Performance results are compared with OFDM and with a conventional FBMC/OQAM system.

4.1 Relevant multi-carrier transceivers in the context of massive MIMO

We consider a MU-mMIMO setup, where there are U MTs and a BS. Each MT is equipped with a single antenna. The BS is equipped with N_{Rx} antennas and serves all U MTs in the cell simultaneously. In what follows, relevant multi-carrier transceivers in the context of mMIMO systems will be discussed.

4.1.1 OFDM transceiver

OFDM is the predominant modulation technique used in the mMIMO literature. The OFDM transmitter for MU-mMIMO systems follows the one described in Section 2.1.1 for each user. Note that all users modulated together in the mMIMO system are allocated the same frequency subband. Consequently, the sample k of the OFDM signal, denoted $s(k)$, can be expressed mathematically as follows:

$$\boldsymbol{s}(k) = \sum_{u=1}^{U} \sum_{n=-\infty}^{\infty} \sum_{m=s}^{s+N_c-1} a_n(m-s) e^{i2\pi \frac{(k-L_{CP})m}{M}}, k \in [\![0, M + L_{CP} - 1]\!] \tag{4.1}$$

s represents the index of the first subcarrier of the allocated subband and $a_n(m)$ is the complex user's transmitted QAM symbol number m assigned to the subcarrier index $m+s$, at time index n.

To demodulate the received signal and reconstruct the transmitted QAM symbols, the OFDM receiver applies dual operations to the ones performed by the transmitter. In fact, due to the increased dimension of large-scale MIMO systems, a low-complexity signal detection algorithm is required. Low-complexity linear detection algorithms such as ZF perform near-optimally if the number of antennas at the BS tends to infinity [119]. Indeed, if r_j denotes the received signal on antenna index j, it represents a combination of all the signals coming from different users consisting of several OFDM symbols. Then a FFT of size N is required to demodulate one OFDM symbol after eliminating the CP. The received signals from all users are then separated by a ZF equalization stage having as equalization matrix the pseudo inverse operator $(.)^+$ of the CFR $\boldsymbol{C_n}(m) = \boldsymbol{H_n}^+(m)$ for the received symbol n at frequency bin m.

In fact, in MU-mMIMO systems, the expected performance gains can be largely hindered by frequency and time synchronization errors between the users. Moreover, both the MU CFO estimation and compensation problems [120] are quite different from those in conventional SU communication systems [121]. Therefore, preserving orthogonality across subcarriers generally requires resorting to computationally expensive techniques for mMIMO that may penalize beyond 5G system requirements in terms of throughput, energy efficiency, and latency [122]. Moreover, the orthogonality of preamble training sequences can be largely affected by TOs and/or CFOs for OFDM systems, and hence penalizing the performance [123]. Hence, taking into account the aforementioned shortcomings of OFDM, and the stringent requirements of beyond 5G systems, there has been a regain of interest in alternative waveforms designed to address OFDM

drawbacks in order to fully benefit from mMIMO technologies.

4.1.2 FBMC transceiver

It was shown in [124] [125] that FBMC/OQAM represents an appealing alternative waveform to OFDM thanks to its advantages in terms of resilience against synchronization errors, its very low level of OOBPL and its higher BW efficiency by avoiding the introduction of a CP. Extending such advantages to mMIMO would largely benefit the objective of satisfying the considerable constraints of B5G systems. The PPN-FBMC receiver discussed in Section 2.2.4.1 is generally adopted at the transmitter side in mMIMO systems due to its low computational complexity. Therefore, in a MU scenario, equations (2.12), and (2.13) will be modified as follows:

$$\boldsymbol{s}(k) = \sum_{n=-\infty}^{+\infty} g\left(k - n\frac{M}{2}\right)\boldsymbol{x_n}(k) \tag{4.2}$$

with

$$\boldsymbol{x_n}(k) = \sum_{m=0}^{M-1} (-1)^{nm}\boldsymbol{a_n}(m)\phi_n(m)e^{i2\pi\frac{km}{M}} \tag{4.3}$$

where $\boldsymbol{a_n}(m) \in \mathbb{C}^{U\times 1}$ are the users' PAM symbols at time slot n, subcarrier index m, and $\boldsymbol{s}(k) \in \mathbb{C}^{U\times 1}$ is a vector containing the transmitted signals of all users.

The use of FBMC in mMIMO systems was investigated in [126], with results obtained for a sample set of channel responses generated using the IEEE802.16 broadband channel model (SUI-4) [127]. Its so-called self-equalization property, which results in a channel flattening effect, was revealed through simulations. In SISO transmissions, by using a large number of subcarriers, FBMC takes advantage of the fact that while each subcarrier band is narrow, it has an approximately flat gain and so suffers from a negligible level of ISI. However, in mMIMO systems, channel distortion is smoothed. As a result, the requirement of adopting a large number of subcarriers in FBMC systems is relaxed. This results in a lower complexity and latency caused by the analysis and synthesis filter banks. Moreover its sensitivity to CFOs decreases due to the increase in the subcarrier spacing Δf. In [128] the authors propose a simple FBMC PF design intended to eliminate antenna array correlation, allowing the system to reach arbitrarily high SIR values when increasing the number of BS antennas. The authors have also shown that there is a small difference (around 1.5 dB) between the SIR of CP-OFDM and PPN-FBMC with their proposed modified PF. However, they simply considered a normalized exponentially decaying channel in their simulations. Therefore, the SIR difference may get higher for more realistic channels. In [129], the PPN-FBMC low complexity data detector was implemented at the receiver side preceded by a frequency domain equalization for the received FBMC symbols. However, it was shown that the FBMC waveform with this receiver is outperformed by OFDM in the context of large-scale MIMO systems over the WINNER-Phase2 channel model due to the PPN structure of the receiver. The prior-art on FBMC-based mMIMO being still in its early stages, these systems require careful examination and investigation for being able to draw definitive conclusions.

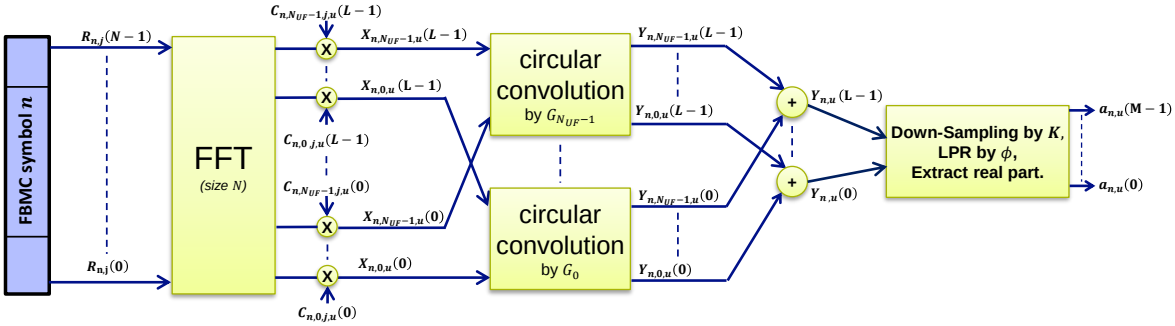

Figure 4.1: FBMC/OQAM OS massive MIMO Receiver.

4.2 Proposed OS-based FBMC receivers in the context of massive MIMO

The FBMC-OS receiver was proposed for SISO transmissions in [13]. The basic principle of the FBMC-OS receiver is to integrate an OS-based time-domain equalizer with FBMC demodulation. Associated with the NPR1 short PF, this receiver was shown to achieve improved robustness against TOs and multipath channels with long delay spreads while reducing the computational complexity in comparison to existing FBMC receivers found in the literature [13]. Actually, there is a lot of interest in using short PF with FBMC since it enables the support of short frame sizes for low latency communication. This can significantly reduce the computational complexity, and higher power efficiency can be obtained when compared to long PFs. Thus, implementing the OS-based FBMC receivers in the context of mMIMO becomes particularly interesting.

4.2.1 Overlap-Save FBMC receiver with massive MIMO

Figure 4.2 depicts the FBMC-OS receiver in the context of mMIMO. Let N_{Rx} be the number of antennas deployed at the receiver side, and U be the total number of users. At the output m of the size $N = N_{UF}M$ FFT, the received signal $R_{n,m}(j)$ at receiver antenna j, symbol index n, is expressed as

$$R_{n,m}(j) = \sum_{k=0}^{N-1} r_j \left(k + n\frac{M}{2}\right) e^{-i\frac{2\pi km}{N}} \tag{4.4}$$

To ease notations, the received signal of all antennas can be combined into a vector $\boldsymbol{R_n}(m) = [R_{n,m}(1), ..., R_{n,m}(N_{Rx})]$. Note that $\boldsymbol{R_n}(m)$ is a combination of all the signals coming from different users consisting of several FBMC symbols. As for OFDM, MIMO equalization is performed directly after FFT as $\boldsymbol{X_n}(m) = \boldsymbol{C_n}(m) \times \boldsymbol{R_n}(m)$, where $\boldsymbol{X_n}(m)$ is the equalized signal for all users, and $\boldsymbol{C_n}(m) \in \mathbb{C}^{U \times N_{Rx}}$ is the ZF equalizer matrix at frequency bin m defined in Section 4.1.1.

Then, N_{UF} stages of circular convolution by the frequency shifted responses of the PF is performed on $\boldsymbol{X_n}(m)$, where N_{UF} is an integer number referred to as the up-sampling factor used

for the OS technique. Thus, the output of each filtering stage vector is

$$\boldsymbol{Y_n}(m,\ell) = \sum_{p=-\Delta}^{\Delta} G_\ell(p)\boldsymbol{X_n}\Big(\ell + (m-p)N_{UF}\Big) \tag{4.5}$$

where $\Delta = (N_G - 1)/2$, N_G denotes the number of non-truncated filter coefficients, and G is the frequency shifted response of the PF that can be deduced from its impulse response g as follows:

$$G_\ell(p) = e^{i\frac{\pi\ell}{N_{UF}}} \sum_{k=0}^{M-1} g(k) e^{i\frac{2\pi\ell(k-M/2)}{N}} e^{-i\frac{2\pi pk}{M}} \tag{4.6}$$

The Analysis Filter Bank (AFB) output $\boldsymbol{Y_n}(m)$, $m \in [\![0, M-1]\!]$, is obtained by summing each filtering stage vector outputs as follows:

$$\boldsymbol{Y_n}(m) = \sum_{\ell=0}^{N_{UF}-1} \boldsymbol{Y_n}(m,\ell) \tag{4.7}$$

Finally, the transmitted data symbols $\hat{\boldsymbol{a}}_{\boldsymbol{n}}$(m) of all users are recovered after extracting the real part of the down-sampled (by K; $K = 1$ for short filters) and linear phase rotated ϕ_n filtering stage outputs

$$\hat{\boldsymbol{a}}_{\boldsymbol{n}}(m) = \Re\Big(\boldsymbol{Y_n}(Km)\phi_n^*(m)\Big) \tag{4.8}$$

4.2.2 Overlap-Save-Block FBMC receiver with massive MIMO

The FBMC-OSB receiver can be seen as an FBMC-OS receiver where the FFT is applied on a block of FBMC symbols. Hence, only one FFT is required to process all symbols in a given block. Furthermore, in the particular scenario of low mobility, it can be sufficiently accurate to assume that the channel response remains static over a given block, which reduces the equalization complexity. This is particularly interesting in mMIMO systems, as the equalization step is quite complex. Indeed, through similar demodulation steps to FBMC-OS, at the output m of the size N FFT, the received signal $R_{n,m,b}(j)$ at receiver antenna j, symbol index n in a block b, is expressed as

$$R_{n,m,b}(j) = \sum_{k=0}^{N-1} r_{b,j}\left(k + n\frac{M}{2}\right) e^{-i\frac{2\pi km}{N}} \tag{4.9}$$

Similarly, the equalized signal for all users $\boldsymbol{X_{n,b}}(m)$ is

$$\boldsymbol{X_{n,b}}(m) = \boldsymbol{C_{n,b}}(m) \times \boldsymbol{R_{n,b}}(m) \tag{4.10}$$

where $\boldsymbol{C_{n,b}}(m) \in \mathbb{C}^{U \times N_{Rx}}$ is $\boldsymbol{C_n}(m)$ for a block b, and $\boldsymbol{R_{n,b}}(m) = [R_{n,m,b}(1), ..., R_{n,m,b}(N_{Rx})]$ is a combination of all the signals coming from different users consisting of several blocks of FBMC symbols.

Hence, if $\hat{\boldsymbol{a}}_{\boldsymbol{n,b}}$(m) is the recovered PAM symbol at block b and FBMC symbol n for all users, we

have

$$\hat{\boldsymbol{a}}_{\boldsymbol{n},\boldsymbol{b}}(m) = \Re\Big(\boldsymbol{Y}_{\boldsymbol{n},\boldsymbol{b}}(Km)\phi_n^*(m)\Big) \tag{4.11}$$

where $\boldsymbol{Y}_{\boldsymbol{n},\boldsymbol{b}}(m)$ is the AFB output expressed as

$$\boldsymbol{Y}_{\boldsymbol{n},\boldsymbol{b}}(m) = \sum_{\ell=0}^{\mathrm{N}_{UF}-1} \sum_{p=-\Delta}^{\Delta} G_\ell(p)\boldsymbol{X}_{\boldsymbol{n},\boldsymbol{b}}(Km-p,\ell) \tag{4.12}$$

and N_{UF} is chosen so that it is the lowest possible integer value of $\left\lceil 1+\frac{N_s-1}{2K}\right\rceil$ considering that the FFT size must be superior or equal to the block size N_s.

4.3 The proposed analytical study

In this section, we derive analytical SIR expressions in the presence of CFO and TO, as well as an analytical expression for the SIR saturation level in an asymptotic regime (i.e. as the number of antennas N_R at the BS tends to infinity) for each of the proposed receivers in the context of MU-mMIMO. Therefore, the relationship between the transmitted symbols and the recovered symbols must be established in order to get an explicit form of the analytical SIR expression.

4.3.1 Timing offsets

4.3.1.1 Overlap-save FBMC receiver

The robustness of the FBMC-OS$_{N_{UF}}$ receiver to TO can be proved analytically by considering the time domain equalizer in [16] with MU-mMIMO and disregarding multi-path. Hence, the frequency domain equalized signal for all users is

$$\underbrace{\boldsymbol{X}_{\boldsymbol{n}}(m)}_{\in\mathbb{C}^{U\times 1}} = \underbrace{\boldsymbol{C}_{\boldsymbol{n}}(m)}_{\in\mathbb{C}^{U\times N_R}} \times \sum_{k=0}^{N-1} \underbrace{\boldsymbol{r}(k+n\frac{M}{2})}_{\in\mathbb{C}^{N_R\times 1}} e^{-i\frac{2\pi km}{N}} \tag{4.13}$$

Adapting the previous equation in the presence of TO of l_d samples, we have

$$\begin{aligned}\boldsymbol{X}_n(m) &= \boldsymbol{C}_n(m)\boldsymbol{C}_{\boldsymbol{TO}}(m)\sum_{k=0}^{N-1}\boldsymbol{r}\left(k+l_d+n\frac{M}{2}\right)e^{-i\frac{2nkm}{N}}\\ &= \boldsymbol{C}_n(m)\times\sum_{k=0}^{N-1}\boldsymbol{r}\left(k+l_d+n\frac{M}{2}\right)e^{-i\frac{2n(k+l_d)m}{N}}\end{aligned} \tag{4.14}$$

where $\boldsymbol{C}_{\boldsymbol{TO}}(m) = e^{-i\frac{2\pi ml_d}{N'}}$ and $N' = N_{UF}M$.
By applying the following change of variable $k = k + l_d$, then

$$\boldsymbol{X}_n(m) = \boldsymbol{C}_n(m)\times\sum_{k=l_d}^{N+l_d-1}\boldsymbol{r}\left(k+n\frac{M}{2}\right)e^{-i\frac{2nkm}{N}} \tag{4.15}$$

Suppose that $l_d > 0$, then (4.15) becomes

$$\boldsymbol{X_n}(m) = \boldsymbol{C_n}(m) \times \left[\sum_{k=0}^{N-1} \boldsymbol{r}\left(k + n\frac{M}{2}\right) e^{-i\frac{2nkm}{N}} + \sum_{k=0}^{l_d-1} \left(\boldsymbol{r}\left(k + N + n\frac{M}{2}\right) - \boldsymbol{r}\left(k + n\frac{M}{2}\right)\right) \times e^{-i\frac{2nkm}{N}} \right] \tag{4.16}$$

At the output of the OS time-domain equalizer, we have

$$\begin{aligned} \boldsymbol{x_n}(k) &= \sum_{m=0}^{N-1} \boldsymbol{X_n}(m) e^{i\frac{2m\pi(k+l_0)}{N}} \\ &= \boldsymbol{c_n}(k) \times A \end{aligned} \tag{4.17}$$

where $k \in [0, M-1]$, $l_0 = \frac{(N_{UF}-1)M}{2}$,

$$A = \left[\boldsymbol{r}\left(k + l_0 + n\frac{M}{2}\right) + \boldsymbol{\Pi}_{l_d}(k + l_0) \times \left(\boldsymbol{r}\left(k + N + l_0 + \frac{M}{2}n\right) - \boldsymbol{r}\left(k + l_0 + \frac{M}{2}n\right)\right) \right] \tag{4.18}$$

and

$$\boldsymbol{\Pi}_x(k) = \begin{cases} k, & k < x \text{ and } x > 0 \\ 0, & k \geq x \text{ or } x \leq 0 \end{cases} \tag{4.19}$$

By making another change of variable $k = k + l_0$, then (5.27) becomes

$$\boldsymbol{x_n}(k) = \boldsymbol{c_n}(k) \times \left[\boldsymbol{r}\left(k + n\frac{M}{2}\right) + \underbrace{\boldsymbol{I}(k)}_{\text{Interfering signal}} \right] \tag{4.20}$$

where $k \in [l_0, l_0 + M - 1]$, and

$$\boldsymbol{I}(k) = \boldsymbol{\Pi}_{l_d}(k) \left[\boldsymbol{r}\left(k + N + \frac{M}{2}n\right) - \boldsymbol{r}\left(k + \frac{M}{2}n\right) \right]$$

The lowest possible value of l_0 is $\frac{M}{2}$ for $N_{UF} = 2$. Moreover, when $l_d < l_0$, then $\boldsymbol{\Pi}_{l_d}(k) = 0$. When $-l_0 < l_d < 0$, the same conclusion can be obtained through similar development. Hence, this confirms that the $\text{OS}_{N_{UF}}$-FBMC receiver is insensitive to TO lower than 50% of the symbol duration for all $N_{UF} \geq 2$.

4.3.1.2 Overlap-save-block FBMC receiver

Let's also consider the OS time domain equalizer in [16] but applied to a block of FBMC symbols with mMIMO. Adapting equation (4.13) but with a block $\boldsymbol{b}$, the frequency domain equalized

signal for a block $\boldsymbol{b}$ and all users will be

$$\underbrace{\boldsymbol{X_{b,n}}(m)}_{\in \mathbb{C}^{U\times 1}} = \underbrace{\boldsymbol{C_{b,n}}(m)}_{\in \mathbb{C}^{U\times N_R}} \times \sum_{k=0}^{N-1} \underbrace{\boldsymbol{r_b}(k)}_{\in \mathbb{C}^{N_R\times 1}} e^{-i\frac{2\pi km}{N}} \tag{4.21}$$

Actually, in the presence of TO for an OSB receiever, only the first or last FBMC symbol is affected by interference. Hence, adapting the previous equation in the presence of TO and by considering only the first FBMC symbol ($n = 0$), we have

$$\begin{aligned} \boldsymbol{X_{b,0}}(m) &= \boldsymbol{C_{b,0}}(m) \times \boldsymbol{C_{TO}}(m) \sum_{k=0}^{N-1} \boldsymbol{r_b}\,(k + l_d)\, e^{-i\frac{2\pi km}{N}} \\ &= \boldsymbol{C_{b,0}}(m) \times \sum_{k=0}^{N-1} \boldsymbol{r_b}\,(k + l_d)\, e^{-i\frac{2\pi (k+l_d)m}{N}} \end{aligned} \tag{4.22}$$

By neglecting the effect of multi-path and noise, substituting the value of $\boldsymbol{r_b}(k)$ in (4.22), and by applying the change of variable $k = k + l_d$ we have

$$\underbrace{\boldsymbol{X_{b,0}}(m)}_{\in \mathbb{C}^{U\times 1}} = \underbrace{\boldsymbol{C_{b,0}}(m)}_{\in \mathbb{C}^{U\times N_R}} \times \sum_{k=l_d}^{N+l_d-1} \underbrace{\boldsymbol{H}}_{\in \mathbb{C}^{N_R\times U}} \times \underbrace{\boldsymbol{s_b}(k)}_{\in \mathbb{C}^{U\times 1}} e^{-i\frac{2\pi km}{N}} \tag{4.23}$$

Similarly as before, if $l_d > 0$, then equation (4.23) becomes

$$\boldsymbol{X_{b,0}}(m) = \left[\sum_{k=0}^{N-1} \boldsymbol{s_b}(k) e^{-i\frac{2\pi km}{N}} + \sum_{k=N}^{N+l_d-1} \boldsymbol{s_b}(k) e^{-i\frac{2\pi km}{N}} - \sum_{k=0}^{l_d-1} \boldsymbol{s_b}(k) e^{-i\frac{2\pi km}{N}} \right] \tag{4.24}$$

At the output of the OS time domain equalizer applied to a block $\boldsymbol{b}$ we have

$$\boldsymbol{x_{b,0}}(k) = \left[\underbrace{\boldsymbol{s_b}(k)}_{\text{Transmitted signal}} \quad \underbrace{+\boldsymbol{\Pi_{l_d}}(k)\boldsymbol{s_b}(k+N) - \boldsymbol{\Pi_{l_d}}(k)\boldsymbol{s_b}(k)}_{\text{Interfering signal } \boldsymbol{I}_b(k)} \right] \tag{4.25}$$

where $\boldsymbol{\Pi_{l_d}}(k)$ is defined in (5.28).
The interfering term can be expressed as

$$\boldsymbol{I_b}(k) = \boldsymbol{\Pi_{l_d}}(k) g(k) \sum_{m=0}^{M-1} \boldsymbol{\phi_0}(m) \boldsymbol{A'}_m e^{i\frac{2\pi km}{N}} \tag{4.26}$$

where $\boldsymbol{A'}_m = \boldsymbol{a_{b+1,0}}(m) - \boldsymbol{a_{b,0}}(m)$, $\boldsymbol{a_{b+1,0}}(m)$ and $\boldsymbol{a_{b,0}}(m)$ are the transmitted data symbols of distinct users at the first FBMC symbol of blocks $\boldsymbol{b+1}$ and $\boldsymbol{b}$ respectively. Hence, at the output of the AFB we have

$$\boldsymbol{I_b}(m) = \sum_{p=-\frac{M}{2}}^{\frac{M}{2}-1} F_{g_{l_d}}(p) \boldsymbol{\phi_0}(m-p) \boldsymbol{A'}_{m-p} \tag{4.27}$$

where

$$F_{g_{l_d}}(p) = \sum_{k=0}^{M-1} \Pi_{l_d}(k) g^2(k) e^{-i\frac{2\pi km}{N}}$$

Then, after OQAM demodulation, the interference term at the output of the FBMC receiver $\{\boldsymbol{D_b}(m) = \mathrm{R}\left(\boldsymbol{\phi_0^*}(m)\boldsymbol{I_b}(m)\right)\}$ can be expressed as

$$\boldsymbol{D_b}(m) = \Re\left(\sum_{p=-\frac{M}{2}}^{\frac{M}{2}-1} i^{-p} F_{g_{\boldsymbol{l_d}}}(p) \boldsymbol{A'}_{m-p} \right) \tag{4.28}$$

Recall that interference is only introduced at the first FBMC symbol in a block $\boldsymbol{b}$, then

$$\widehat{a_{b,n}}(m) = a_{b,n}(m) + \underbrace{\boldsymbol{D_b}(m)}_{\text{Only for n=0}} + \boldsymbol{T_{b,n}}(m) \tag{4.29}$$

where $\boldsymbol{T_{b,n}}(m)$ represents the interference induced by truncation.
Finally, the SIR expression arising from a TO of l_d samples for the FBMC-OSB receiver can be expressed as

$$\mathbf{SIR}_{\mathrm{OSB}}(l_d) \approx \frac{E\left(\mathbf{a}_{\mathbf{b,n}}^2(m)\right)}{\frac{1}{N_s} E\left(\boldsymbol{D_b}(m)^2\right) + E\left(\boldsymbol{T_{b,n}}(m)^2\right)} \tag{4.30}$$

Since the data $\boldsymbol{a_{b,n}}(m)$ of the users are independent and identically distributed random variables of mean 0 and variance σ^2 then

$$E\left(\boldsymbol{D_b}(m)^2\right) = 2\sigma^2 \sum_{p=-\frac{M}{2}}^{\frac{M}{2}-1} \mathrm{R}\left(i^{-p} F_{g_{l_d}}(p)\right)^2 \tag{4.31}$$

Hence, (4.30) becomes

$$\mathbf{SIR}_{\mathrm{TO,OSB}}(l_d) \approx \frac{\sigma^2}{\frac{1}{N_s} 2\sigma^2 \sum_{p=-\frac{M}{2}}^{\frac{M}{2}-1} \Re\left(i^{-p} F_{g_d}(p)\right)^2 + E\left(\boldsymbol{T_{b,n}}(m)^2\right)} \tag{4.32}$$

4.3.2 Analytical SIR expression in the presence of CFO

4.3.2.1 Overlap-save FBMC receiver

The expression of the received signal by the j^{th} BS antenna provided in (4.4) can be rewritten as

$$R_{n,m,\ell}(j) = \sum_{k=0}^{N-1} r_j\left(k + n\frac{M}{2}\right) e^{-i\frac{2\pi k(N_{UF}m+\ell)}{N}} \tag{4.33}$$

Equivalently, the complete $N_R \times 1$ received signal which is a combination of all the signals stemming from different users consisting of several FBMC symbols can be expressed as

$$\begin{aligned} \boldsymbol{R_n}(m,\ell) &= \sum_{k=0}^{N-1} \boldsymbol{r}\left(k + n\frac{M}{2}\right) e^{-i\frac{2nk(N_{UF}m+\ell)}{N}} \\ &= \sum_{s=0}^{N_{UF}-1} \sum_{k=0}^{M-1} \boldsymbol{r}(p'_n) \times P \end{aligned} \tag{4.34}$$

where $p'_n = k + \frac{M}{2}(2s+n)$ and

$$\begin{aligned} \boldsymbol{R}_n(m,\ell) &= [R_{n,m,\ell}(1), ..., R_{n,m,\ell}(N_R)] \\ \boldsymbol{r}\,(k) &= [r_1\,(k)\,, ..., r_{N_R}\,(k)] \\ P &= e^{-i\frac{2\pi s\ell}{N_{UF}}} e^{-i\frac{2\pi km}{M}} e^{-i\frac{2\pi k\ell}{N_{UF}M}} \end{aligned}$$

After equalization, the frequency domain equalized signal can be expressed as

$$\begin{aligned} \underbrace{\boldsymbol{X}_n(m,l)}_{\in \mathbb{C}^{U\times 1}} &= \underbrace{\boldsymbol{C}_n(m,\ell)}_{\in \mathbb{C}^{U\times N_R}} \times \underbrace{\boldsymbol{R}_n(m,\ell)}_{\in \mathbb{C}^{N_R\times 1}} \\ &= \boldsymbol{C}_n(m,\ell) \times \sum_{s=0}^{N_{UF}-1} \sum_{k=0}^{M-1} \boldsymbol{r}(p'_n) \times P \end{aligned} \tag{4.35}$$

This is followed by a filtering stage as previously mentioned i in Section 4.2.1, which is rearranged in the time domain. Then the ℓ^{th} AFB output is

$$\underbrace{\boldsymbol{Y}_n(m,\ell)}_{\in \mathbb{C}^{U\times 1}} = \boldsymbol{C}_n(m) \sum_{s=0}^{N_{UF}-1} \sum_{k=0}^{M-1} g_\ell(k)\boldsymbol{r}(p'_n) \frac{P}{e^{-i\frac{2\pi k\ell}{N_{UF}M}}} \tag{4.36}$$

where $g_\ell(k)$ represents the ℓ^{th} impulse response of the PF defined as

$$g_\ell(k) = (-1)^\ell e^{-i\frac{2\pi k\ell}{N_{UF}M}} \sum_{m=-\Delta}^{\Delta} \Re\left(G_\ell(m)\right) e^{i\frac{2\pi km}{M}} \tag{4.37}$$

Neglecting the effect of multipath (delay spread) and noise, the complete $N_R \times 1$ received signal is

$$\boldsymbol{r}(k) = \boldsymbol{H} \times \boldsymbol{s}(k) \tag{4.38}$$

where $\boldsymbol{H} \in \mathbb{C}^{N_R\times U}$ is the MIMO channel matrix, and $\boldsymbol{s}(k)$ is the baseband signal defined in (4.2). Substituting (4.2) in (4.38), we get

$$\boldsymbol{r}(k) = \boldsymbol{H} \times \sum_{n'=-\infty}^{+\infty} g\left(k - n'\frac{M}{2}\right) \boldsymbol{x_{n'}}(k) \tag{4.39}$$

By substituting (4.39) in (4.36), the ℓ^{th} AFB output number will be

$$\boldsymbol{Y_n}(m,\ell) = \sum_{s=\mathbf{0}}^{N_{\mathrm{UF}}-1} \sum_{k=0}^{M-1} \sum_{n'=-\infty}^{+\infty} g_\ell(k) g(p'_{n-n'}) \boldsymbol{x_{n'}}(p'_n) \frac{P}{e^{-i\frac{2\pi k\ell}{N_{UF}M}}} \tag{4.40}$$

However, due to the time localization of the NPR1 PF, interference is limited to only neighboring FBMC symbols. Hence, by defining $q = (n - n'), \in [-1, 1]$, (4.40) becomes

$$\boldsymbol{Y}_n(m,\ell) = \sum_{s=0}^{N_{UF}-1} \sum_{q=-1}^{1} \sum_{k=0}^{M-1} g_\ell(k) g(p'_q) \boldsymbol{x}_{n-q}(p'_n) \frac{P}{e^{-i\frac{2\pi k\ell}{N_{UF}M}}} \tag{4.41}$$

In fact the third sum in the previous equation is nothing but the FFT of the inner term. Moreover, since the Fourier transform of a product is the circular convolution of the corresponding transforms, then (4.41) can be written as

$$\begin{aligned} \boldsymbol{Y}_n(m,l) &= \sum_{s=0}^{N_{UF}-1} \sum_{q=-1}^{1} F_{g_{l,s}}(m,q) \otimes \boldsymbol{X_{n-q}}(m) \\ &= \sum_{s=\mathbf{0}}^{N_{UF}-1} \sum_{q=-1}^{1} \sum_{p=-\frac{M}{2}}^{\frac{M}{2}-1} F_{g_{l,s}}\left(p, q\frac{M}{2}\right) \boldsymbol{X_{n-q}}(m-p) \end{aligned} \tag{4.42}$$

where $\otimes$ denotes a circular convolution, and

$$\boldsymbol{X_{n-q}}(m-p) = \boldsymbol{a_{n-q}}(m-p)\boldsymbol{\phi_{n-q}}(m-p) \tag{4.43}$$

$$F_{g_{\ell,s}}(p,q) = \sum_{k=0}^{M-1} g_\ell(k) g\left(k + Ms + q\right) e^{-i\frac{2\pi s\ell}{N_{UF}}} e^{-i\frac{2\pi kp}{M}} \tag{4.44}$$

Substituting (4.43) in (4.42), we get

$$\boldsymbol{Y_n}(m,\ell) = \sum_{s=\mathbf{0}}^{N_{UF}-1} \sum_{(p,q)\in\Omega} F_{g_{\ell,s}}\left(p, q\frac{M}{2}\right) \boldsymbol{a_{n-q}}(m-p) \times \boldsymbol{\phi_{n-q}}(m-p)$$

where $\Omega = \left[-\frac{M}{2}, \frac{M}{2} - 1\right] \times [-1, 1]$.

Finally, by developing (5.11), the estimated data symbols $\widehat{\boldsymbol{a_n}}(m)$ of all users will be

$$\begin{aligned} \widehat{\boldsymbol{a_n}}(m) &= \Re\left[\phi_n^*(m) \sum_{\ell=0}^{N_{UF}-1} \boldsymbol{Y}_n(m,\ell)\right] \\ &= \Re\left[\sum_{(\ell,s)\in\Omega_1} \sum_{(p,q)\in\Omega} \mathrm{i}^{-\boldsymbol{q}-\boldsymbol{p}} F_{g_{\ell,s}}\left(p, q\frac{M}{2}\right) \times \boldsymbol{a_{n-q}}(m-p)\right] \end{aligned} \tag{4.45}$$

where $\Omega_1 = [0, N_{UF} - 1] \times [0, N_{UF} - 1]$.
Actually, in the presence of CFO, the previous equation can be written as

$$\begin{aligned}\widehat{\boldsymbol{a_n}}(m) &= \Re\left[\boldsymbol{C_{CPE}}(n)e^{j\pi nr}\phi_n^*(m)\sum_{(\ell,s)\in\Omega_1}\sum_{(p,q)\in\Omega} g_\ell(k)\times g(p'_q)\boldsymbol{x}_{n-q}(p'_n)e^{-i\frac{2\pi s\ell}{N_{UF}}}e^{-i\frac{2\pi k(m+r)}{N_{UF}}}\right] \\ &= \Re\left[\sum_{(l,s)\in\Omega_1}\sum_{(p,q)\in\Omega} \mathrm{i}^{-\boldsymbol{q}-\boldsymbol{p}}F_{g_{l,s}}\left(p+r, q\frac{M}{2}\right)\times \boldsymbol{a_{n-q}}(m-p)\right]\end{aligned} \tag{4.46}$$

where r is the CFO normalized to the subcarrier spacing Δf, and $\boldsymbol{C_{CPE}}(n) = e^{j\pi nr}$ is the Common Phase Error (CPE) compensation term introduced by CFO.
Keeping in mind that $\boldsymbol{a_n}(m)$ are independent and identically distributed random variables with zero mean, then the SIR expression arising from a CFO of r is

$$\mathbf{SIR_{OS,CFO}}(r) = \frac{\left(\sum_{(\ell,s)\in\Omega_1}\Re\left(F_{g_{\ell,s}}(r,0)\right)\right)^2}{\sum_{(\ell,s)\in\Omega_1}\sum_{(p,q)\in\Omega^0}\Re\left(\mathrm{i}^{-q-p}F_{g_{\ell,s}}\left(r,q\frac{M}{2}\right)\right)^2} \tag{4.47}$$

where Ω_0 is $\Omega/(0,0)$.

4.3.2.2 Overlap-save-block FBMC receiver

Through similar development, equation (4.12) can be adapted to obtain the expression of the recovered PAM symbols $\widehat{\boldsymbol{a_{b,n}}}$ of all users in a block $\boldsymbol{b}$ when a CFO r is applied, as follows:

$$\widehat{\boldsymbol{a_{b,n}}}(m) = \Re\left[\sum_{(l,s)\in\Omega_1}\sum_{(p,n)\in\Omega_2} i^{-p}F_{g_{l,s}}\left(p+r, n\frac{M}{2}\right)\times(-1)^{n(m-p)}\boldsymbol{a_{b,n}}(m-p)\right] \tag{4.48}$$

where $\Omega_2 = \left[-\frac{M}{2}, \frac{M}{2}-1\right]\times[0, N_s-1]$, and

$$F_{g_{\ell,s}}(p,n) = \sum_{k=0}^{M-1} g_\ell(k)g\left(k+n+sM\right)e^{-i\frac{2\pi s\ell}{N_{UF}}}e^{-i\frac{2\pi kp}{M}}$$

Hence, the SIR expression arising from a CFO of r for the OSB receiver becomes:

$$\mathbf{SIR_{OSB,CFO}}(r) = \frac{\left(\sum_{(l,s)\in\Omega_1}\sum_{n=0}^{Ns-1}\Re\left(F_{g_{l,s}}\left(r,n\frac{M}{2}\right)\right)\right)^2}{\sum_{(l,s)\in\Omega_1}\sum_{(p,n)\in\Omega_2^0}\Re\left(\mathrm{i}^{-p}F_{g_{l,s}}\left(r,n\frac{M}{2}\right)\right)^2} \tag{4.49}$$

4.3.3 Analysis of the asymptotic behavior

When the number of antennas at the BS tends to infinity, the channel distortions tend to average out. As a result, the Signal-to-Intereference plus noise ratio (SINR) saturates at a predetermined

level depending on system parameters. This establishes an upper limit for the SINR performance of the system. We will determine its analytical expression. For that, we neglect the effect of noise, because the noise contribution fades away in an asymptotic regime. By adapting equations (4.2) and (4.3), in the presence of multipath and absence of noise the received signal at the j^{th} BS antenna can be expressed as

$$\begin{aligned} r_j(k) &= \sum_{l'=0}^{L-1}\sum_{u=0}^{U-1}\sum_{n'=-\infty}^{+\infty}\sum_{m'=0}^{M-1} a_{n',m'} g_{m'}(k - n'\frac{M}{2} - l') \times \phi_{n'}(m') h_{j,u}(l') \\ &= \sum_{u=0}^{U-1}\sum_{n'=-\infty}^{+\infty}\sum_{m'=0}^{M-1} a_{n',m'} g_{m'}(k - n'\frac{M}{2})\phi_{n'}(m') * h_{j,u}(k) \end{aligned} \tag{4.50}$$

where $(*)$ denotes a linear convolution, $h_{j,u}(l')$ is the channel impulse response between a user u and the j^{th} BS with $l' \in [0, L-1]$, L is the total number of paths, and $g_m(k) = g(k)e^{j\frac{2\pi mk}{M}}$ is the PF modulated to center frequency of subcarrier m. Equivalently, for N_{Rx} antennas the previous equation can be written as

$$\boldsymbol{r}(k) = \sum_{n'=-\infty}^{\infty}\sum_{m'=0}^{M-1} \phi_{n'}(m') \times P' \times \boldsymbol{a_{n',m'}} \tag{4.51}$$

where

$$P' = \begin{bmatrix} P_{1,1}(k) & \dots & P_{1,U}(k) \\ \vdots & \ddots & \vdots \\ P_{N_R,1}(k) & \dots & P_{N_R,U}(k) \end{bmatrix}$$

$P_{j,u}(k) = g_{m'}(k - n'\frac{M}{2}) * h_{j,u}(k)$, and $\boldsymbol{a_{n',m'}} \in \mathbb{C}^{U\times 1}$ is a vector containing all transmitted data symbols of the users at subcarrier m' and at time index n'. Adapting (4.36) we have

$$\boldsymbol{Y}_n(m,\ell) = \boldsymbol{C_n(m)} \times \sum_{s=0}^{N_{UF}-1}\left(\sum_{n'=-\infty}^{\infty}\sum_{m'=0}^{M-1} H_{mm',nn'} \times \boldsymbol{a_{n',m'}}\phi_{n'}(m')\right) \tag{4.52}$$

where $\boldsymbol{H_{mm',nn'}}$ is an $N_{Rx} \times U$ matrix that can be expressed as

$$\boldsymbol{H_{mm',nn'}} = \begin{bmatrix} H^{1,1}_{mm',nn'} & \dots & H^{1,U}_{mm',nn'} \\ \vdots & \ddots & \vdots \\ H^{N_R,1}_{mm',nn'} & \dots & H^{N_R,U}_{mm',nn'} \end{bmatrix} \tag{4.53}$$

along with

$$H^{j,u}_{mm',nn'} = g_{m'}(p'_{n-n'}) * h_{j,u}(p'_n) * g_{m,\ell}(k)$$

and

$$g_{m,\ell}(k) = (-1)^{\ell} e^{-i\frac{2\pi s\ell}{N_{UF}}} \sum_{k=0}^{M-1} g(k) e^{-i\frac{2\pi km}{M}}$$

Similarly, interference is limited to only neighboring FBMC symbols. Hence, (4.52) becomes

$$\boldsymbol{Y}_n(m,\ell) = \boldsymbol{C_n(m)} \sum_{s=0}^{N_{UF}-1} \left(\sum_{(q,m')\in\Omega_3} H_{mm',n(n-q)} \times \boldsymbol{a_{n-q,m'}} \phi_{n-q}(m') \right) \tag{4.54}$$

where $\Omega_3 = [-1,1][0,M-1]$.

Adapting equations (4.7) and (5.11), the estimated data symbols of the users will be

$$\begin{aligned} \widehat{\boldsymbol{a}}_{n,m} &= \mathrm{R}\left[\sum_{(\ell,s)\in\Omega_1} \boldsymbol{C_n(m)} \times \sum_{(q,m')\in\Omega_3} \boldsymbol{H_{mm',n(n-q)}} \times \boldsymbol{a_{n-q,m'}} \phi_{n-q}(m') \phi_n^*(m) \right] \\ &= \mathrm{R}\left[\sum_{(\ell,s)\in\Omega_1} \sum_{(q,m')\in\Omega_3} \boldsymbol{G_{mm',n(n-q)}} \boldsymbol{a}_{n-q,m'} \times \phi_{n-q}(m') \phi_n^*(m) \right] \end{aligned} \tag{4.55}$$

where $\boldsymbol{G_{mm',nn(n-q)}}$ is an $U \times U$ matrix defined as $\boldsymbol{C_n(m) H_{mm',n(n-q)}}$.

In order to compute the elements of $\boldsymbol{G_{mm',n(n-q)}}$ in the asymptotic regime, let us recall the law of large numbers in probability theory. Let a and b be two random vectors each with n identically independent elements. As a result of the law of large numbers (i.e as n tends to infinity), the random variable $\frac{1}{n} a^H b$ will almost converge to $Cab = E[a_i^* b_i]$, with $i = 1, ..., n$.
Similarly, in our case when the number of antennas at the BS N_R tends to infinity, the law of large numbers can be used to compute the elements of $\boldsymbol{G_{mm',n(n-q)}}$.
The ZF equalizer matrix is defined as $\left(\boldsymbol{H_m}^H \boldsymbol{H_m}\right)^{-1} \boldsymbol{H_m}^H$, where $\boldsymbol{H_m}$ is the matrix of channel coefficients of the center of the m^{th} subcarrier (i.e $H_m^{j,u} = \sum_{l'=0}^{L-1} h_{j,u}(l') e^{-j\frac{2\pi m l'}{M}}$).
Note that $\left(\frac{1}{N_R} \boldsymbol{H_m}^H \boldsymbol{H_m}\right)^{-1}$ tends to $\boldsymbol{I_U}$ as N_R tends to infinity. Then according to the previously introduced law of large numbers, the elements in $\boldsymbol{G_{mm',n(n-q)}}$ will converge to

$$G^{u,u'}_{mm',n(n-q)} \rightarrow \mathbb{E}\left\{ \left(H_m^{j,u}\right)^* H^{j,u'}_{mm',n(n-q)} \right\} \tag{4.56}$$

Substituting the value of $H^{j,u}_{mm',n(n-q)}$, then (4.56) will be

$$G^{u,u'}_{mm',n(n-q)} \rightarrow g_{m'}(p'_q) * \mathbb{E}\left\{ \left(H_m^{j,u}\right)^* h_{j,u'}(p'_n) \right\} * g_{m,\ell}(k) \tag{4.57}$$

where

$$\begin{aligned} \mathbb{E}\left\{ \left(H_m^{j,u}\right)^* h_{j,u}(p'_n) \right\} &= \sum_{l'=0}^{L-1} \mathbb{E}\left\{ h^*_{j,u}(l') h_{j,u'}(p'_n) \right\} e^{j\frac{2\pi l' m}{M}} \\ &= \rho_u(p'_n) e^{j\frac{2\pi p'_n m}{M}} \delta^{uu'} \\ &= \rho_{m,u}(p'_n) \delta^{uu'} \end{aligned} \tag{4.58}$$

where $\rho_{m,u}(l') = \rho_u(l') e^{j\frac{2\pi l' m}{M}}$ is the channel Power Delay Profile (PDP) of the u^{th} user modulated to the m^{th} subcarrier.
The left hand side term of (4.58) tends to zero when $u \neq u'$. This is due to the fact that the

effect of multi-user interference vanishes as the number of antennas at the BS tends to infinity. However, residual self interference is experienced by the user when $u = u'$. Therefore, for a given user u and starting from (4.57), the equivalent CIR between the transmitted data symbols at subcarrier m' and the received ones at subcarrier m tends to

$$g_{m'}(p'_q) * \rho_{m,u}(p'_n) * g_{m,\ell}(k) \tag{4.59}$$

As a result, the SINR for a user u saturates to

$$\mathbf{SINR}^{u}_{m,n} \rightarrow \frac{\sum_{(l,s)\in\Omega_1} \Re^2\left\{G_{mm,nn}\right\}}{\sum_{(l,s)\in\Omega_1} \sum_{(m',q)\in\Omega\neq(m,0)} \Re^2\left\{G_{mm',n(n-q)}\right\}} \tag{4.60}$$

4.4 Performance evaluation and comparisons of the considered methods

In this section, we first describe the used filtered discrete channel model, the simulation tool and the antenna array structure. Then, the performance of the FBMC-OS and FBMC-OSB receivers, using the NPR1 short PF, is evaluated in the context of mMIMO. Several channel impairments are considered such as timing offsets, Doppler effect, and carrier frequency offsets. The results are then compared to the OFDM waveform with 4 and 16-QAM. In our simulations, the CSI is assumed to be perfectly estimated at the receiver side. Furthermore, the number of non-truncated filter coefficients is set to $N_G = 7$ for an SIR of 55 dB [130]. For the FBMC-OS-based receivers, the up-sampling factor used for the OS technique is set to $N_{UF} = 4$ which is a good compromise between system performance and complexity. The number of FBMC symbols in a block N_s for the FBMC-OSB receiver is set to 7. This is reflected by the OS_4-FBMC and OSB_7-FBMC receiver notations.

4.4.1 Simulation setup

4.4.1.1 Channel model

In rapidly changing environments, a discrete multipath channel model has, in general, a variable number of paths in addition to variable path gains. However, for reference channels it can be assumed that the number of discrete components is constant. Consider a channel model consisting of L paths, then for antenna k, and user u, the channel impulse response $h_u(k,t)$ is given by

$$h_u(k,t) = \sum_{m=1}^{L} b_{m,u}(k)\delta(t - \tau_{m,u}(k)) \tag{4.61}$$

where m is the path index, $\tau_{m,u}(k)$ and $b_{m,u}(k)$ are the path delay and path complex amplitude of the u^{th} user respectively.

According to [131], when the differential delays are small compared to the simulation sampling time T_s or are not integer multiples of T_s, it is advantageous to band limit the channel by design to obtain better simulation properties. Hence, the CIR is band-limited using an ideal

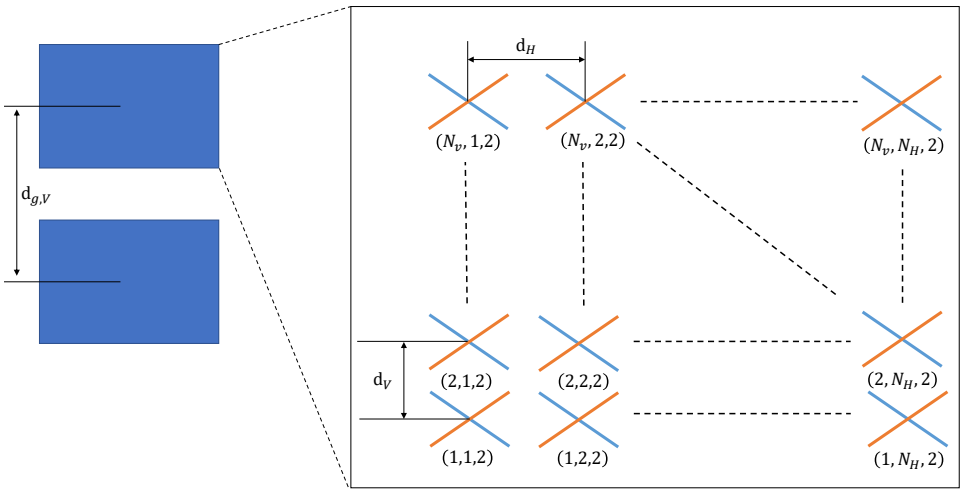

Figure 4.2: Antenna array structure.

rectangular filter. Thus, the filtered discrete channel impulse response is given by

$$\tilde{h}(k,n) = \sum_{m=1}^{L} b_{m,u}(k) sinc(\frac{\tau_{m,u}(k)}{T_s} - n) \tag{4.62}$$

where $-N_1 \leq n \leq N_2$, N_1 and N_2 are the tap indices chosen such that $\tilde{h}(k,n)$ is small when n is less than N_1 or larger than N_2, and $sinc(x) = sin(x)/x$ [131]. In our simulations, the tap indices are chosen such that the value of $\tilde{h}(k,n)$ at the relevant tap indices is larger by at least 1% of its maximum.

According to [132], if the maximum distance between antenna elements divided by the speed of light ($d_{\max}/c$) is much smaller than $\frac{1}{B}$ value, where B is the transmission BW, the delay value can be assumed independent of antenna index k, i.e. $\tau_{m,u}(k) = \tau_{m,u}$.

4.4.1.2 Simulation tool

For our simulations, the 5G QuaDRiga simulation tool explained in Chapter 2 is used to generate realistic radio channels. Chosen parameters follow the 5G standard [21] with 64 cross-polarized antennas at the BS.

4.4.1.3 Antenna array structure

For the 3D-Urban-Macro Non-Line-of-Sight (Uma-NLOS) and 3GPP-38.901-Rural Macro (Rma) models of the 5G QuaDRiga channel, the antenna array at the BS is 25 meters high and consists of two co-located rectangular sub-arrays, each with 32 antennas as in [133]. Each sub-array is denoted by (N_V, N_H, N_P), where $N_H = 2$ is the number of columns, $N_V = 8$ is the number of antenna elements with the same polarization in each column, and $N_P = 2$ is the number of polarization as proposed in [134]. Therefore, with $N_{gV} = 2$ vertical antenna panels, the

Parameters	**Value**
Carrier frequency	3.5 GHz
Cyclic prefix	36
Channel model	'3GPP_3D_Uma'
Channel type	NLOS
Total number of subcarriers	512 subcarriers
Sub-band size	300 subcarriers
Number of UE	4
BS height	25 m
Number of BS antennas	64
Number of vertical/horizontal panels	2/1
Vertical and horizontal antennas spacing	42.85 mm

Table 4.1: Massive MIMO simulation parameters

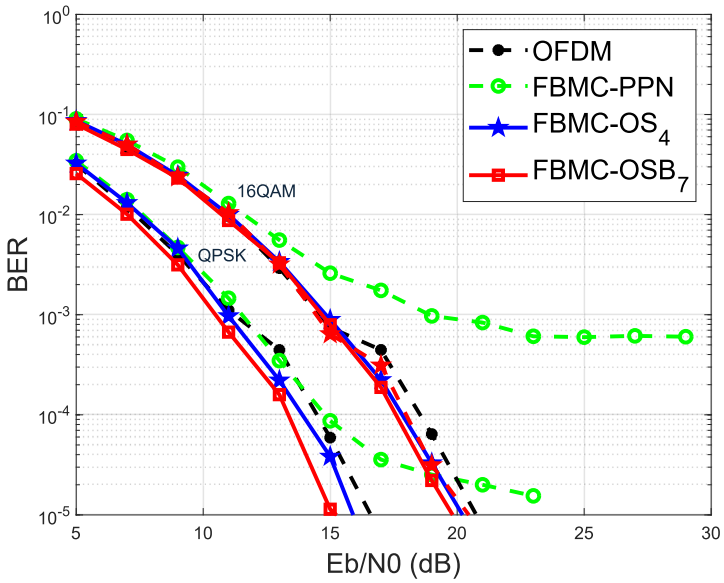

Figure 4.3: BER performance comparison of different receivers over the 5G QuaDRiga fading channel under the '3GPP-3D-Uma-NLOS' scenario', with 4 users and 64 Rx antennas.

number of antennas is calculated as $\{N_{RX} = N_{gV} \times N_V \times N_H \times N_P = 64\}$. With λ being the carrier wavelength, the 2 antenna panels are spaced in the vertical direction with a spacing of $d_{gV} = \lambda$, and the antenna units placed inside each panel are uniformly spaced in the horizontal direction with a spacing of $d_H = 0.5\lambda$ and in the vertical direction with a spacing of $d_V = 0.5\lambda$, where $\lambda = 85.7$ mm for a carrier frequency $f_c = 3.5$ GHz. Specific simulation parameters are summarized in Table 4.1.

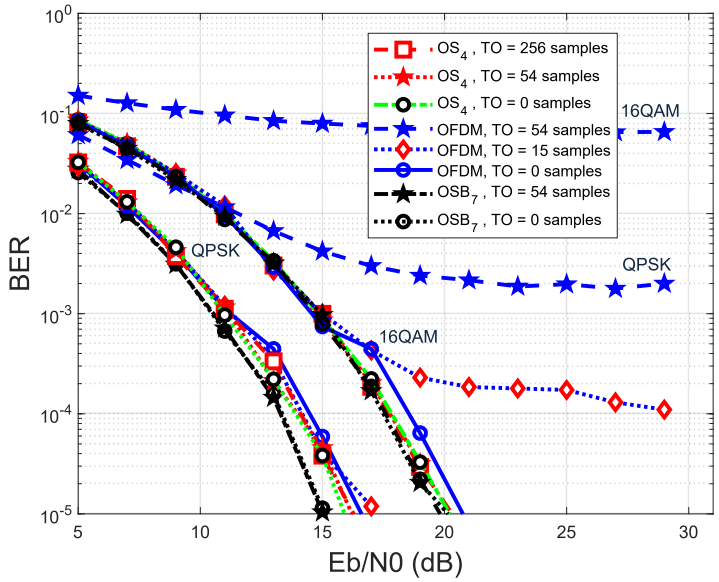

Figure 4.4: BER performance comparison of different receivers in the presence of timing offset over the 5G QuaDRiga fading channel under the '3GPP-3D-Uma-NLOS' scenario', with 4 users and 64 Rx antennas.

4.4.2 Performance over static channel

The BER performance of the OS-based FBMC receivers is compared to OFDM on the 5G channel with the 3D-Uma-NLOS scenario. The channel is considered to be static (i.e: the users are stationary).

4.4.2.1 Performance over multipath channels

Although one of the historic drawbacks of FBMC compared to OFDM resides in the difficulty of efficiently supporting mMIMO systems because of the lack of orthogonality in the complex plane between neighboring OQAM symbols, we can see in Figure 4.3 that OFDM is outperformed by the proposed FBMC waveform thanks to the OS-based FBMC receivers. Indeed, the FBMC-OSB_7 receiver shows the best performance. Furthermore, since the PPN-FBMC technique was widely adopted in prior-art related to mMIMO, it was taken as reference for FBMC proposals. As depicted in Figure 4.3, PPN-FBMC offers the worst performance, suffering from an error floor. This result is expected as it was previously demonstrated with SISO transmissions in [130].

4.4.2.2 Robustness against timing offset

In order to reduce power consumption in future beyond 5G systems, two scenarios can be considered:

- Relaxed synchronization: users transmit data simultaneously. However, because each user

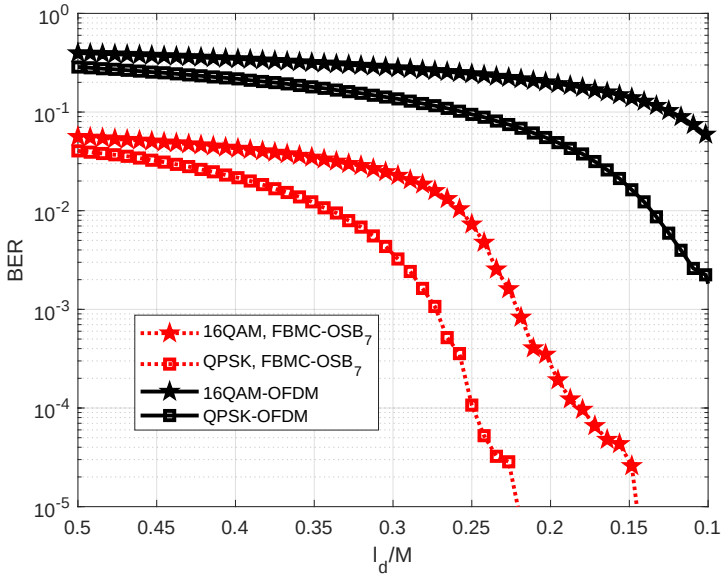

Figure 4.5: Timing offset evaluation in terms of BER for the OSB$_7$-FBMC and OFDM receivers over the 5G QuaDRiga fading channel under the '3GPP-3D-Uma-NLOS' scenario', with 4 users and 64 Rx antennas.

is located at a different geographical distance from the BS, the corresponding signal is affected by a distinct propagation delay. This can result into overlapping signals that lead to intereference. The receiver must be able to compensate for the introduced TO in order to avoid the penalizing effects of interference .

- Asynchronous communication: users transmit independently, hence avoiding any need for a common time reference. In other words, there is no time synchronization among the scheduled users leading to a time mismatch between them that can reach up to 50% of the symbol duration.

In these scenarios, the resulting synchronization errors cause a LPR for each subcarrier. For FBMC and the proposed receivers, this can be totally compensated after CE and equalization. Therefore, if l_d is the time offset in number of samples, then the frequency domain compensation term is expressed as $C_{TO}(m) = e^{-i\frac{2\pi m l_d}{N'}}$ where $N' = M$ for OFDM, and $N' = N_{UF}M$ for the OS-based FBMC receivers. It is assumed that the TO l_d is perfectly known at the receiver side. For our simulations, the receiver is considered perfectly time-aligned when the first sample processed by the FFT is the sample located at the middle of the CP length, so that both positive and negative TO values can be supported.

It is well known that OFDM is highly sensitive to TOs. Therefore, a TO of 15 samples is applied to the OFDM waveform, that corresponds to approximately 42% of L_{CP}. Figure 4.4 shows the BER performance of all considered receivers in the presence and absence of TO. As depicted in the figure, with the 16QAM modulation scheme, the OFDM waveform starts to suffer from a performance degradation. This confirms that OFDM is highly sensitive to TO impairments. After that, a TO of 54 samples is applied that corresponds to 10.55% of the symbol

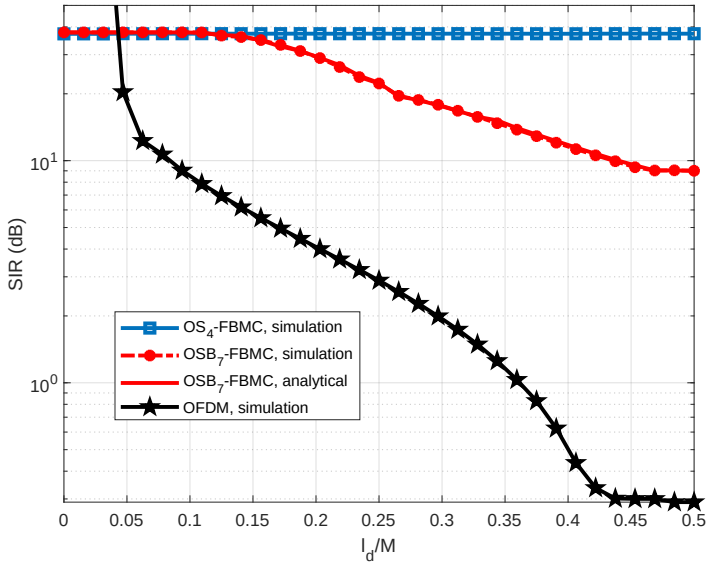

Figure 4.6: SIR evaluation for the OS-based receivers in the presence of TOs with 4 users and 64 receiving antennas.

period and is 3 times greater than the CP size. As depicted in Figure 4.4, unlike OFDM, the OS-based FBMC receivers show robustness against a timing offset of 54 samples where their BER performance wasn't affected at all as shown in the same figure.

Regarding the OS$_4$-FBMC receiver, a TO of 256 samples (half the symbol duration) was applied, and as depicted in the same Figure 4.4, there is no effect observed on the BER performance, which means that the OS$_4$-FBMC receiver is able to support any TO value less than half the symbol duration which makes it adequate for asynchronous communication in the context of mMIMO.

Unlike the OS$_4$-FBMC receiver, the OSB$_7$-FBMC receiver cannot support any TO value less than half the symbol duration, because, for certain TO value the generated interference will no longer be limited, resulting in irreducible errors. Since in the FBMC-OSB receiver, FBMC symbols are transmitted in blocks and demodulated all at once in the frequency domain, the receiver processing window must, to some extent, be aligned with the received blocks. However, because of the ramp-up and ramp-down of the PF, the FBMC-OSB receiver is less susceptible to TO impairments than OFDM.

Actually, in order to know what is the maximum value of the TO such that the OSB$_7$-FBMC receiver will still able to limit interference, we plot in Figure 4.5 the BER performance versus l_d/M of the OSB$_7$-FBMC and OFDM receivers. For this simulation, noise is removed, corresponding to a transmission at infinite SNR.

As depicted in the figure, the OSB$_7$-FBMC receiver with QPSK can support a TO of 22% of the symbol period for an error floor less than 10^{-5}. However, with 16QAM modulation scheme, it can only support a TO up to 14% of the symbol period. For larger TO values, the error floor gradually increases showing that the interference introduced is not limited. However, it is worth noting that the OSB$_7$-FBMC receiver is more robust against TO than OFDM in mMIMO, as it

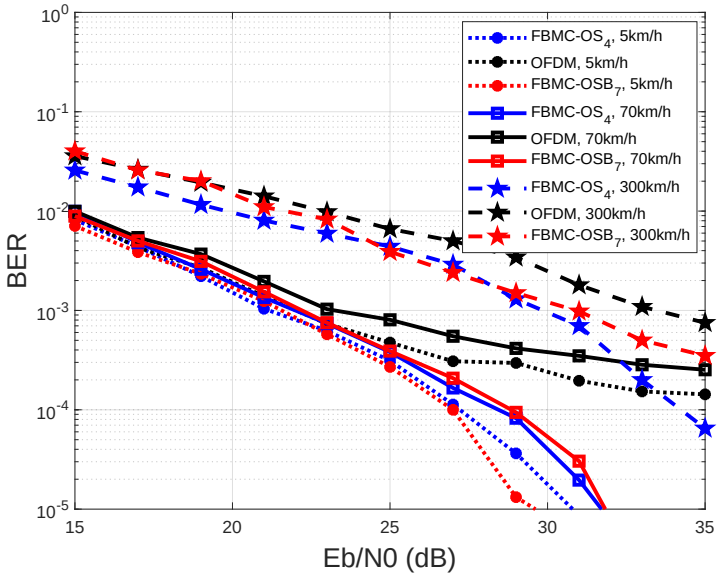

Figure 4.7: BER performance for different receivers over the non-static 5G QuaDRiga fading channel under the '3GPP-3D-Uma-NLOS' scenario', with 4 users and 64 Rx antennas.

was also the case in SISO transmissions [13].

In order to validate the robustness of the OS receivers to TO impairments, we plot in Figure 4.6 the SIR obtained by simulation for the OS_4-FBMC, and the OSB_7-FBMC receivers, as well as the SIR determined by evaluating (4.32) under the 3D-Uma-NLOS scenario. As depicted in the figure, the SIR of the OS_4-FBMC receiver is unaffected by TO, supporting the analytical study performed in Section 4.3.1.1 and the previous simulations on BER depicted in Figure 4.4. Unlike the OS_4-FBMC receiver, the OSB_7-FBMC receiver, cannot support any TO less than half the symbol duration, as illustrated and validated analytically in the same figure. In fact, according to Figure 4.6, the SIR of the OSB_7-FBMC receiver achieves a constant value up to a TO of 12% of the symbol duration, showing that the introduced interference is limited. The SIR gradually decreases as the TO value increases showing that the introduced interference is no longer limited. Finally, OFDM is free from any interference when $l_d < \frac{L_{CP}}{2}$, but it is clearly outperformed by FBMC associated to the OS-based receiver for larger TO values.

4.4.3 Asynchronous communication

The 5G network is designed to accommodate new and highly demanding scenarios such aseMMCs, which requires asynchronous communication. The latter is considered as a cornerstone for grant-free spectrum and massive access, since it allows each user to transmit at an independent time reference without the need for time synchronization among all scheduled users. However, this can lead to time misalignment between users, which may vary within the same subband. To investigate the performance of the FBMC-OS_4 receiver for asynchronous communications compared to OFDM, we consider 4 users transmitting asynchronously in time and then evaluate the BER over the 5G QuaDRiga channel under the 3GPP-38.901-Rma scenario with a cell radius of 10 km, as shown in Figure 4.8. Both receivers show similar BER performance when the users are perfectly

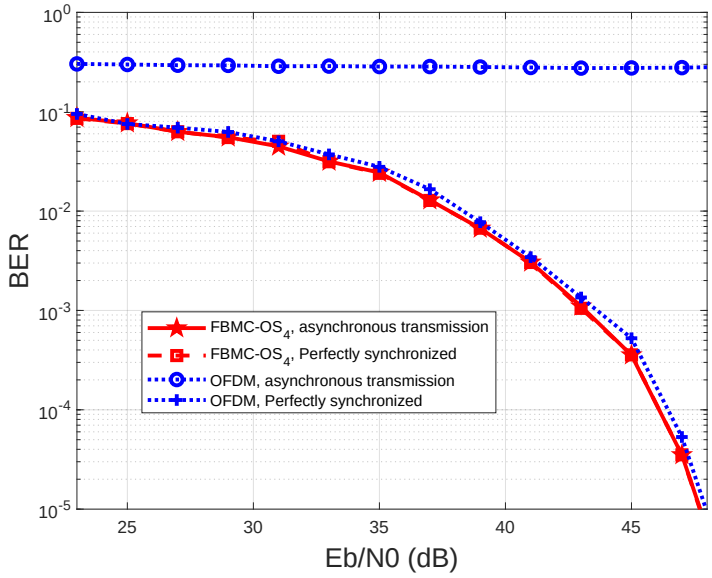

Figure 4.8: BER performance comparison for asynchronous transmissions over the 5G QuaDRiga channel under the 3GPP-38.901-Rma scenario with 4 users and 64 receiving antennas.

synchronized, but when users send signals at independent time references within the same band, OFDM suffers from an irreducible error floor, while the BER performance for the FBMC-OS_4 receiver remains unaffected, showing the same performance as perfectly synchronized users. This confirms the support of the FBMC-OS receiver for asynchronous communications.

4.4.4 Performance over non-static channel

It is well known that OFDM is very sensitive to CFOs caused by Doppler spread/shift [116,135]. In fact, the impact of Doppler spread/shift on the system performance is worse in MU-mMIMO systems since the achievable gains of mMIMO heavily depend on the accuracy of frequency synchronization.

4.4.4.1 Doppler spread

We consider users moving with speeds of 5, 70, and 300 km/h and test the BER performance of FBMC when using the OS-based FBMC receivers compared to OFDM on the non-static 5G channel with the 3D-Uma-NLOS scenario. The results are shown in Figure 4.7. The BER performance is degraded compared to that in a static channel. For a speed of 5km/h, similar BER levels are obtained for all considered receivers when Eb/N0 $<$ 25 dB. However, OFDM shows the worst BER performance when Eb/N0 $>$ 25 dB. Despite the fact that the maximum Doppler shift is substantially less than Δf, OFDM has around a 10^{-4} error floor due to its low frequency localization. Similar observations can be made with a speed of 70 km/h, presented in the same Figure 4.7. OFDM once again shows the worst performance. The OS-based FBMC receivers have similar performance and outperform OFDM. For a speed of 300km/h, the performance is highly degraded for all receivers. The OSB_7-FBMC receiver performs worse than the OS_4-

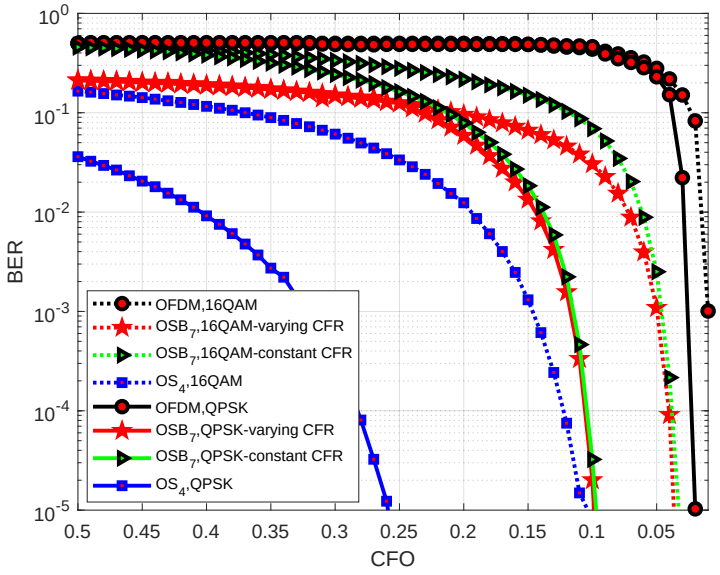

Figure 4.9: Carrier frequency offset evaluation in terms of BER for different receivers with 4 users and 64 Rx antennas.

FBMC receiver, yet it's worth noting how it outperforms OFDM as the latter suffers from an error floor of approximately 10^{-3}. In fact, it's noteworthy how the OS_4-FBMC receiver offers the best performance, but it comes at the expense of system simplicity when compared to OFDM.

4.4.4.2 Robustness against carrier frequency offset

CFO also arises when the transmitter and receiver's local oscillators have a frequency misalignment. which can happen more frequently when employing low-cost equipment. Mathematically, this corresponds to a LPR of the received baseband samples. In reality, CFO causes two types of impairments at the receiver. The first one is the CPE, which may be easily compensated in the frequency domain if the CFO is estimated. The second drawback is ICI, which is caused by frequency domain misalignment of the transmitter and receiver PFs. The second drawback is a significant problem for OFDM because of its low frequency localization. However, the Frequency Domain Compensation (FDC) technique can be used to compensate the CFO for FBMC [130], resulting in a large reduction in the ICI caused by the CFO. This is a key benefit for FBMC since it relaxes the frequency synchronization requirement, allowing for higher speeds and the use of low-cost oscillators. In this regard, we study the robustness of each receiver to CFO resulting from the frequency misalignment of local oscillators.

Figure 4.9 shows the BER performance versus CFO for all receivers without noise (infinite SNR). In this case, the CPE term to compensate is $e^{j\pi nr}$ where r is the CFO relative to Δf, which is assumed to be perfectly known at the receiver side. As expected, OFDM shows the worst performance. In the FBMC-OSB receiver described before, equalization is performed for each FBMC symbol n in a block b. This increases the equalization complexity compared to the OFDM signal, however, allows to accurately compensate fast varying channels. Hence, with QPSK, the OSB_7-FBMC receiver with varying CFR can tolerate a CFO of 10% of Δf for an

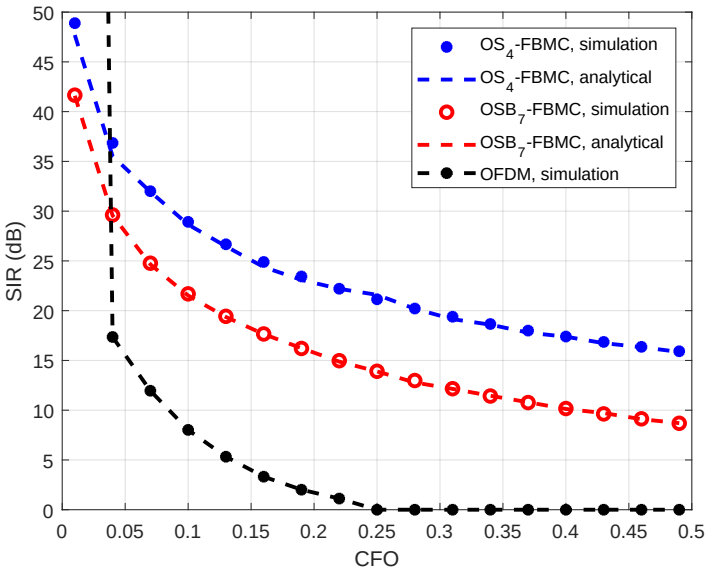

Figure 4.10: SIR evaluation for the OS-based receivers in the presence of CFO.

error floor of around 10^{-5}, however, only 4% of Δf with the 16-QAM modulation scheme. For larger CFO values, the error floor gradually increases showing that the interference introduced is not limited. On the other hand, it is assumed that the equalizer coefficients $\boldsymbol{C_{b,n}}(m)$ in (4.10) are independent of n ($\boldsymbol{C_{b,n}}(m) = \boldsymbol{C_b}(m)$). This means that the channel is constant over a block b in the OSB$_7$-FBMC receiver, which reduces the equalization complexity but degrades the performance at larger CFOs as shown in the same figure. The OS$_4$-FBMC receiver offers the best performance, where it can support a CFO of 26% and 10% of Δf with the QPSK and 16QAM modulation schemes respectively for an error floor around 10^{-5}.

In order to validate the accuracy of our analytical study for the OS-based receivers in the presence of CFO impairments, we plot in Figure 4.10 the SIR obtained by simulation for the OS$_4$-FBMC and the OSB$_7$-FBMC receivers, as well as the SIR determined by evaluating equations (4.47) and (4.49). The results are then compared to the OFDM receiver. As depicted in the figure, the OS receiver is more robust than the FBMC-OSB receiver against CFOs. The simulation results are confirmed analytically as depicted in the same figure. Concerning OFDM, the SIR simulation results also confirm its high sensitivity to CFOs compared to the OS-based FBMC receivers.

4.4.5 Performance in an asymptotic regime

In this section, we PERFORM the analysis carried out in Section 4.3.3 as well as the efficiency of our proposed receivers in an asymptotic regime. The noise level is chosen so that the SNR at the input of the BS antennas is equal to 10 dB. Note that, the noise contribution fades away as the number of antennas at the BS tends to infinity. The NPR1 PF is used unless explicitly mentioned otherwise. Figure 4.11 compares the SINR performance for different FBMC receivers over different channels and OFDM is chosen as a benchmark. First, we compared the saturation

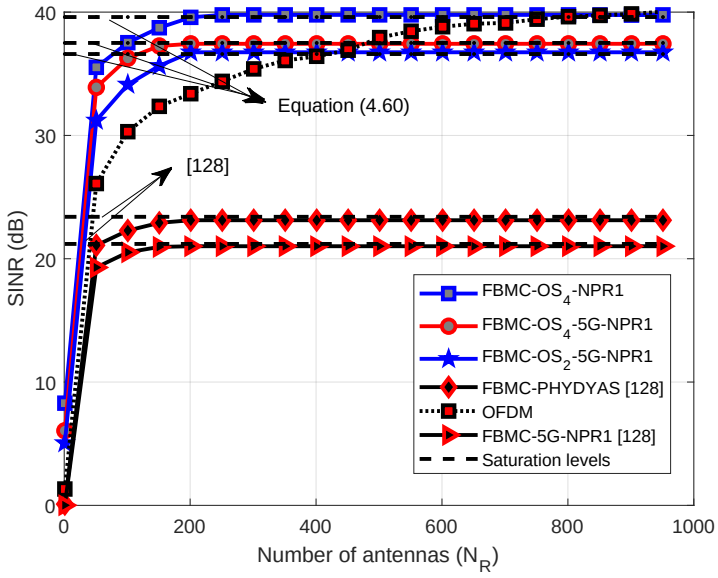

Figure 4.11: SIR saturation level comparison for different FBMC receivers considering different channels with 4 users and 64 receiving antennas.

level for the OS receiver achieved in (4.60) to that obtained in [128]. For that, the same channel (delay spread = 40 samples) and parameters are used for a fair comparison.
As depicted in the figure, the saturation level obtained for the OS_4-FBMC receiver is 16.2 dB larger than the one obtained in [128]. This confirms the superiority of the FBMC-OS receiver since it was also confirmed analytically using (4.60) and equation (17) in [128]. It is worth noting that the delay spread (40 samples) of the channel is slightly larger than the CP duration of OFDM (36 samples). Although this represents only a difference of 10%, OFDM fails to outperform the OS_4-FBMC receiver.

It is worth noting that the channel used in [128] is non-realistic and a lower saturation level might be obtained over a realistic one. For that, we compare the SIR saturation level of the OS_4-FBMC receiver to that of a PPN receiver over the 5G channel in the 3D-Uma-NLOS scenario. As depicted in the same figure, the SIR saturation level decreased by around 2.2 dB with the PPN receiver and by 2.1 dB for the OS_4-FBMC receiver. Using a different up-sampling factor for the OS receiver will decrease the SIR saturation level by around 1.1 dB as was confirmed also by simulation.

4.4.6 Performance in the presence of adjacent interferers

It is well known that the MU interference vanishes in mMIMO systems. Therefore, in this subsection, we consider a communication in which several users transmit data on adjacent frequency bands. However, the communication is done asynchronously in time. As a result, signals arrive with random delays.

In this scenario, we examine 3 transmission channels operating in parallel on 1.5 MHz bands (i.e 4.5 MHz). The second transmission will be considered as the “main” transmission which will be demodulated by the receiver. The other two transmissions will be treated as interferers

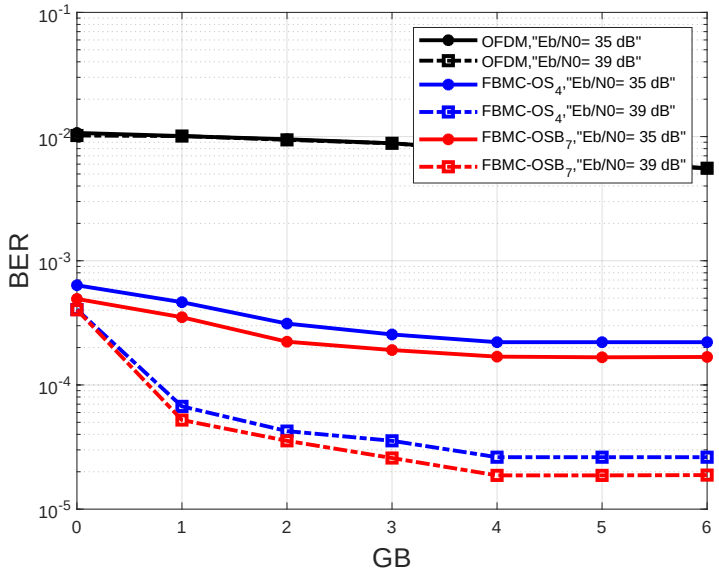

Figure 4.12: Comparison of performance versus GB size for all receivers over the 5G QuaDRiga fading channel under the '3GPP-3D-Uma-NLOS' scenario' considering $P_s = 0$ dBW, 3 users, 64 Rx antennas and different E_b/N_0 values.

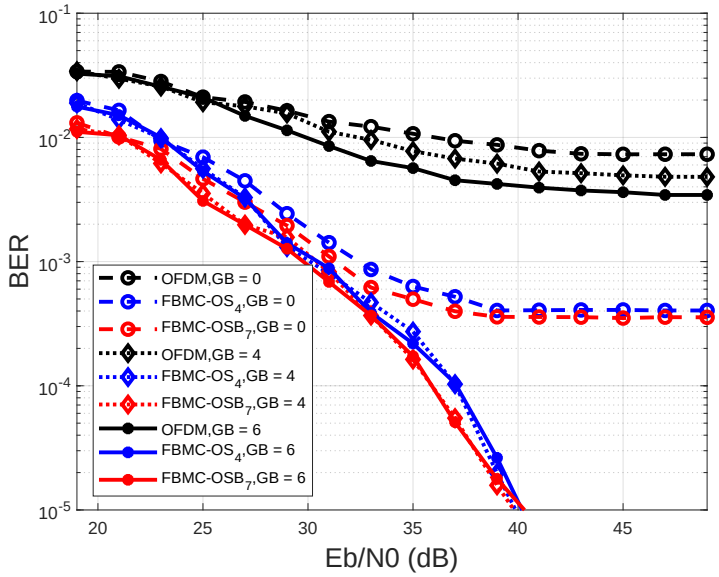

Figure 4.13: BER performance comparison for all receivers over the 5G Quadriga fading channel under the '3GPP-3D-Uma-NLOS' scenario' considering $P_s = 0$ dBW, with 3 users, and 64 Rx antennas.

with the main transmission. The transmit powers of all transmissions are assumed to be equal and normalized to $P_s = 0$ dBW.

Figure 4.13 compares the BER performance of all receivers in the context of mMIMO. Several GB lengths (in number of subcarriers) are considered. With no GB (GB = 0), the performance of all receivers is highly degraded due to the high level of interference resulting from adjacent transmissions. Therefore, it is essential to introduce GBs to limit interference at the

cost of a reduction in the transmission rate. A compromise between system performance and achieved throughput is hence applied.

When GB = 4, OFDM shows the worst performance due to the low frequency localization of OFDM where it is highly affected by the adjacent interferers leading to the highest error floor when compared to FBMC. However, FBMC augmented by the OS-based receivers is more robust against adjacent interferers thanks to the frequency localization of the NPR1 PF.

Similar conclusions can be made with GB = 6. Actually, it is worth noting that the BER performance of the OS_4-FBMC and the OSB_7-FBMC receivers is unaffected. This is because there is no interference stemming from adjacent transmissions. In fact, in order to know how many GBs are necessary to avoid any adjacent interference for the OS-based FBMC receivers, we plot in Figure 4.12 the BER performance of all considered receivers versus the GB size at E_b/N_0 = 35 dB and 39 dB. For E_b/N_0 = 35 dB, the BER performance of the OS-based FBMC receivers remains constant after 4 GBs, implying that all the adjacent interference is avoided. Unlike FBMC, even a GB size of 6 is insufficient to avoid adjacent interference for OFDM.

Similar conclusions can be made with E_b/N_0 = 39 dB. Furthermore, despite the increase in the value of E_b/N_0, OFDM does not improve its results compared to the E_b/N_0 = 35 dB case. Therefore, we can deduce that FBMC augmented by the OS-based receivers requires less GBs than OFDM. Hence, FBMC is more bandwidth-efficient under such a scenario.

4.5 Summary

In this chapter, we extended the OS-based FBMC receivers (FBMC-OS and FBMC-OSB) to support mMIMO technology. This extension aimed to enhance system robustness against long delay spread channels and TOs when using short PFs.

One noteworthy finding is that the FBMC-OS receiver can still support asynchronous communications when short PFs are utilized for mMIMO. On the other hand, the FBMC-OSB receiver, while unable to support asynchronous communications, exhibits superior resilience against TO compared to OFDM. This characteristic makes it an excellent choice for relaxed synchronization, as demonstrated through analytical and simulation studies. Additionally, the FBMC-OSB receiver is less complex than the FBMC-OS receiver when both employ the same FFT size. The proposed analytical derivation of the SINR largely reduces the design time for selecting the OSB receiver parameters during the quest for the best performance/complexity trade-off tailored for the intended application.

When faced with multipath channels, both FBMC-OS and FBMC-OSB receivers outperform OFDM. Furthermore, the performed analytical study confirms that the OS-based FBMC receivers are robust against CFOs.

Moreover, we conducted an asymptotic study on the performance of FBMC combined with the proposed receivers in the context of mMIMO systems. The results indicate that increasing the number of BS antennas does not allow the SINR to increase unbounded while still outperforming OFDM.

The validation process shows that the results obtained from the proposed analytical study align with those obtained from simulations. Additionally, simulation results verify the superiority of the FBMC OS-based receivers over OFDM in the presence of adjacent interferers.

Considering the additional advantages introduced by the proposed contributions in this chapter, FBMC with short PFs becomes a viable competitor to OFDM in the context of MU-mMIMO and emerges as an appealing solution for meeting the requirements of beyond 5G air interfaces.

Chapter 5

Novel single and multi-user pilot structures and associated channel estimation for FBMC/OQAM systems

Accurate CE plays a crucial role in harnessing the full potential of mMIMO such as improved SE and resilience against challenging channel conditions, as well as for leveraging the benefits of the MCO technique proposed in Chapter 3. Unlike OFDM, FBMC/OQAM shows only real-field orthogonality. Therefore, corresponding signals suffer from intrinsic interference, penalizing its reliability and motivating the use of alternative CE techniques. Furthermore, typical CE methods for mMIMO-FBMC systems require large training overheads, particularly for a large number of users or for flat-fading channel conditions over each subcarrier band. To address these issues, we propose in this chapter a preamble-based PS that reduces the training overhead by interleaving user pilots in frequency while re-introducing the possibility of applying conventional OFDM CE techniques, particularly the LS method in the context of SU and MU scenarios. Performed simulations over the 5G QuaDRiga channel show that the proposed PS improves SE while delivering the best performance in both preamble-based MU-mMIMO and SU systems. Furthermore, the proposed method significantly improves SE compared to the available solutions in the literature that require a large number of GBs for separating the pilots of different users, while enabling the usage of conventional CE techniques for OFDM.

5.1 Relevant Pilot structure and CE techniques

The CE process in FBMC/OQAM systems differs from that in traditional OFDM systems due to the loss of complex orthogonality. The majority of current CE methods rely on the frequency domain model with the IAM approach and assume that the symbol period is significantly greater than the maximum channel delay spread [136]. Alternative methods include time domain models where the frequency domain pilots are utilized to estimate the time domain CIRs with no constraint on the length of the symbol interval [137] [96] [97]. This section presents a detailed description of the aforementioned models that exist in the literature. Then we propose a novel PS design that permits employing conventional CE techniques and shows significant advantages in terms of performance and SE.

5.1.1 Frequency domain models

Considering a time-invariant channel, the received signal can be expressed as follows:

$$r(k) = h(k) * s(k) + \eta(k) \tag{5.1}$$

where h is the CIR, $\eta(k)$ is the AWGN term, and s is the transmitted signal defined in (2.12). By assuming that the preamble pilots have time index $n = 0$, and are not subject to interference by the data symbols due to the insertion of enough GBs in-between, the received pilot on the m^{th} subcarrier is obtained by [136]

$$\hat{a}_{m,0} \approx H_{m,0}\left(a_{m,0} + a^{c}_{m,0}\right) + \eta_{m,0} \tag{5.2}$$

where $a^{c}_{m,0}$ represents the intrinsic interference and is expressed as follows:

$$\begin{aligned} a^{c}_{m,0} &= \sum_{i=0, i\neq m}^{M-1} \zeta^{m,0}_{i,0} a_{i,0} \\ \zeta^{p,q}_{m,n} &= \sum_{k=-\infty}^{\infty} g_{m,n}[k] g^{*}_{p,q}[k] \\ H_{m,0} &= \sum_{0}^{L} h[k] e^{-2j\pi mk/M} \end{aligned} \tag{5.3}$$

where $H_{m,0} = \sum_{0}^{L} h[k] e^{-2j\pi mk/M}$ represents the complex CFR at the m^{th} subcarrier, L is the total number of paths, g the impulse response of the PF, and $\eta_{m,n}$ is the demodulated noise at the (m, n)-th position given as

$$\eta_{m,n} = \sum_{k=-\infty}^{\infty} \eta[k] g\left[k - n\frac{M}{2}\right] e^{-j2\pi mk/M} \phi^{*}_{n}(m) \tag{5.4}$$

Considering the frequency domain model in equation (5.2), CE based on the IAM method

is given by [136]

$$\widehat{H}_{m,0} = \frac{\hat{a}_{m,0}}{a_{m,0} + a^{c}_{m,0}} \tag{5.5}$$

Indeed, if the channel delay spread is considerably smaller than the symbol interval, the IAM method exhibits favorable CE performance. Nevertheless, if the channel delay spread is not adequately small compared to the symbol interval, the use of the IAM method would lead to significant deterioration in the accuracy of the CE.

The IAM approach is improved in [138] by considering the transmission of purely real and imaginary pilot values. This enhancement is particularly interesting for short PFs as their short duration allows for complete separation of the pilots from the data. A study in [139] shows that when an IAM-based CE technique is employed, FBMC/OQAM with a short PF performs better than OFDM by 2.3 dB and outperforms FBMC/OQAM with a long PF by 0.3 dB. Similar findings are reported in [140]. However, the IAM-based techniques suffer from high PAPR, which makes it vulnerable to non-linear distortions caused by the HPA [141].

5.1.2 Time domain models

As an alternative approach to the frequency domain models, time domain models for CE were investigated. The demodulated pilot symbol at the frequency bin m and time symbol n can be written as

$$\hat{a}_{m,n} = \sum_{k=-\infty}^{\infty} r(k) g(k - n\frac{M}{2}) e^{-j2\pi mk/M} \phi^{*}_{n}(m) \tag{5.6}$$

According to [137], by substituting (2.12), (2.13) and (5.1) in (5.6), the received pilot vector $\boldsymbol{P_r}$ can be expressed as follows:

$$\boldsymbol{P_r} = \boldsymbol{A}\boldsymbol{h} + \boldsymbol{\eta} \tag{5.7}$$

where $\boldsymbol{h} = [h(0), ..., h(L-1)]$ is a vector containing the channel taps, $\boldsymbol{\eta} = [\eta_{0,n}, ..., \eta_{M-1,n}]$ is the noise vector, and A is an $M \times L$ matrix with its entry on the m^{th} row and l^{th} column is defined as

$$\begin{aligned} A(m,l) = \sum_{k=-\infty}^{\infty} \sum_{m'=0}^{M-1} \sum_{n'=-\infty}^{\infty} & a_{m',n'} g\left[k - l - n'\frac{M}{2}\right] \\ & \times g\left[k - n\frac{M}{2}\right] e^{j2\pi(m'-m)k/M} \\ & \times e^{j\pi(m'+n'-m-n)/2} e^{-j2\pi m' l/M}. \end{aligned} \tag{5.8}$$

Added to the filtering operation, the orthogonality of FBMC/OQAM in the real domain leads to a correlation of the noise vector elements in (5.7).
Therefore, the conventional LS CE method used for OFDM systems [142] cannot be readily applied [137]. To solve this issue, the authors in [137] included the channel noise correlation

matrix $\boldsymbol{C}$ in the LS method as follows:

$$\hat{\mathbf{h}} = (\mathbf{A}^{\mathrm{H}}\mathbf{C}^{-1}\mathbf{A})^{-1}\mathbf{A}^{\mathrm{H}}\mathbf{C}^{-1}\mathbf{P}_{\mathbf{r}} \tag{5.9}$$

along with

$$\boldsymbol{C} = \begin{pmatrix} \sigma^2 & \sigma^2\zeta_{0,0}^{1,0} & \cdots & \sigma^2\zeta_{0,0}^{M-2,0} & \sigma^2\zeta_{0,0}^{M-1,0} \\ \sigma^2\zeta_{1,0}^{0,0} & \sigma^2 & \cdots & \sigma^2\zeta_{1,0}^{M-2,0} & \sigma^2\zeta_{1,0}^{M-1,0} \\ \vdots & \vdots & \ddots & \vdots & \vdots \\ \sigma^2\zeta_{M-2,0}^{0,0} & \sigma^2\zeta_{M-2,0}^{1,0} & \cdots & \sigma^2 & \sigma^2\zeta_{M-1,0}^{M-0} \\ \sigma^2\zeta_{M-1,0}^{0,0} & \sigma^2\zeta_{M-1,0}^{1,0} & \cdots & \sigma^2\zeta_{M-1,0}^{M-2,0} & \sigma^2 \end{pmatrix} \tag{5.10}$$

The authors of [137] have shown that applying (5.9) outperforms the frequency domain IAM method. However, extra GBs are necessary to separate the pilot signals of different users in a MU CE scenario, hence penalizing SE.

To avoid GB insertion between the pilots of different users, the authors in [143] proposed an alternative PS that relies on interleaving user pilots in frequency. Following this method, each user employs N_p instead of M pilots, where N_p corresponds to the channel length of a user and three FBMC guard symbols were inserted between the pilots and data symbols to shield the pilots from interference. While spectrally efficient thanks to the the absence of guard symbols, this method leads to intrinsic interference due to the experienced correlation between the estimates of different user channels. To avoid a performance penalty, it is necessary to explicitly consider intrinsic interference when applying (5.9) during the estimation process. However, this leads to a higher computational complexity. Moreover, the authors of [143] simply considered an exponentially decaying channel in their simulations. Therefore, the performance may differ for more realistic channels.

To overcome the aforementioned drawbacks, we propose next a new PS as an alternative efficient solution that enables the use of the conventional LS CE method, improves its accuracy while avoiding guard symbol insertion between user pilots. Moreover, the proposal requires only one FBMC symbol as a guard interval between pilots and data symbols.

5.2 Proposed pilot structure design and channel estimation technique

5.2.1 Single user scenario

One of the pilot sequences used in the 5G NR wireless system is the Zadoff-Chu (ZC) sequence [144]. The latter has a constant amplitude zero autocorrelation (CAZAC) property that is preserved even when it is processed by an IFFT/FFT since the output samples remain a ZC sequence. Moreover, their low PAPR makes them an attractive choice for CE. On the other hand, due to the fact that FBMC systems only exhibit orthogonality within the real domain, it

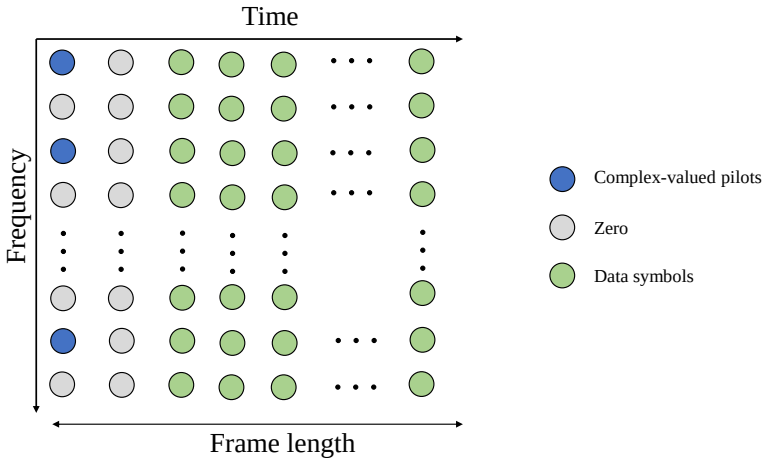

Figure 5.1: Proposed FBMC/OQAM pilot structure for uplink SU CE.

is not possible to load adjacent subcarriers with complex-valued pilots since the latter must be shielded from interference.

To solve this issue, we propose assigning complex pilots to even frequency indices and keeping the neighboring FBMC subcarrier positions vacant or inactive. Therefore, if $\boldsymbol{P} = [a_0(0), a_2(1), ..., a_{\boldsymbol{M}}(M/2)]^T \in \mathbb{C}^{M/2\times 1}$ is a vector containing complex-valued elements generated from a ZC sequence, the transmitted pilots $\boldsymbol{A_T}$ can be expressed mathematically as follows:

$$\boldsymbol{A_T} = \begin{cases} a_m(k) & \text{if } m = 2k, \text{where } 0 \leq k \leq M/2-1 \\ 0, & \text{otherwise} \end{cases} \tag{5.11}$$

along with

$$a_m(k) = e^{\frac{-j\pi k^2}{M/2}} \text{ where } 0 \leq k \leq M/2-1 \tag{5.12}$$

Following the proposed PS, the complex-valued ZC sequences can still be employed for FBMC/OQAM, along with the CE techniques considered for OFDM. However, a sufficient number of guard symbols must be introduced among the training and data symbols to ensure their total isolation, resulting in a data rate loss. In fact, the required number of FBMC guard symbols depends on the overlapping factor of the considered PF. Therefore, we propose to employ the NPR1 short PF since only 1 FBMC symbol is necessary as a guard interval to perfectly isolate the pilots from the data, leading to a minimal data rate loss [12].

Figure 5.1 depicts the proposed PS in the uplink. Using equation (5.1), and by adopting the filtering stage in the time domain, the received pilot symbol can be expressed as in equation (5.7) with the matrix $\boldsymbol{A}$ modified as follows:

$$\boldsymbol{A} = \begin{cases} A_{m,l} & \text{if } m = 2k, \text{where } k \in Z \\ 0, & \text{otherwise} \end{cases}$$

where its entry $A_{m,l}$ on the even subcarrier indices m and l^{th} row is defined in equation (5.8).

As mentioned earlier, the noise correlation must be included in the LS channel due to the lack of complex orthogonality. However, with the suggested PS that employs odd subcarriers as GBs and the short NPR1 PF, the correlation between noise components can be computed as follows:

$$\begin{aligned}\mathrm{Cov}\left[\eta_{m,n},\eta_{m',n'}\right] &= \mathbb{E}\left[\eta_{m,n}\eta^{*}_{m',n'}\right] - \mathbb{E}\left[\eta_{m,n}\right]\mathbb{E}\left[\eta^{*}_{m',n'}\right] \\ &= \mathbb{E}\left[\left(\sum_{k=-\infty}^{+\infty}\eta[k]g[k-n\frac{M}{2}]e^{-j2\pi mk/M}\phi_n(m)\right)\right. \\ &\left.\times\left(\sum_{k=-\infty}^{+\infty}\eta^{*}[k]g[k-n^{'}\frac{M}{2}]e^{j2\pi m^{'}k/M}\phi^{*}_{n'}(m^{'})\right)\right] \\ &= \sigma^2\sum_{k=-\infty}^{\infty}g(k-n\frac{M}{2})g(k-n^{'}\frac{M}{2}) \\ &\times e^{j2\pi(m^{'}-m)\frac{k}{M}}\phi_n(m)\phi^{*}_{n'}(m^{'})\end{aligned} \tag{5.13}$$

where σ^2 is the noise variance.

By making the change of variable $k = k + n\frac{M}{2}$, the previous equation can be rewritten as follows:

$$\begin{aligned}\mathrm{Cov}\left[\eta_{m,n},\eta_{m',n'}\right] &= \sigma^2\sum_{k=-\infty}^{\infty}g(k)g(k+(n-n^{'})\frac{M}{2}) \\ &\times e^{j2\pi(m^{'}-m)\frac{k}{M}}\phi_n(m)\phi^{*}_{n'}(m^{'}) \\ &= \sigma^2(i^{p+q})\sum_{k=0}^{M}g(k)g(k+q\frac{M}{2})e^{j2\pi\frac{kp}{M}}\end{aligned} \tag{5.14}$$

where $p = m - m^{'}$, and $q = n - n^{'}$ with $(p,q) \neq (0,0)$.

Since the NPR1 PF has a short duration in time, the interference only affects adjacent FBMC symbols. This means that the value of q is limited to -1, or 1. Additionally, the proposed pilot structure includes a GB as the neighboring FBMC symbol, making the correlation between noise components negligible in equation (5.14) (i.e., $\mathrm{Cov}\left[\eta_{m,n},\eta_{m',n'}\right] \approx 0$). Therefore, the assumption of uncorrelated noise is valid, and the conventional LS method used in OFDM systems can be applied without considering the noise correlation matrix, reducing the complexity.

Hence, equation (5.9) will reduce to the conventional LS channel estimate as follows:

$$\hat{\mathbf{h}} = (\mathbf{A}^{\mathrm{H}}\mathbf{A})^{-1}\mathbf{A}^{\mathrm{H}}\mathbf{P_r} \tag{5.15}$$

In fact, the estimated CIR above $\hat{\boldsymbol{h}}$ has most of its power concentrated on a few first samples $L^{'}$, and therefore can be divided into two parts as follows:

$$\hat{\boldsymbol{h}_{\boldsymbol{LS}}}(n) = \begin{cases} \boldsymbol{h}(n) + \boldsymbol{\eta}(n), & \text{if } 0 \leq n \leq L^{'} - 1 \\ \boldsymbol{\eta}(n), & \text{otherwise} \end{cases} \tag{5.16}$$

Therefore, it is advantageous to denoise the above channel estimate. Denoising is the process of eliminating noise from a noisy signal. The estimated channel in 5.15 can be observed to be corrupted by noise. Hence, the CIR can be considered as a noisy signal, and denoising it can lead to an improved CIR estimation. Denoising can be performed by pruning the CIR coefficients using a threshold. Hence, we apply an M point Inverse Discrete Cosine Transform-Type-IV (IDCT4) on $\hat{\boldsymbol{h}_{\boldsymbol{LS}}}(n)$. Next, we consider only the first $L^{'}$ taps and pad the rest with zeros. This translates mathematically as follows:

$$\hat{\boldsymbol{h}}^{'}_{\mathbf{LS}}(n) = \begin{cases} \mathbf{IDCT4_M}(\boldsymbol{h}(n) + \boldsymbol{\eta}(n)), & \text{if } 0 \leq n \leq L^{'} - 1 \\ 0, & \text{otherwise} \end{cases} \tag{5.17}$$

where $L^{'}$ is the channel delay spread in samples.

In fact, some channel taps included in the first part of the previous equation may be insignificant. Therefore, to accurately select the significant channel taps, we first estimate the noise power as follows:

$$\hat{\sigma}^2_{\boldsymbol{\eta}} = \frac{1}{N - L^{'}} \sum_{n=L^{'}}^{N-1} |\boldsymbol{\eta}(n)|^2 \tag{5.18}$$

Next, we select the significant channel taps according to the following rule

$$\hat{\boldsymbol{h}}^{'}_{\mathbf{LS}}(n) = \begin{cases} \hat{\boldsymbol{h}}^{'}_{\mathbf{LS}}(n), & \text{if } \beta(n) > \sigma^2_{\boldsymbol{\eta}} \\ 0, & \text{otherwise} \end{cases} \tag{5.19}$$

where $\beta(n)$ is the power of $\hat{\boldsymbol{h}}^{'}_{\mathbf{LS}}(n)$ at tap index n.

Eventually, the CE is then obtained by taking the Discrete Cosine Transform-type-IV (DCT4) of equation (5.19) as follows:

$$\hat{H}_{\mathrm{DCT4}}[m] = \mathbf{DCT4_M}(\hat{\boldsymbol{h}_{\boldsymbol{LS}}}^{'}(n)) \tag{5.20}$$

where $m = 2k$, along with $0 \leq k \leq M/2$

Note that the above equation gives the channel estimate only for the even subcarrier indices since the odd subcarriers were vacant. Therefore, the channel on the odd subcarriers can be interpolated using Makima's method in [145].

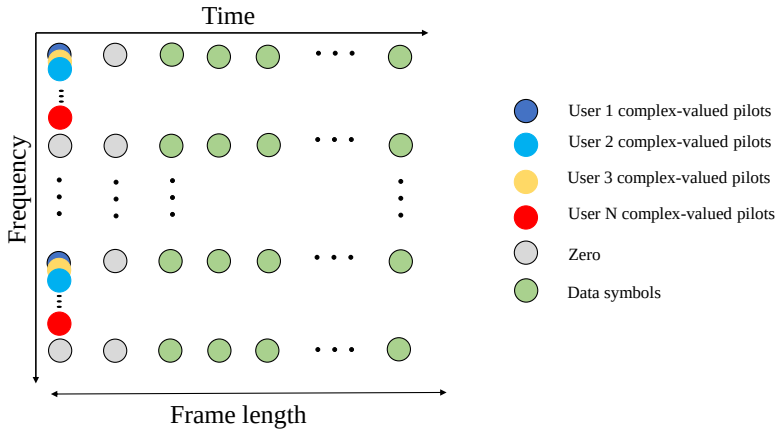

Figure 5.2: Proposed FBMC/OQAM pilot structure for uplink MU CE.

5.2.2 Multi-user scenario

To ensure the orthogonality for the pilots of multiple users in the uplink, guard symbols are typically required. However, most of the available solutions in the literature are not efficient in terms of spectral usage as discussed previously in Section 5.1.2. To address this issue, we extend the SU PS along with the time domain CE technique that was discussed in Section 5.2.1 to a MU uplink scenario. We show how the extended PS reduces MU CE to SU.

In this regard, we propose to circularly shift the pilots of different users within the same band as shown in Figure 5.2. Note that the frequency resources used for pilot signals of different users are mutually inclusive. This means that each frequency slot is used by all users, however, the pilot signal of a user u is a circular shift of the $u+1$ pilot signal. This translates mathematically as follows:

$$\boldsymbol{A}_{\boldsymbol{T_u}} = \begin{cases} a^u_{m,n}(k) & \text{if } m = 2k, \text{where } 0 \leq k \leq M/2 \\ 0, & \text{otherwise} \end{cases} \tag{5.21}$$

along with

$$\begin{aligned} a^{u+1}_{m,n}(k) &= a^u_{i,n}(k) \\ i &= (\mathbf{mod}_{L_{ZC}}(m + \frac{L_{ZC}}{U})) \end{aligned} \tag{5.22}$$

such that

$$\frac{L_{ZC}}{U} \leq DS$$

where **mod** is the modulo operator, $L_{ZC} = \frac{M}{2}$ is the ZC sequence length, and DS is the average delay spread of all users.

The absence of guard symbols between user pilots leads to intrinsic inter-user interference. The presence of this latter translates into an inter-user dependency of the information used for computing the channel estimation. As a result, intrinsic interference from a user u_2 to another user u_1 denoted by $\zeta^{u_1}_{u_2}$ must be considered for CE.

Therefore, with U being the total number of users, the demodulated pilot signal on subcarrier m, time index n can be mathematically expressed as

$$\begin{aligned} p_{m,n} = & \sum_{u=1}^{U} \sum_{l=0}^{L_u-1} \sum_{k=-\infty}^{\infty} \sum_{m'=0}^{M-1} \sum_{n'=-\infty}^{\infty} a^u_{m',n'} g(k-l-n'\frac{M}{2}) \\ & \times g(k-n\frac{M}{2}) e^{j2\pi(m'-m)k/M} e^{j\pi(m'+n'-m-n)/2} \\ & e^{-j2\pi m'l/M} h_u(l) + \eta_{m,n}. \end{aligned} \tag{5.23}$$

where $h_u(l)$ is the u^{th} user CIR of length L_u.

To ease notations, the above equation can be expressed in a vector form as follows:

$$\overline{\boldsymbol{P}} = \overline{\boldsymbol{A}\boldsymbol{h}} + \overline{\boldsymbol{\eta}} \tag{5.24}$$

where

$$\begin{aligned} \overline{\boldsymbol{h}} &= [\boldsymbol{h_1}, ..., \boldsymbol{h_U}] \\ \boldsymbol{h_u} &= [h_u(0), ..., h_u(L_u-1)] \\ \overline{\boldsymbol{P}} &= [\boldsymbol{P_{r_1}}, ..., \boldsymbol{P_{r_U}}] \\ \boldsymbol{P_{r_u}} &= [p_0{}^u, 0, p_2{}^u, 0, ..., 0, p^u_{M/2-2}, 0] \\ \overline{\boldsymbol{\eta}} &= [\boldsymbol{\eta_0}, ..., \boldsymbol{\eta_u}] \end{aligned}$$

and

$$\overline{\mathbf{A}} = \begin{bmatrix} \mathbf{A}_1 & \boldsymbol{\zeta}^{\mathbf{2}}_{\mathbf{1}} & \cdots & \boldsymbol{\zeta}^{\boldsymbol{U}}_{\mathbf{1}} \\ \boldsymbol{\zeta}^{\mathbf{1}}_{\mathbf{2}} & \mathbf{A}_2 & \cdots & \boldsymbol{\zeta}^{\boldsymbol{U}}_{\mathbf{2}} \\ \vdots & \vdots & \ddots & \vdots \\ \boldsymbol{\zeta}^{\mathbf{1}}_{\boldsymbol{U}} & \boldsymbol{\zeta}^{\mathbf{2}}_{\boldsymbol{U}} & \cdots & \mathbf{A}_U \end{bmatrix} \tag{5.25}$$

where $\boldsymbol{A_u}$ is a $\frac{M}{2} \times L_u$ matrix with its m^{th} row and l^{th} column defined as

$$\begin{aligned} A_u(m,l) = & \sum_{k=-\infty}^{\infty} \sum_{m'=0}^{M-1} \sum_{n'=-\infty}^{\infty} a^u_{m',n'} g\left[k-l-n'\frac{M}{2}\right] \\ & \times g\left[k-n\frac{M}{2}\right] \times e^{j2\pi(m'-m)k/M} \\ & e^{j\pi(m'+n'-m-n)/2} e^{-j2\pi m'l/M} \end{aligned}$$

along with $\boldsymbol{\zeta}^{\boldsymbol{j}}_{\boldsymbol{j'}}$ is an $\frac{M}{2} \times L_{j'}$ matrix with its m^{th} row and l^{th} column defined as

$$\begin{aligned}\zeta_{j'}^{j} &= \sum_{k=-\infty}^{\infty}\sum_{m'=0}^{M-1}\sum_{n'=-\infty}^{\infty} a_{m',n'}^{j'} g\left[k-l-n'\frac{M}{2}\right] \\ &\times g\left[k-n\frac{M}{2}\right]\times e^{j2\pi(m'-m)k/M} \\ &e^{j\pi(m'+n'-m-n)/2} e^{-j2\pi m' l/M} \\ &= A_j(\mathbf{mod}_{L_{ZC}}(m+\frac{L_{ZC}}{U}, l)\end{aligned} \tag{5.26}$$

Using equation (5.15), and neglecting noise correlation as previously discussed, the LS CE can be obtained as

$$\hat{\mathbf{h}} = (\overline{\mathbf{A}}^{\mathrm{H}}\overline{\mathbf{A}})^{-1}\overline{\mathbf{A}}^{\mathrm{H}}\overline{\mathbf{P}} \tag{5.27}$$

where $\hat{\mathbf{h}} = [\hat{\mathbf{h}_1}, ..., \hat{\mathbf{h}_U}]$.

In fact, the proposed PS for a MU scenario shifts the intrinsic interference caused by user pilots to the noise part. In other words, the estimated channel in equation (5.27) can be divided into two parts: the CIR part and the noise plus intrinsic interference part. Under the light of this definition, equation (5.16) is modified as follows:

$$\hat{h_{j_{LS}}}(n) = \begin{cases} \hat{h_j}(n) + \eta_j(n), & \text{if } 0 \le n \le L_j - 1 \\ \sum_{j'} \boldsymbol{\zeta}_{\boldsymbol{j'}}^{\boldsymbol{j}} \hat{\boldsymbol{h}_{\boldsymbol{j}}'} + \eta_j(n), & \text{otherwise} \end{cases} \tag{5.28}$$

Next, by adopting equation (5.17) for denoising the estimated impulse response for the i^{th} user, the second part can be neglected, which modifies equation (5.19) to

$$\hat{\sigma}_{\boldsymbol{\eta}}^2 = \frac{1}{i - L'}\sum_{n=L'}^{i-1} |\boldsymbol{\eta}(n)|^2 \tag{5.29}$$

where i is the circular shift applied for the j^{th} user defined in (5.22).

Hence, the intrinsic interference in MU CE can be ignored and therefore, equation (5.25) reduces to a diagonal matrix as follows:

$$\overline{\mathbf{A}} = \begin{bmatrix} \mathbf{A}_1 & 0 & \cdots & 0 \\ 0 & \mathbf{A}_2 & \cdots & 0 \\ \vdots & \vdots & \ddots & \vdots \\ 0 & 0 & \cdots & \mathbf{A}_U \end{bmatrix} \tag{5.30}$$

As a result, the CE for MU reduces to a SU one, where the channel estimate of the u^{th} user can be computed by adopting equations (5.17) (5.19) and (5.20).

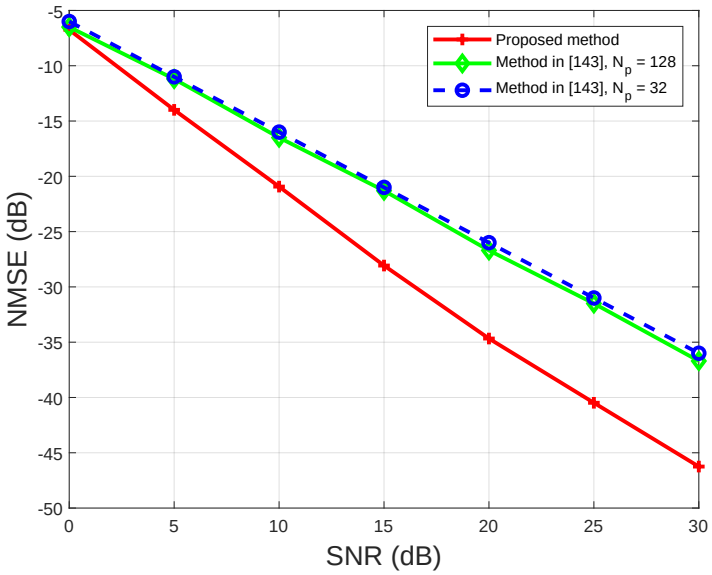

Figure 5.3: NMSE performance comparison of the proposed technique compared with the one in [143] for SU.

5.3 Performance evaluation and comparison

We first evaluate the NMSE and SR of the proposed CE technique for SU and MU scenarios compared to CE techniques presented in the literature [137, 143]. This is followed by a performance evaluation of the proposed CE approach over the multi-path 5G QuaDRiga channel under the 3GPP-3D-Uma-NLOS scenario using BER simulations.

In our simulations, the OFDM and the OS-FBMC receiver using the NPR1 short PF are considered. The number of non-truncated filter coefficients is set to $N_G = 7$ for a SIR of 55 dB [12]. For the OS-FBMC receiver, the upsampling factor N_{UF} is set to 4 leading to the FBMC-OS_4 receiver notation. This choice represents a good compromise between system performance and complexity.

5.3.1 NMSE results

We evaluate in this section the estimation performance of the proposed CE technique compared to that in [137] and [143] for SU and MU scenarios, using the NMSE metric defined as

$$\text{NMSE} = \frac{\sum_{l=0}^{L-1} |\hat{h}[l] - h[l]|^2}{\sum_{l=0}^{L-1} |h[l]|^2} \tag{5.31}$$

We consider 1 user which employs the PS in Figure 5.1, with $M = 128$ subcarriers and 4-QAM modulation. A random channel model with exponential PDP of $\alpha(l) = e^{-\beta l}$ is considered as in [143], where $l \in [0, ..., L-1]$.

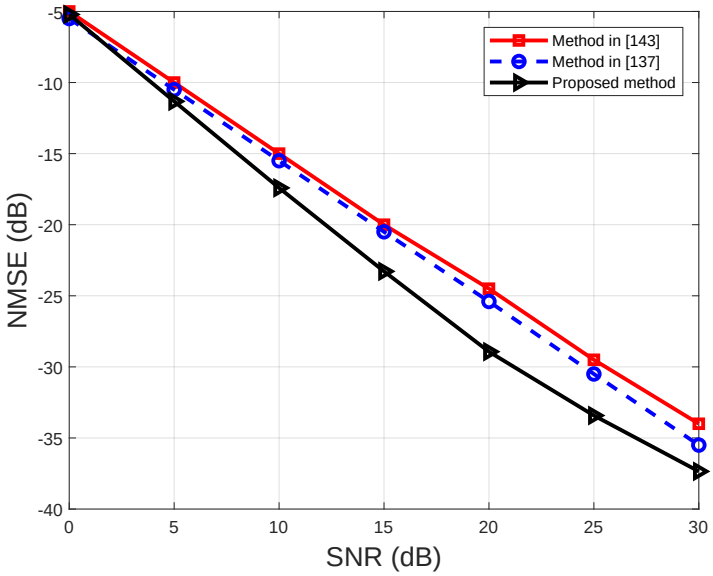

Figure 5.4: NMSE performance comparison of the proposed technique compared with the one in [143] for MU scenario with 4 users.

5.3.1.1 Single user

Figure 5.3 compares the NMSE of the proposed CE technique with SU to that in [143] with $L = 32$. The authors in [143] had already shown that the number of pilots has a negligible effect on the accuracy of the CE. This was also confirmed in our results. Applying the proposed PS and CE techniques described in Section 5.2.1 improves the NMSE when compared to [143] as depicted in the same figure.

5.3.1.2 Multi-user

Figure 5.4 compares the NMSE of the proposed CE technique to that in [143] and [137] for a MU scenario with 4 users and $L = 32$. While not applying any specific processing to target intrinsic interference as described in Section 5.2.1, the proposed PS and CE techniques outperform the competing methods from prior-art while considerably reducing the required complexity.

5.3.2 Sum-rate results

To fully benefit from the advantages of mMIMO technologies, accurate CE is required. While the use of FBMC in mMIMO channels has been proposed in the literature, applying most of the current CE techniques to MU channels can result in a considerable BW efficiency loss. This is because guard symbols are necessary to distinguish between the pilots of various users.

The CE technique described in Section 5.2.2 can be a solution for all the above problems. The insertion of guard symbols between the pilots of various users is not necessary for the proposed solution. In addition, the deployment of training pilots in a highly compact topology allows for simultaneous estimation of all user channel responses at the BS.

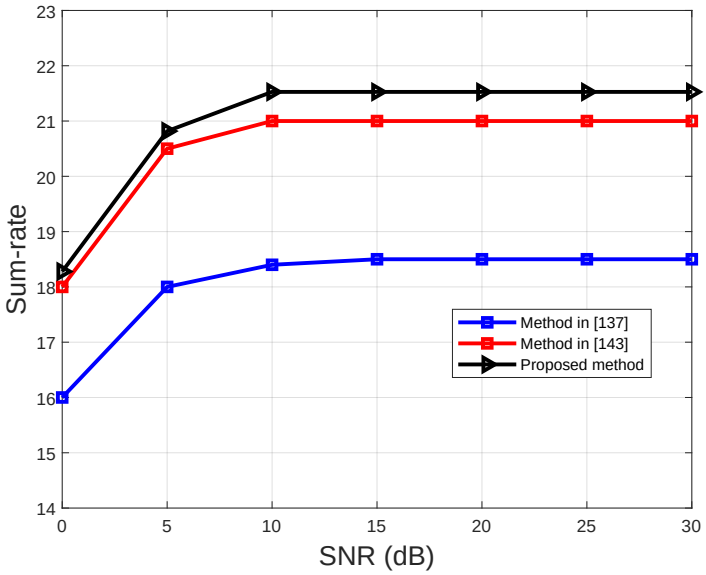

Figure 5.5: SR performance comparison between the proposed technique and that in [143].

To highlight the advantages of the proposed PS in MU-mMIMO scenario, we compare in Figure 5.5 the SR of the proposed technique to that in [143] considering the same channel model defined in Section 5.3.1 with $L = 16$, a frame length of 84 FBMC symbols along with the SR expression defined as follows:

$$\mathrm{SR} = \gamma \sum_{u=1}^{U} \log_2(1 + \mathrm{SINR}_u) \tag{5.32}$$

where γ is the training loss and SINR_u is the signal to interference plus noise ratio of the u^{th} user. From Figure 5.5, we can clearly see that the proposed method exhibits higher SR than the method of [143]. This improvement is due to the fact that the proposed method employs only 2 FBMC symbols for training compared to 4 in [143], added to the improved NMSE performance depicted previously in Figure 5.4.

Figure 5.5 further compares the SR performance to [137] where the latter utilizes 128 subcarriers for estimating each user's channel. This implies that [137] incurs four times the training overhead as compared to our proposed approach. Indeed, this becomes even more significant when the number of users increases.

5.3.3 BER results

We study the performance of the proposed CE technique in terms of BER simulations considering OFDM and the FBMC-OS receiver over the static and non-static 5G QuaDRiga channel in two cases: first by employing the proposed CE technique and second by assuming that the channel is perfectly estimated at the receiver side. Chosen parameters follow the 5G standard [21]. Specific simulation parameters are summarized in Table 4.1 with 2 users rather than 4.

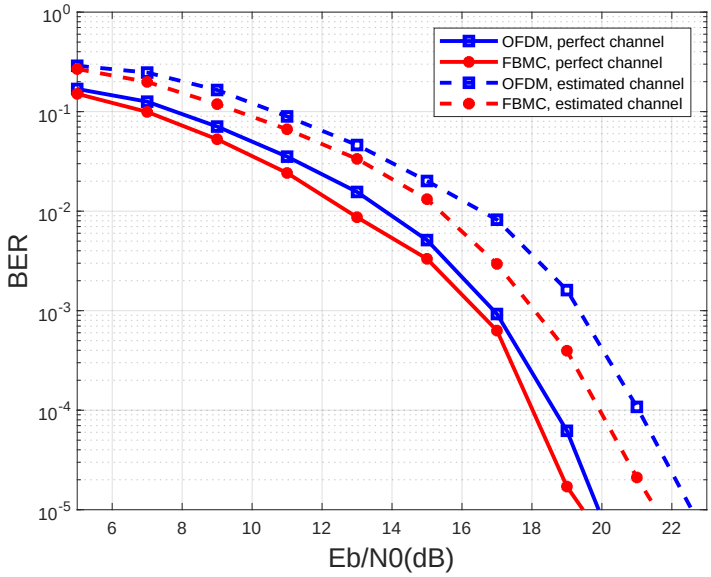

Figure 5.6: BER performance comparison between OFDM and FBMC-OS receiver by employing the proposed CE technique over the 5G QuaDRiga channel under the '3D-Uma-NLOS' scenario with 2 users and 64 receiving antennas.

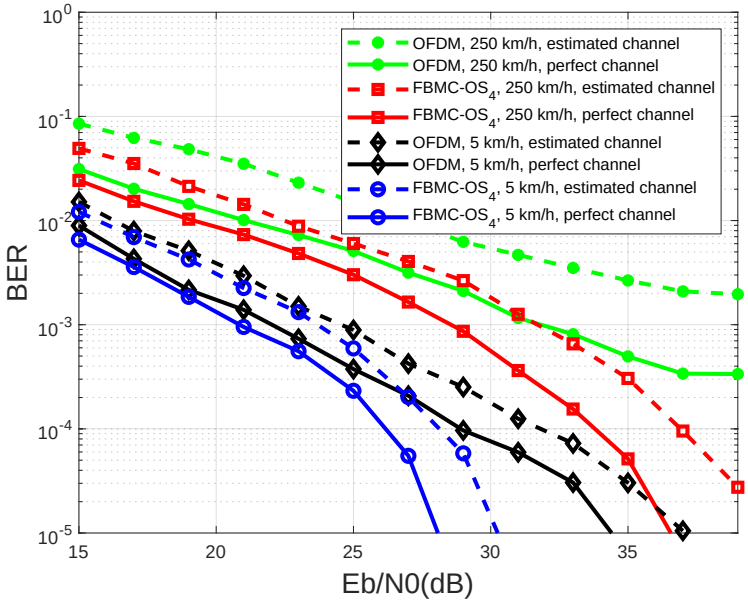

Figure 5.7: BER performance comparison between OFDM and FBMC-OS receiver by employing the proposed CE technique over the non-static 5G QuaDRiga channel under the '3D-Uma-NLOS' scenario with speeds of 5 and 250 km/h, 2 users and 64 receiving antennas.

5.3.3.1 Static channel

Figure 5.6 compares the BER performance of the OFDM and FBMC-OS$_4$ receivers for the two aforemetioned cases. The FBMC-OS4 receiver outperforms OFDM in both cases. Despite the fact that CE has been known to be an open issue for FBMC/OQAM systems due to the absence of complex orthogonality, applying the proposed PS along with the CE technique described in

Section 5.2 outperforms OFDM.

5.3.3.2 Non-static channel

We consider now two users moving with speeds of 5 and 250 km/h and evaluate the BER performance of FBMC when using the OS-based FBMC receivers compared to OFDM. The non-static 5G channel with the 3D-Uma-NLOS scenario was considered for the two aforementioned cases as well. The results are shown in Figure 5.7.

The BER performance is degraded compared to that in a static channel. For a speed of 5km/h, similar BER levels are obtained for the considered receivers when Eb/N0 < 25 dB in both cases. However, OFDM shows the worst BER performance when Eb/N0 > 25 dB.

For a speed of 250km/h, the performance is highly degraded for both receivers. Yet it is worth noting how the OS-$_4$-FBMC receiver outperforms OFDM when employing the proposed CE as shown in the figure. Considering OFDM, the BER performance when emulating the CE technique is further degraded compared to FBMC/OQAM. This is due to its low frequency localization.

5.4 Summary

In this chapter, we proposed a novel PS along with a CE technique for FBMC/OQAM systems considering a SU scenario. In opposition to prior practices, the proposed model does not impose the symbol interval to be much longer than the maximum channel delay spread. We then extended these proposals for a joint MU-CE approach in a MU scenario and mMIMO systems, in which the pilots for different users are interleaved in frequency by a simple circular shift without the need for any guard symbols between them. This results in a high reduction in training overhead which becomes significant when the number of users increases. Accordingly, the proposed method significantly improves SE compared to the available solutions in the literature that require a large number of GB for separating the pilots of different users, while offering the best achievable known performance to date.

Chapter 6

Conclusions and future work

6.1 Conclusions

SE plays a crucial role in mobile communication networks, especially due to the increasing scarcity of spectrum resources and the continuous growth of mobile data traffic. To address the need for SE enhancement, various techniques have been explored in the literature. However, existing techniques that relax the orthogonality condition, such as FTN, have limited performance under severe channel conditions or suffer from high computational complexity.

In this context, a novel transmission technique called MCO is proposed to overcome these limitations in Chapter 3. The MCO technique intentionally overlaps neighboring subcarriers of adjacent users, offering a new approach for SE enhancement. In the context of waveform comparison, two waveforms are considered: OFDM and FBMC/OQAM.

It is found that the MCO-augmented FBMC/OQAM outperforms OFDM over the 5G QuaDRiga channel, both in the presence and absence of TO impairments. FBMC/OQAM achieves a remarkable 66% higher SE gain compared to OFDM. This highlights the superiority of FBMC/OQAM in terms of SE performance and its potential as a waveform candidate for future mobile communication networks.

Indeed, by introducing the MCO technique and demonstrating the advantages of FBMC/OQAM over OFDM, Chapter 3 contributes to the development of efficient SE enhancement techniques for single antenna systems. The proposed approach offers a promising solution for improving SE while addressing complexity issues and the challenges posed by channel conditions, paving the way for more efficient and effective mobile communication systems.

Despite the enhancement of SE through the MCO technique, there is a growing demand for even higher levels of SE in certain 6G applications. To address this concern, leveraging large-scale MIMO systems emerges as a promising solution.

The literature mostly examines the use of PPN and FS receivers with long PFs like MMB4 PF in the context of mMIMO systems. However, these receivers have several drawbacks. Firstly, the PPN receiver exhibits lower performance compared to OFDM. Secondly, the utilization of long PFs augmented by the aforementioned receivers leads to a prohibitivecomputational complexity, hindering its wider adoption.

On the other hand, employing short PFs compromises the ability to support asynchronous communication and results in performance degradation. This is because the performance of FBMC/OQAM over multipath channels depends on the ratio between the delay spread and the filter length.

In recent years, OS-based FBMC receivers have been introduced in the realm of SISO transmissions. These receivers offer several advantages, including improved performance over doubly dispersive channels when using short PFs, specifically the NPR1 PF. Additionally, they exhibit robustness against imperfect synchronization and support relaxed and asynchronous communications.

In this context, Chapter 4 extends the FBMC-OS receiver and its corresponding advantages to the context of mMIMO systems. To reduce computational complexity, the OSB design is further extended for mMIMO systems. Under the assumption that the channel response remains static within a given block, which is plausible in scenarios with low mobility, the equalization complexity is reduced. This is particularly beneficial for mMIMO systems due to the complexity of the equalization step.

Through the performed analytical study, the proposed receivers for mMIMO systems confirm their improved performance over doubly dispersive channels, robustness against CFOs and TOs, and their support of relaxed synchronization and asynchronous communications.

Accurate CE is crucial for maximizing the benefits of mMIMO, such as improved SE and resilience against challenging channel conditions. It is also essential for leveraging the advantages of the MCO technique proposed in Chapter 3.

Unlike OFDM, FBMC/OQAM exhibits only real-field orthogonality. Consequently, the transmitted signals suffer from intrinsic interference, compromising reliability and motivating the exploration of alternative CE techniques.

Furthermore, conventional CE methods for mMIMO-FBMC systems often require large training overhead, especially when dealing with a large number of users or flat-fading channel conditions over each subcarrier band. To address these issues, Chapter 5 proposes a PS that reduces the training overhead by interleaving users' pilots in frequency domain. Conventional OFDM CE technique, particularly the LS method, is employed within the context of SU and MU scenarios.

Simulations conducted over the 5G QuaDRiga channel demonstrate that the proposed PS improves SE while achieving the best performance in both preamble-based MU-mMIMO and SU systems. Additionally, the proposed method significantly enhances SE compared to existing literature solutions that rely on a large number of GBs to separate different users' pilots. Despite using conventional CE techniques, the proposed method outperforms these solutions while reducing the number of required GBs.

6.1.1 Trade-offs

We provide a summary and comparison of the relevant KPIs between the original FBMC/OQAM waveform and the considered variant, highlighting the recent advances proposed in this thesis.

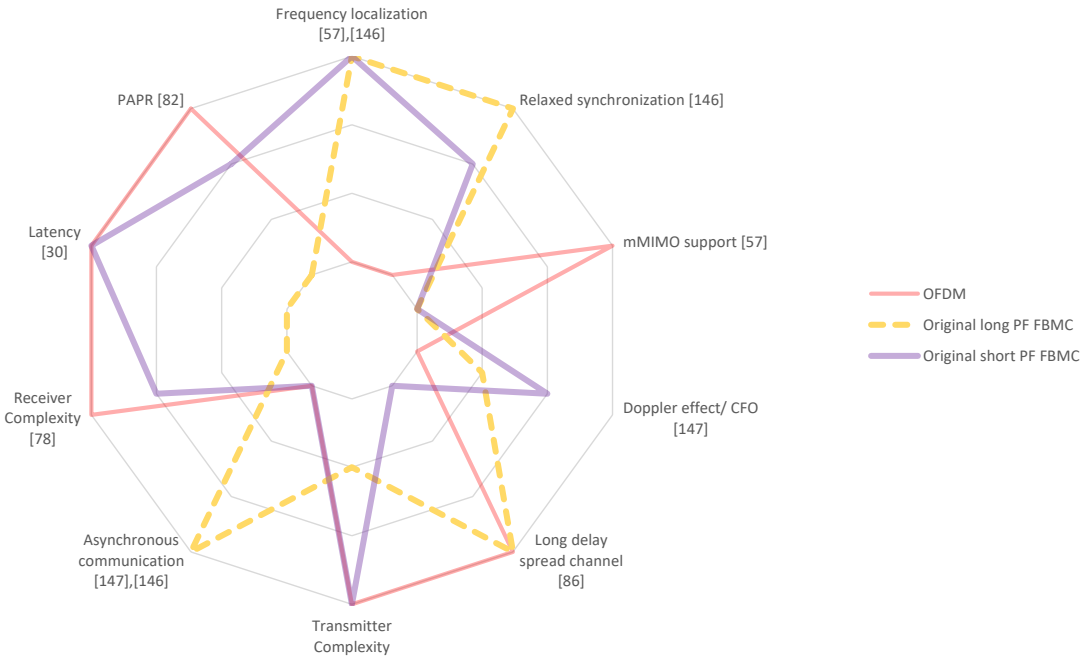

Figure 6.1: Comparison of different properties between original FBMC and OFDM waveforms. A larger circle radius represents a better system performance.

This provides a comprehensive snapshot of the current status of FBMC/OQAM when compared to OFDM.

Fig. 6.1 summarizes the KPIs for the original FBMC with long and short filters and for OFDM. At a first glance, it may seem that the long-filtered FBMC is complementary to OFDM in terms of the selected KPIs. Due to its simple implementation and robustness to multi-path, OFDM has been adopted in multiple standards, including 5G. Despite the aforementioned advantages, OFDM still suffers from several drawbacks, including slightly lower SE and high sensitivity to imperfect synchronization due to its low frequency localization.

Concerning OFDM, the TO at the receiver must be within the CP length to guarantee a reliable communication. However, the propagation delay of the transmitted signal will be constantly changing due to the user and/or transmitter mobility, introducing time-variant TOs. Since the TA mechanism is implemented to overcome such variable timing misalignment in current 5G systems [21], the BS monitors each user's uplink timing, requiring additional hand-shake rounds. However, for mMTC, it is desirable to establish a simplified access procedure that enables GF communication. Therefore, the first requirement derived from the aforementioned problem is asynchronous communication. Yet, the latter cannot be supported by OFDM, which may hinder its adoption in future communication systems requiring ultra-low latency and reliability, such as autonomous vehicles.

The original FBMC associated with long PFs is robust to long-delay spread channels. It also supports asynchronous communications when utilizing a FS-FBMC receiver [146], which is crucial for some 6G-IoT applications, including driver attention monitoring. However, the combined use of a long PF and a FS implementation comes at the cost of a high transceiver complexity. Indeed, on one hand, the computation of a larger FFT is required for the FS-based

Figure 6.2: Radar chart illustrating the set of beyond 5G relevant KPI and tradeoffs for OFDM and several variants of the original and the largely improved FBMC waveforms. A larger circle radius represents a better system performance. The green shaded area corresponds to the flexibility that can be attained by the FBMC-OS receivers, according to the selected parameters N_s and N_{UF}.

implementation, and on the other hand, higher processing capabilities are required for the PPN implementation.

Another well-known drawback of the original FBMC resides in its difficulty to support efficient mMIMO systems and channel estimation techniques due to intrinsic interference [57]. Furthermore, a significant drawback of FBMC employing long PFs resides in the introduction of a ramp-up and ramp-down at the beginning and end of each transmitted frame. Consequently, this results in a higher PAPR level compared to OFDM and compromises the support of short-frame sizes for low-latency communications. Few solutions have been investigated to address the latency problem that came at the cost of an increased transmitter complexity and a higher OOBPL. Therefore, further progress was needed in order to effectively support short frame sizes and low latency with long PFs.

To address complexity problems, short PFs ($K = 1$) including TFL1 and the QMF1 have been previously proposed. Additionally, FBMC with short PFs is more robust against CFO than with long PFs [147]. However, the use of short filters comes with its share of drawbacks, namely a reduced robustness against long-delay spread channels and a lack of support for asynchronous communications [147] which are crucial for low latency applications requiring GF access.

In summary, the introduction of short filters achieves a different KPI tradeoff, especially in

terms of performance/complexity, as seen in Fig. 6.1. Therefore, the ability to devise a flexible FBMC transceiver capable of striking different KPI tradeoffs became particularly appealing in the quest for addressing major FBMC drawbacks while retaining its advantages.

Fig. 6.2 compares the KPIs of the largely improved FBMC/OQAM to that of OFDM and the original FBMC receiver with a long PF. The shaded region delimited by the KPIs of the FBMC-OS receiver and that of the FBMC-OSB receiver can be explored by the designer to strike tradeoff levels better adjusted for the application requirements and constraints.

Another KPI presented in Fig. 6.2, which is a constraint for many 6G-IoT applications, is latency. Indeed, it is directly impacted by the system parameters N_{UF} and N_s. It can be approximated if we consider that it is directly related to the TTI regardless of the propagation delay, hardware latency, and retransmission mechanisms. In fact, FEC codes in modern communication systems require receiving the entire frame before decoding. Therefore, the latency of the FBMC-OSB receiver $L_{NG\text{-}OSB_{Ns}}$ can be approximated as the number of samples in a frame ($M(N_s+1)/2$) divided by the sampling frequency as follows:

$$L_{NG\text{-}OSB_{Ns}} = \frac{M(N_s+1)}{2 \times F_s}.$$

On the other hand, the FBMC-OS receiver increases the latency, albeit not to the same extent as the original FS_4-FBMC receiver. This is due to the addition of $M(N_{UF}-1)/2$ samples to demodulate the last FBMC symbol in each frame.

Furthermore, the frame length impacts the data rate for the OSB_{N_s}-FBMC receiver. Therefore, for a fair comparison, the latency of such a receiver must be compared to that of OFDM, with both having the same data rate loss. The data rate loss of the OSB_{N_s}-FBMC receiver can be written as follows:

$$DR_{loss,FBMC} = \frac{1}{N_s+1}.$$

This comes from the filter-related ramp-up and ramp-down observed at the beginning and end of each frame. Regarding the OFDM waveform, the addition of a CP for each OFDM symbol consisting of M samples leads to the following data rate loss

$$DR_{loss,OFDM} = \frac{L_{CP}}{M+L_{CP}}.$$

Considering the 5G standard [21], the data rate loss due to a CP size 4.68 μs is approximately 6.6%. For the same target DR_{loss}, the number of FBMC symbols N_s in a block must be 14 symbols. This corresponds to $N_{UF} = 8$ and a frame composed of $7.5 \times M$ samples. It is worth mentioning that this corresponds to 1 resource block that is composed of 7 OFDM symbols, including the CP [21]. Therefore, the FBMC-OSB receiver with short PFs can achieve the same latency ($L_{OSB_{Ns}} = 7.5 \times M/F_s = 0.535\ ms$) as OFDM for the same data rate loss.

Other KPIs might also play a major role in the waveform selection for some 6G-IoT applications. Despite the existing trade-off between receiver complexity and the support for asynchronous communications, all the OS-based FBMC receivers can support relaxed synchroniza-

tion.

Furthermore, channel estimation which has been a major issue for FBMC/OQAM systems due to the loss of complex orthogonality is no longer present now thanks to the proposed PS.

Finally, another significant KPI which might hinder the co-existence of multiple services concerns spectral leakage. Indeed, FBMC with long PFs exhibits better spectrum confinement than with short PFs [12]. Added to the advantages brought on by the proposed MCO technique, the largely improved FBMC waveform is able to properly address this problem even with short PFs.

OFDM shows the worst spectral confinement of all considered waveforms, requiring a large number of GBs to avoid compromising efficient multiple access (or service) support under impairments [148]. However, thanks to the proposed MCO technique, GB insertion can be avoided, resulting in improved SE. Nevertheless, it is important to note that the efficiency of the MCO technique is highly reliant on the accuracy of synchronization, which unfortunately poses a significant challenge for OFDM.

In summary, the largely improved FBMC transceivers are able to overcome the main drawbacks of the original FBMC and OFDM waveforms as depicted in Fig. 6.2.

6.2 Future work

Based on the work conducted in this thesis, several ideas are proposed for future work and further investigations.

PAPR

The high PAPR is a persistent issue in FBMC. Assuming an infinite number of FBMC symbols are transmitted consecutively, the PAPR of the FBMC signal is similar to that of OFDM, regardless of the chosen PF. However, in practical scenarios where frames have a finite duration, the PAPR of FBMC signals slightly increases due to the ramp-up and ramp-down at the beginning and end of each frame. Unlike OFDM, pre-coding techniques used to reduce PAPR, such as FFT pre-coding in SC-OFDM, cannot be directly applied to FBMC due to its OQAM scheme. When these techniques are adapted for FBMC, the reduction in PAPR is not as significant as in the case of OFDM. The extent of reduction depends on the overlapping factor K, where a shorter PF (K = 1) has the potential for higher PAPR reduction compared to longer PFs (K = 4). However, regardless of the filter type, pre-coded FBMC still exhibits higher PAPR than pre-coded OFDM. Furthermore, FBMC is more susceptible to non-linearities in HPAs compared to OFDM. In such cases, FBMC may experience spectral regrowth, leading to significant degradation in spectral confinement, which is one of the main advantages of FBMC over OFDM. Hence, it is crucial to explore solutions that effectively reduce PAPR in FBMC, thereby facilitating its wider adoption in real-world applications.

A recent article introduces a novel approach to address the PAPR issue in FBMC [149]. The proposed technique combines FFT-based precoding with a low-complexity Selective Mapping (SLM) method [150]. The SLM technique involves transmitting QAM symbols with different

phase rotations or interleaving schemes, resulting in C modulated signals. Among these signals, the one with the lowest PAPR is selected, and its index is transmitted separately as Side Information (SI). Traditionally, SLM techniques are complex and have a negative impact on data rate. However, the SLM technique proposed in [149] for FBMC requires only 2 bits of SI per FBMC symbol, making it more efficient. Additionally, the processing is performed in the time domain after the FFT, reducing complexity.

The results of the study indicate that FBMC utilizing the proposed SLM technique with MMB4 achieves a lower PAPR compared to OFDM. Since the use of shorter PFs typically contributes to further PAPR reduction when compared to longer PFs, it would be interesting to explore how to adapt this technique for short PFs.

5G proof-of-concept platform

In recent years, the research team has developed a platform capable of simulating 5G scenarios for SISO transmissions and LoS propagation.

Their primary focus has been on the hardware implementation of the waveform transmitter, recognizing it as the most critical component in terms of complexity and energy consumption for uplink communication. On the receiver side, they have implemented typical FBMC receivers (FS and PPN). However, a possible improvement consists of designing and implementing optimized hardware architectures for the OS-based FBMC receivers that utilize common processing units such as FFT and Finite Impulse Response (FIR) filters.

Currently, the platform only supports SISO communication. Nonetheless, given that mMIMO techniques are widely adopted in 5G, and that the OS-based receivers are extended to support mMIMO systems in this thesis, a significant improvement to the platform would involve integrating support for mMIMO technology. This would primarily entail changing the current RF board, which currently accommodates only one antenna for transmission and one for reception.

MCO scheme extension to mMIMO

The MCO scheme proposed in Chapter 3, was originally designed for SISO transmissions. However, since SE is a crucial element of cellular communication networks, added to the continuous growth in mobile data traffic in wireless networks, there is a regain of interest in further enhancing SE for mMIMO systems.

In mMIMO systems, the users' channels are supposed to be asymptotically orthogonal if the number of antennas at the receiver side is much greater than the number of users (i.e: $N_{Rx} \gg U$). Following this constraint, one cannot increase unbounded the number of users in a subband for improving the SE indefinitely. Indeed, there is a compromise between system performance and SE, because increasing the number of users will lead to a degradation in system performance.

To address this challenge, the MCO technique can be employed to potentially enhance the SE while maintaining optimal performance. The key idea is to overlap the subcarriers of adjacent

subbands, with each subband accommodating different users. By doing so, the proposed MCO procedure outlined in Chapter 3 can be applied to investigate its effectiveness in improving SE within the context of mMIMO systems.

Essentially, the concept is to carefully manage the allocation of subcarriers and users across multiple subbands, leveraging the advantages of mMIMO while considering the limitations imposed by channel orthogonality and system performance. By exploring the potential of the MCO scheme in the context of mMIMO, we aim to strike a balance between achieving high SE and ensuring satisfactory overall system performance.

Sensing

Sensing is a fundamental functionality for many IoT services such as emergency call localization, area imaging, and personal radar. [151].

The advent of the millimeter waves and the availability of even larger bandwidths (in THz ranges) improve localization accuracy boosted by high-definition imaging and frequency spectroscopy.

Composed of frequency-modulated continuous waves, chirps signals were generally used for short-range radar systems. However, such modulation schemes cannot provide high data rates. Moreover, the radar signals have to compete for the same spectrum resources as wireless communications waveforms.

For addressing these problems, there is a trend of merging the sensing (radar) and communication systems [151–153]. Their integration can help decrease power consumption, reduce hardware costs, and improve SE. In this case, waveform design plays a central role since it should provide a single waveform capable of performing simultaneous communications and sensing tasks.

Adopted in 5G systems, OFDM cannot be directly used for joint communications and sensing since it can lead to a full duplex self-interference problem. This problem can be aggravated by its high OOBPL and any encountered channel impairments due to its high sensitivity to CFOs and TOs.

FBMC augmented by the OS-based receivers is a promising alternative for joint sensing and communications. Indeed, a recent work [154] proposed a joint radar communication transmitter system based on FBMC waveform. Results showed a better performance in radar targeting and improved BER performance in multipath channels compared to OFDM. However, the introduction of the FS-FBMC receiver associated with MMB4 PF highly increased the computational complexity. Motivated by these excellent results, it may be advantageous to investigate the use of FBMC-OS transceivers in this context.

Bibliography

[1] T. S. Rappaport, W. Roh, and K. Cheun, "Mobile's millimeter-wave makeover," *IEEE Spectrum*, vol. 51, no. 9, pp. 34–58, 2014.

[2] B. Aazhang, P. Ahokangas, H. Alves, M.-S. Alouini, J. Beek, H. Benn, M. Bennis, J. Belfiore, E. Strinati, F. Chen, K. Chang, F. Clazzer, S. Dizit, D. Kwon, M. Giordiani, W. Haselmayr, J. Haapola, E. Hardouin, E. Harjula, and P. Zhu, *Key drivers and research challenges for 6G ubiquitous wireless intelligence (white paper)*, 09 2019.

[3] S. J. Nawaz, S. K. Sharma, B. Mansoor, M. N. Patwary, and N. M. Khan, "Non-coherent and backscatter communications: Enabling ultra-massive connectivity in 6g wireless networks," *IEEE Access*, vol. 9, pp. 38 144–38 186, 2021.

[4] K. David and H. Berndt, "6G Vision and Requirements: Is There Any Need for Beyond 5G?" *IEEE Veh. Technol. Mag.*, vol. 13, no. 3, pp. 72–80, 2018.

[5] Z. Zhang, Y. Xiao, Z. Ma, M. Xiao, Z. Ding, X. Lei, G. K. Karagiannidis, and P. Fan, "6g wireless networks: Vision, requirements, architecture, and key technologies," *IEEE Vehicular Technology Magazine*, vol. 14, no. 3, pp. 28–41, 2019.

[6] L. ke, P. Chengkang, Z. Zhimin, H. Lajos, s. Xuemen, G. Yingjie Jay, Z. Ding, H. Haas, W. Tong, P. Zhu, G. Yang, J. Wang, E. G. Larsson, H. Q. Ngo, W. Hong, H. Wang, D. Hou, J. Chen, Z. Chen, Z. Hao, G. Y. Li, R. Tafazolli, Y. Gao, H. V. Poor, G. P. Fettweis, and Y.-C. Liang, "Towards 6g wireless communication networks: vision, enabling technologies, and new paradigm shifts," *Science China Information Sciences*, vol. 64, no. 1, pp. 1869–1919, 2020.

[7] S. J. Nawaz, S. K. Sharma, M. N. Patwary, and M. Asaduzzaman, "Next-generation consumer electronics for 6g wireless era," *IEEE Access*, vol. 9, pp. 143 198–143 211, 2021.

[8] A. Alalewi, I. Dayoub, and S. Cherkaoui, "On 5g-v2x use cases and enabling technologies: A comprehensive survey," *IEEE Access*, vol. 9, pp. 107 710–107 737, 2021.

[9] H. Abou-zeid, F. Pervez, A. Adinoyi, M. Aljlayl, and H. Yanikomeroglu, "Cellular v2x transmission for connected and autonomous vehicles standardization, applications, and enabling technologies," *IEEE Consumer Electronics Magazine*, vol. 8, no. 6, pp. 91–98, 2019.

[10] T. Hwang, C. Yang, G. Wu, S. Li, and G. Ye Li, "Ofdm and its wireless applications: A survey," *IEEE Transactions on Vehicular Technology*, vol. 58, no. 4, pp. 1673–1694, 2009.

[11] S. Alamouti, "A simple transmit diversity technique for wireless communications," *IEEE Journal on Selected Areas in Communications*, vol. 16, no. 8, pp. 1451–1458, 1998.

[12] J. Nadal, C. A. Nour, and A. Baghdadi, "Design and Evaluation of a Novel Short Prototype Filter for FBMC/OQAM Modulation," *IEEE Access*, vol. 6, pp. 19 610–19 625, 2018.

[13] J. Nadal, F. Leduc-Primeau, C. A. Nour, and A. Baghdadi, "Overlap-save fbmc receivers," *IEEE Transactions on Wireless Communications*, vol. 19, no. 8, pp. 5307–5320, 2020.

[14] E. G. Larsson, O. Edfors, F. Tufvesson, and T. L. Marzetta, "Massive mimo for next generation wireless systems," *IEEE Communications Magazine*, vol. 52, no. 2, pp. 186–195, 2014.

[15] S. A. Busari, K. M. S. Huq, S. Mumtaz, L. Dai, and J. Rodriguez, "Millimeter-wave massive mimo communication for future wireless systems: A survey," *IEEE Communications Surveys Tutorials*, vol. 20, no. 2, pp. 836–869, 2018.

[16] D. Materra, M. Tanda, and M. Bellanger, "Filter bank multicarrier with PAM modulation for future wireless systems," in *Signal Proc.*, vol. 120, 2016, p. 594–606.

[17] J. He, K. Yang, and H.-H. Chen, "6g cellular networks and connected autonomous vehicles," *IEEE Network*, vol. 35, no. 4, pp. 255–261, 2021.

[18] M. Giordani, M. Polese, M. Mezzavilla, S. Rangan, and M. Zorzi, "Toward 6g networks: Use cases and technologies," *IEEE Communications Magazine*, vol. 58, no. 3, pp. 55–61, 2020.

[19] S. Weinstein and P. Ebert, "Data transmission by frequency-division multiplexing using the discrete fourier transform," *IEEE Transactions on Communication Technology*, vol. 19, no. 5, pp. 628–634, 1971.

[20] T. Hwang, C. Yang, G. Wu, S. Li, and G. Li, "Ofdm and its wireless applications: A survey," *IEEE Transactions on Vehicular Communications*, vol. 58, no. 4, pp. 1673–1694, 2009.

[21] 3GPP TR 138 901, v15.0.0, "5G; Study on channel model for frequencies from 0.5 to 100 GHz", 2018.

[22] F. Schaich, B. Sayrac, M. Schubert, H. Lin, K. Pedersen, M. Shaat, G. Wunder, and A. Georgakopoulos, "Fantastic-5g: 5g-ppp project on 5g air interface below 6 ghz," in *European Conference on Network and Communications*, 2016.

[23] Mahmood, N.H. and Böcker, S. and Munari, A. and Clazzer, F. and Moerman, Ingrid and Mikhaylov, K. and Lopez, O. and Park, O.-S. and Mercier, E. and Bartz, H.

and Jäntti, R. and Pragada, R. and Ma, Y. and Annanperä, E. and Wietfeld, C. and Andraud, M. and Liva, G. and Chen, Y. and Garro, E. and Burkhardt, F. and Alves, H. and Liu, C.-F. and Sadi, Y. and Dore, J;-B. and Kim, E. and Shin, J. and Park, G.-Y. and Kim, S.-K. and Yoon, C. and Anwar, K. and Seppänen, P., "White paper on critical and massive machine type communication towards 6G," p. 28, 2020. [Online]. Available: https://www.6gchannel.com/wp-content/uploads/2020/04/6g-white-paper-critical-massive-type-communication.pdf

[24] W. Saad, M. Bennis, and M. Chen, "A Vision of 6G Wireless Systems: Applications, Trends, Technologies, and Open Research Problems," *IEEE Netw.*, vol. 34, no. 3, pp. 134–142, 2020.

[25] C. She, C. Sun, Z. Gu, Y. Li, C. Yang, H. V. Poor, and B. Vucetic, "A tutorial on ultrareliable and low-latency communications in 6g: Integrating domain knowledge into deep learning," *Proceedings of the IEEE*, vol. 109, no. 3, pp. 204–246, 2021.

[26] K. I. Pedersen, T. E. Kolding, F. Frederiksen, I. Z. Kovacs, D. Laselva, and P. E. Mogensen, "An overview of downlink radio resource management for utran long-term evolution," *IEEE Communications Magazine*, vol. 47, no. 7, pp. 86–93, 2009.

[27] X. Zhang, L. Zhang, P. Xiao, D. Ma, J. Wei, and Y. Xin, "Mixed numerologies interference analysis and inter-numerology interference cancellation for windowed ofdm systems," *IEEE Transactions on Vehicular Technology*, vol. 67, no. 8, pp. 7047–7061, 2018.

[28] A. B. Kihero, M. S. J. Solaija, and H. Arslan, "Inter-numerology interference for beyond 5g," *IEEE Access*, vol. 7, pp. 146 512–146 523, 2019.

[29] D. Demmer, R. Gerzaguet, J.-B. Dore, and D. Le Ruyet, "Analytical study of 5g nr embb co-existence," in *2018 25th International Conference on Telecommunications (ICT)*, 2018, pp. 186–190.

[30] S. Eldessoki, D. Wieruch, and B. Holfeld, "Impact of waveforms on coexistence of mixed numerologies in 5g urllc networks," in *WSA 2017; 21th International ITG Workshop on Smart Antennas*, 2017, pp. 1–6.

[31] E. Memisoglu, A. B. Kihero, E. Basar, and H. Arslan, "Guard band reduction for 5g and beyond multiple numerologies," *IEEE Communications Letters*, vol. 24, no. 3, pp. 644–647, 2020.

[32] A. Yazar and H. Arslan, "Reliability enhancement in multi-numerology-based 5g new radio using ini-aware scheduling," *EURASIP Journal on Wireless Communications and Networking*, pp. 1687–1499, 2019.

[33] FANTASTIC-5G, Deliverable D2.1, "Air interface framework and specification of system level simulations," May 2016.

[34] Z. Huang, L. Bai, X. Cheng, X. Yin, P. E. Mogensen, and X. Cai, "A non-stationary 6g v2v channel model with continuously arbitrary trajectory," *IEEE Transactions on Vehicular Technology*, vol. 72, no. 1, pp. 4–19, 2023.

[35] A. Triwinarko, I. Dayoub, and S. Cherkaoui, "Phy layer enhancements for next generation v2x communication," *Vehicular Communications*, vol. 32, p. 100385, 2021. [Online]. Available: https://www.sciencedirect.com/science/article/pii/S2214209621000541

[36] F. Tariq, M. R. A. Khandaker, K.-K. Wong, M. A. Imran, M. Bennis, and M. Debbah, "A speculative study on 6g," *IEEE Wireless Communications*, vol. 27, no. 4, pp. 118–125, 2020.

[37] I. F. Akyildiz, A. Kak, and S. Nie, "6g and beyond: The future of wireless communications systems," *IEEE access*, vol. 8, pp. 133 995–134 030, 2020.

[38] Z. Zhang, Y. Xiao, Z. Ma, M. Xiao, Z. Ding, X. Lei, G. K. Karagiannidis, and P. Fan, "6g wireless networks: Vision, requirements, architecture, and key technologies," *IEEE Vehicular Technology Magazine*, vol. 14, no. 3, pp. 28–41, 2019.

[39] NGMN Alliance, "Ngmn 5g white paper, version 1.0,."

[40] https://quadriga-channel-model.de/.

[41] Y. d. J. Bultitude and T. Rautiainen, "Ist-4-027756 winner ii d1. 1.2 v1. 2 winner ii channel models," *EBITG, TUI, UOULU, CU/CRC, NOKIA, Tech. Rep*, 2007.

[42] R. C. Jones, "A new calculus for the treatment of optical systemsi. description and discussion of the calculus," *J. Opt. Soc. Am.*, vol. 31, no. 7, pp. 488–493, Jul 1941. [Online]. Available: https://opg.optica.org/abstract.cfm?URI=josa-31-7-488

[43] M. Kasmi, S. Mhatli, F. Bahloul, I. Dayoub, and K. Oh, "Performance analysis of ufmc waveform in graded index fiber for 5g communications and beyond," *Optics Communications*, vol. 454, p. 124360, 2020. [Online]. Available: https://www.sciencedirect.com/science/article/pii/S0030401819307060

[44] T. Wild, F. Schaich, and Y. Chen, "5g air interface design based on universal filtered (uf-)ofdm," in *2014 19th International Conference on Digital Signal Processing*, 2014, pp. 699–704.

[45] F. Schaich and T. Wild, "Relaxed synchronization support of universal filtered multi-carrier including autonomous timing advance," in *2014 11th International Symposium on Wireless Communications Systems (ISWCS)*, 2014, pp. 203–208.

[46] F. Conceição, M. Gomes, V. Silva, R. Dinis, A. Silva, and D. Castanheira, "A survey of candidate waveforms for beyond 5g systems," *Electronics*, vol. 10, no. 1, 2021. [Online]. Available: https://www.mdpi.com/2079-9292/10/1/21

[47] R. Hadani, S. Rakib, A. Molisch, C. Ibars, A. Monk, M. Tsatsanis, J. Delfeld, A. Goldsmith, and R. Calderbank, "Orthogonal time frequency space (otfs) modulation for millimeter-wave communications systems," in *2017 IEEE MTT-S International Microwave Symposium (IMS)*. IEEE, 2017, pp. 681–683.

[48] R. Hadani, S. Rakib, M. Tsatsanis, A. Monk, A. J. Goldsmith, A. F. Molisch, and R. Calderbank, "Orthogonal time frequency space modulation," in *2017 IEEE Wireless Communications and Networking Conference (WCNC)*, 2017, pp. 1–6.

[49] V. S. Bhat, S. G. Dayanand, and A. Chockalingam, "Performance analysis of otfs modulation with receive antenna selection," *IEEE Transactions on Vehicular Technology*, vol. 70, no. 4, pp. 3382–3395, 2021.

[50] W. Shen, L. Dai, J. An, P. Fan, and R. W. Heath, "Channel estimation for orthogonal time frequency space (otfs) massive mimo," *IEEE Transactions on Signal Processing*, vol. 67, no. 16, pp. 4204–4217, 2019.

[51] P. Raviteja, K. T. Phan, Y. Hong, and E. Viterbo, "Interference cancellation and iterative detection for orthogonal time frequency space modulation," *IEEE Transactions on Wireless Communications*, vol. 17, no. 10, pp. 6501–6515, 2018.

[52] A. Farhang, A. RezazadehReyhani, L. E. Doyle, and B. Farhang-Boroujeny, "Low complexity modem structure for ofdm-based orthogonal time frequency space modulation," *IEEE Wireless Communications Letters*, vol. 7, no. 3, pp. 344–347, 2018.

[53] K. R. Murali and A. Chockalingam, "On otfs modulation for high-doppler fading channels," in *2018 Information Theory and Applications Workshop (ITA)*, 2018, pp. 1–10.

[54] F. Lampel, H. Joudeh, A. Alvarado, and F. M. J. Willems, "Orthogonal time frequency space modulation based on the discrete zak transform," *Entropy*, vol. 24, no. 12, 2022. [Online]. Available: https://www.mdpi.com/1099-4300/24/12/1704

[55] R. Hadani and A. M. Monk, "Otfs: A new generation of modulation addressing the challenges of 5g," *ArXiv*, vol. abs/1802.02623, 2018.

[56] Y. Jiang, M. K. Varanasi, and J. Li, "Performance analysis of zf and mmse equalizers for mimo systems: An in-depth study of the high snr regime," *IEEE Transactions on Information Theory*, vol. 57, no. 4, pp. 2008–2026, 2011.

[57] M. Bellanger, "FBMC physical layer: A primer," PHYDYAS FP7 Project Document, Tech. Rep., Jan. 2010.

[58] R. Nissel, S. Schwarz, and M. Rupp, "Filter Bank Multicarrier Modulation Schemes for Future Mobile Communications," *IEEE J. Sel. Areas Commun.*, vol. 35, no. 8, pp. 1768–1782, 2017.

[59] B. Hirosaki, "An Orthogonally Multiplexed QAM System Using the Discrete Fourier Transform," *IEEE Trans. Commun.*, vol. 29, no. 7, pp. 982–989, 1981.

[60] M. Bellanger, "FS-FBMC: An alternative scheme for filter bank based multicarrier transmission," in *5th International Symposium on Communications, Control and Signal Processing*, 2012, pp. 1–4.

[61] M. Alrwashdeh and Z. Kollár, "Analysis of quantization noise in FBMC transmitters," *Digital Signal Processing*, vol. 131, p. 103760, 2022.

[62] M. Bellanger, "FS-FBMC: A flexible robust scheme for efficient multicarrier broadband wireless access," in *Proc. Globecom Workshops*, 2012, pp. 192–196.

[63] V. Berg, J.-B. Doré, and D. Noguet, "A flexible FS-FBMC receiver for dynamic access in the TVWS," in *Proc. CROWNCOM*, 2014, pp. 285–290.

[64] C. Kim, Y. H. Yun, K. Kim, and J.-Y. Seol, "Introduction to QAM-FBMC: From Waveform Optimization to System Design," *IEEE Commun. Mag.*, vol. 54, no. 11, pp. 66–73, 2016.

[65] B. Le Floch, M. Alard, and C. Berrou, "Coded orthogonal frequency division multiplex," *Proc. IEEE*, vol. 83, no. 6, pp. 982–996, 1995.

[66] M. El Tabach, J.-P. Javaudin, and M. Helard, "Spatial data multiplexing over ofdm/oqam modulations," in *Proc. ICC*, 2007, pp. 4201–4206.

[67] R. Zakaria and D. Le Ruyet, "A Novel Filter-Bank Multicarrier Scheme to Mitigate the Intrinsic Interference: Application to MIMO Systems," *IEEE Trans. Wirel. Commun.*, vol. 11, no. 3, pp. 1112–1123, 2012.

[68] S. Taheri, M. Ghoraishi, P. Xiao, and L. Zhang, "Efficient Implementation of Filter Bank Multicarrier Systems Using Circular Fast Convolution," *IEEE Access*, vol. 5, pp. 2855–2869, 2017.

[69] C. Le, S. Moghaddamnia, and J. Peissig, "On the Performance of Alamouti Scheme in 2 x 2 MIMO-FBMC Systems," in *Proc. ICOF*, 2016, pp. 1–6.

[70] H. Zhang, D. Le Ruyet, and M. Terre, "Spectral Efficiency Analysis in OFDM and OFDM/OQAM Based Cognitive Radio Networks," in *Proc. VTC-Spring*, 2009, pp. 1–5.

[71] M. Renfors, T. Ihalainen, and T. H. Stitz, "A block-Alamouti scheme for filter bank based multicarrier transmission," in *Proc. EW*, 2010, pp. 1031–1037.

[72] D. Pinchon, P. Siohan, and C. Siclet, "Design techniques for orthogonal modulated filterbanks based on a compact representation," *IEEE Transactions on Signal Processing*, vol. 52, no. 6, pp. 1682–1692, 2004.

[73] M. Lanoiselée, B. Jahan, C. Gallard, H. Lin, D. Elleouet, and P. Siohan, "Comparative evaluation on real-time hardware platforms of coded ofdm/qam and ofdm/oqam systems," in *2012 International Symposium on Wireless Communication Systems (ISWCS)*, 2012, pp. 186–190.

[74] D. Pinchon and P. Siohan, "Derivation of analytical expressions for flexible pr low complexity fbmc systems," in *21st European Signal Processing Conference (EUSIPCO 2013)*, 2013, pp. 1–5.

[75] H. Malvar, "Modulated qmf filter banks with perfect reconstruction," *Electronics Letters*, vol. 26, pp. 906 – 907, 07 1990.

[76] M. Bellanger, D. Mattera, and M. Tanda, "Lapped-ofdm as an alternative to cp-ofdm for 5g asynchronous access and cognitive radio," in *2015 IEEE 81st Vehicular Technology Conference (VTC Spring)*, 2015, pp. 1–5.

[77] C. Lele, R. Legouable, and P. Siohan, "Iterative scattered pilot channel estimation in OFDM/OQAM," in *Proc. SPAWC*, 2009, pp. 176–180.

[78] D. Dasalukunte, S. Mehmood, and V. Öwall, "Complexity analysis of iota filter architectures in faster-than-nyquist multicarrier systems," in *2011 NORCHIP*, 2011, pp. 1–4.

[79] R. Mounzer, M. Crussiere, J.-F. Helard, and Y. Nasser, "Peak-to-average power ratio reduction in a multi-carrier signal," Jul. 23 2019, uS Patent 10,361,897.

[80] K. Hariss, Y. Nasser, H. El Mokdad, K. Y. Kabalan, and Y. Jaffal, "Are side-band tones beneficial for papr reduction in fbmc?" in *2015 IEEE 16th International Workshop on Signal Processing Advances in Wireless Communications (SPAWC)*, 2015, pp. 111–115.

[81] S. Rosati, E. Candreva, Y. Nasser, S. Yun, G. Corazza, R. Mounzer, J. Hélard, and A. Mourad, "Papr reduction techniques for the next generation of mobile broadcasting," in *2012 19th International Conference on Telecommunications (ICT)*, 2012, pp. 1–6.

[82] B. Elmaroud, M. Faqihi, M. Abbad, and D. Aboutajdine, "On the impact of prototype filter length on the PAPR reduction of FBMC signals," *Int. J. Eng. Technol.*, vol. 6, pp. 1951–1960, 2014.

[83] M. Bellanger, "Efficiency of filter bank multicarrier techniques in burst radio transmission," in *2010 IEEE Global Telecommunications Conference GLOBECOM 2010*, 2010, pp. 1–4.

[84] M. Bellanger, M. Renfors, T. Ihalainen, and C. A. da Rocha, "Ofdm and fbmc transmission techniques: a compatible high performance proposal for broadband power line communications," in *ISPLC2010*, 2010, pp. 154–159.

[85] D. Qu, F. Wang, Y. Wang, T. Jiang, and B. Farhang-Boroujeny, "Improving spectral efficiency of fbmc-oqam through virtual symbols," *IEEE Transactions on Wireless Communications*, vol. 16, no. 7, pp. 4204–4215, 2017.

[86] B. Farhang-Boroujeny, "OFDM Versus Filter Bank Multicarrier," *IEEE Signal Process. Mag.*, vol. 28, no. 3, pp. 92–112, 2011.

[87] D. Mattera, M. Tanda, and M. Bellanger, "Filter bank multicarrier with PAM modulation for future wireless systems," *Signal Process.*, vol. 120, pp. 594–606, 2016.

[88] P. Banelli, S. Buzzi, G. Colavolpe, A. Modenini, F. Rusek, and A. Ugolini, "Modulation Formats and Waveforms for 5G Networks: Who Will Be the Heir of OFDM?: An overview of alternative modulation schemes for improved spectral efficiency," *IEEE Signal Processing Magazine*, vol. 31, no. 6, pp. 80–93, 2014.

[89] J. G. Andrews, S. Buzzi, W. Choi, S. V. Hanly, A. Lozano, A. C. K. Soong, and J. C. Zhang, "What Will 5G Be?" *IEEE Journal on Selected Areas in Communications*, vol. 32, no. 6, pp. 1065–1082, 2014.

[90] P. Yang, Y. Xiao, M. Xiao, and S. Li, "6G Wireless Communications: Vision and Potential Techniques," *IEEE Network*, vol. 33, no. 4, pp. 70–75, 2019.

[91] T. L. Marzetta, "Noncooperative Cellular Wireless with Unlimited Numbers of Base Station Antennas," *IEEE Trans. on Wireless Commun.*, vol. 9, no. 11, pp. 3590–3600, 2010.

[92] P. Siohan, C. Siclet, and N. Lacaille, "Analysis and design of ofdm/oqam systems based on filterbank theory," *IEEE Transactions on Signal Processing*, vol. 50, no. 5, pp. 1170–1183, 2002.

[93] P. Singh, B. U. Rani, H. B. Mishra, and K. Vasudevan, "Neighbourhood detection-based zf-v-blast architecture for mimo-fbmc-oqam systems," in *2018 IEEE Global Communications Conference (GLOBECOM)*, 2018, pp. 1–6.

[94] C. Lélé, J.-P. Javaudin, R. Legouable, A. Skrzypczak, and P. Siohan, "Channel estimation methods for preamble-based ofdm/oqam modulations," *European Transactions on Telecommunications*, vol. 19, pp. 741–750, 11 2008.

[95] D. Kong, D. Qu, and T. Jiang, "Time domain channel estimation for oqam-ofdm systems: Algorithms and performance bounds," *IEEE Transactions on Signal Processing*, vol. 62, no. 2, pp. 322–330, 2014.

[96] P. Singh and K. Vasudevan, "Time domain channel estimation for mimo-fbmc/oqam systems," *Wireless Personal Communications*, vol. 108, 10 2019.

[97] M. Caus and A. I. Perez-Neira, "Transmitter-receiver designs for highly frequency selective channels in mimo fbmc systems," *IEEE Transactions on Signal Processing*, vol. 60, no. 12, pp. 6519–6532, 2012.

[98] E. Kofidis, "Preamble-based estimation of highly frequency selective channels in mimo-fbmc/oqam systems," in *Proceedings of European Wireless 2015; 21th European Wireless Conference*, 2015, pp. 1–6.

[99] A. Mishra, V. Shrivastava, S. Banerjee, and W. Arbaugh, "Partially overlapped channels not considered harmful," vol. 34, 06 2006, pp. 63–74.

[100] Z. Feng and Y. Yang, "How much improvement can we get from partially overlapped channels?" in *2008 IEEE Wireless Communications and Networking Conference*, 2008, pp. 2957–2962.

[101] H. Liu, H. Yu, X. Liu, C.-N. Chuah, and P. Mohapatra, "Scheduling multiple partially overlapped channels in wireless mesh networks," in *2007 IEEE International Conference on Communications*, 2007, pp. 3817–3822.

[102] J. Fan, S. Guo, X. Zhou, Y. Ren, G. Y. Li, and X. Chen, "Faster-than-nyquist signaling: An overview," *IEEE Access*, vol. 5, pp. 1925–1940, 2017.

[103] F. Rusek and J. Anderson, "The two dimensional mazo limit," in *Proceedings. International Symposium on Information Theory, 2005. ISIT 2005.*, 2005, pp. 970–974.

[104] J. E. Mazo, "Faster-than-nyquist signaling," *The Bell System Technical Journal*, vol. 54, no. 8, pp. 1451–1462, 1975.

[105] A. Prlja and J. B. Anderson, "Reduced-complexity receivers for strongly narrowband intersymbol interference introduced by faster-than-nyquist signaling," *IEEE Transactions on Communications*, vol. 60, no. 9, pp. 2591–2601, 2012.

[106] F.-M. Han, M. Jin, and H.-X. Zou, "Binary symbol recovery via ℓ_∞ minimization in faster-than-nyquist signaling systems," *IEEE Transactions on Signal Processing*, vol. 62, no. 20, pp. 5282–5293, 2014.

[107] J. B. Anderson and F. Rusek, "Improving ofdm: Multistream faster-than-nyquist signaling," in *4th International Symposium on Turbo Codes Related Topics; 6th International ITG-Conference on Source and Channel Coding*, 2006, pp. 1–5.

[108] T. Xu and I. Darwazeh, "A soft detector for spectrally efficient systems with non-orthogonal overlapped sub-carriers," *IEEE Communications Letters*, vol. 18, no. 10, pp. 1847–1850, 2014.

[109] *IEEE International Conference on Communications, ICC 2017, Paris, France, May 21-25, 2017*. IEEE, 2017. [Online]. Available: http://ieeexplore.ieee.org/xpl/mostRecentIssue.jsp?punumber=7985734

[110] F. Ganhão, B. Cunha, L. Bernardo, R. Dinis, and R. Oliveira, "A high throughput h-arq technique with faster-than-nyquist signaling," in *2014 International Conference on Telecommunications and Multimedia (TEMU)*, 2014, pp. 122–126.

[111] R. Dinis, B. Cunha, F. Ganhao, L. Bernardo, R. Oliveira, and P. Pinto, "A hybrid arq scheme for faster than nyquist signaling with iterative frequency-domain detection," in *2015 IEEE 81st Vehicular Technology Conference (VTC Spring)*, 2015, pp. 1–5.

[112] z. Esad Ankaralı, A. Şahin, and A. Şahin, "Intentional-overlapping for multicarrier schemes based on user-specific filters," *Analog Integr Circ Sig Process*, vol. 78, pp. 683–690, 2013.

[113] M. Hamamura and S. Tachikawa, "Bandwidth efficiency improvement for multi-carrier systems," in *IEEE 15th International Symposium on Personal, Indoor and Mobile Radio Communications (IEEE Cat. No.04TH8754)*, vol. 1, 2004, pp. 48–52 Vol.1.

[114] A. Sahin, I. Guvenc, and H. Arslan, "A survey on multicarrier communications: Prototype filters, lattice structures, and implementation aspects," *IEEE Communications Surveys Tutorials*, vol. 16, no. 3, pp. 1312–1338, 2014.

[115] 3GPP TS 38.212 V17.3.0; Technical Specification Group Radio Access Network; NR; Multiplexing and channel coding ", Release 17 2022.

[116] K. Sathananthan and C. Tellambura, "Probability of error calculation of OFDM systems with frequency offset," *IEEE Trans. on Commun.*, vol. 49, no. 11, pp. 1884–1888, 2001.

[117] A. Hamdan, L. Ros, H. Hijazi, C. Siclet, and A. Al-Ghouwayel, "On multi-carrier systems robustness to doppler in fast varying flat fading wireless channel," *Digital Signal Processing*, vol. 117, p. 103189, 2021. [Online]. Available: https://www.sciencedirect.com/science/article/pii/S1051200421002281

[118] D. Passos, H. Balbi, R. Carrano, and C. Albuquerque, "Asynchronous Radio Duty Cycling for Green IoT: State of the Art and Future Perspectives," vol. 57, no. 9, pp. 106–111, 2019.

[119] F. Rusek, D. Persson, B. K. Lau, E. G. Larsson, T. L. Marzetta, O. Edfors, and F. Tufvesson, "Scaling Up MIMO: Opportunities and Challenges with Very Large Arrays," *IEEE Signal Process. Mag.*, vol. 30, no. 1, pp. 40–60, 2013.

[120] P. Sabeti, A. Farhang, N. Marchetti, and L. Doyle, "CFO Estimation for OFDM-Based Massive MIMO Systems in Asymptotic Regime," *IEEE 10th Sensor Array and Multichannel Signal Process.*, pp. 99–103, 2018.

[121] T. Schmidl and D. Cox, "Robust frequency and timing synchronization for OFDM," *IEEE Trans. on Commun.*, vol. 45, no. 12, pp. 1613–1621, 1997.

[122] P. Banelli, S. Buzzi, G. Colavolpe, A. Modenini, F. Rusek, and A. Ugolini, "Modulation formats and waveforms for 5g networks: Who Will Be the Heir of OFDM?: An overview of alternative modulation schemes for improved spectral efficiency," *IEEE Signal Process. Mag.*, vol. 31, no. 6, pp. 80–93, 2014.

[123] F. Yang, P. Cai, H. Qian, and X. Luo, "Pilot contamination in massive mimo induced by timing and frequency errors," *IEEE Trans. on Wireless Commun.*, vol. 17, no. 7, pp. 4477–4492, 2018.

[124] M. Bellanger, "Fs-fbmc: An alternative scheme for filter bank based multicarrier transmission," in *2012 5th International Symposium on Communications, Control and Signal Processing*, 2012, pp. 1–4.

[125] B. Farhang-Boroujeny, "Ofdm versus filter bank multicarrier," *IEEE Signal Processing Magazine*, vol. 28, no. 3, pp. 92–112, 2011.

[126] A. Farhang, N. Marchetti, L. E. Doyle, and B. Farhang-Boroujeny, "Filter Bank Multicarrier for Massive MIMO," *IEEE 80th Veh. Tech. Conf. (VTC2014-Fall)*, pp. 1–7, 2014.

[127] K. Hari, D. Baum, A. Rustako, R. Roman, and D. Trinkwon, "Channel models for fixed wireless applications," *IEEE 802.16 Broadband wireless access working group*, 2003.

[128] A. Aminjavaheri, A. Farhang, L. E. Doyle, and B. Farhang-Boroujeny, "Prototype filter design for FBMC in massive MIMO channels," *IEEE Intl. Conf. on Commun. (ICC)*, pp. 1–6, 2017.

[129] N. E. Tunali, M. Wu, C. Dick, and C. Studer, "Linear large-scale MIMO data detection for 5G multi-carrier waveform candidates," *49th Asilomar Conf. on Signals, Systems and Computers*, pp. 1149–1153, 2015.

[130] J. Nadal, C. A. Nour, and A. Baghdadi, "Design and Evaluation of a Novel Short Prototype Filter for FBMC/OQAM Modulation," *IEEE Access*, vol. 6, pp. 19 610–19 625, 2018.

[131] M. C. Jeruchim, P. Balaban, and K. S. Shanmugan, *Simulation of Communication Systems, Kluwer Academic/Plenum*, 2000.

[132] A. Osinsky, A. Ivanov, and D. Yarotsky, "Theoretical Performance Bound of Uplink Channel Estimation Accuracy in Massive MIMO," *IEEE Intern. Conf. on Acoustics, Speech and Signal Proc. (ICASSP)*, pp. 4925–4929, 2020.

[133] A. Ivanov, A. Osinsky, D. Lakontsev, and D. Yarotsky, "High Performance Interference Suppression in Multi-User Massive MIMO Detector," *IEEE 91st Veh. Tech. Conf. (VTC2020-Spring)*, 2020.

[134] G. Liu, X. Hou, and J. Jin, "3-D-MIMO With Massive Antennas Paves the Way to 5G Enhanced Mobile Broadband: From System Design to Field Trials," *IEEE J. on Selected Areas in Commun.*, vol. 35, no. 6, pp. 1222–1233, 2017.

[135] Y. Nasser, M. d. Noes, L. Ros, and G. Jourdain, "Sensitivity of ofdm-cdma systems to carrier frequency offset," in *2006 IEEE International Conference on Communications*, vol. 10, 2006, pp. 4577–4582.

[136] C. Lele, P. Siohan, R. Legouable, and J.-P. Javaudin, "Preamble-based channel estimation techniques for ofdm/oqam over the powerline," in *2007 IEEE International Symposium on Power Line Communications and Its Applications*, 2007, pp. 59–64.

[137] D. Kong, D. Qu, and T. Jiang, "Time domain channel estimation for oqam-ofdm systems: Algorithms and performance bounds," *IEEE Transactions on Signal Processing*, vol. 62, no. 2, pp. 322–330, 2014.

[138] J. Du and S. Signell, "Novel preamble-based channel estimation for ofdm/oqam systems," in *2009 IEEE international conference on communications*. IEEE, 2009, pp. 1–6.

[139] C. Lele, P. Siohan, and R. Legouable, "2 db better than cp-ofdm with ofdm/oqam for preamble-based channel estimation," in *2008 IEEE International Conference on Communications*. IEEE, 2008, pp. 1302–1306.

[140] C. Lélé, J.-P. Javaudin, R. Legouable, A. Skrzypczak, and P. Siohan, "Channel estimation methods for preamble-based ofdm/oqam modulations," *European Transactions on Telecommunications*, vol. 19, no. 7, pp. 741–750, 2008.

[141] E. Kofidis, D. Katselis, A. Rontogiannis, and S. Theodoridis, "Preamble-based channel estimation in ofdm/oqam systems: A review," *Signal processing*, vol. 93, no. 7, pp. 2038–2054, 2013.

[142] A. S. Ahmed, M. M. Hamdi, M. S. Abood, A. M. Khaleel, M. Fathy, and S. H. Khaleefah, "Channel estimation using ls and mmse channel estimation techniques for mimo-ofdm systems," in *2022 International Congress on Human-Computer Interaction, Optimization and Robotic Applications (HORA)*, 2022, pp. 1–6.

[143] H. Hosseiny, A. Farhang, and B. Farhang-Boroujeny, "Spectrally efficient pilot structure and channel estimation for multiuser fbmc systems," in *ICC 2020 - 2020 IEEE International Conference on Communications (ICC)*, 2020, pp. 1–7.

[144] D. Chu, "Polyphase codes with good periodic correlation properties (corresp.)," *IEEE Transactions on Information Theory*, vol. 18, no. 4, pp. 531–532, 1972.

[145] H. Akima, "A new method of interpolation and smooth curve fitting based on local procedures," *J. ACM*, vol. 17, no. 4, p. 589–602, oct 1970. [Online]. Available: https://doi.org/10.1145/321607.321609

[146] D. Mattera, M. Tanda, and M. Bellanger, "Analysis of an FBMC/OQAM scheme for asynchronous access in wireless communications," *EURASIP J. Adv. Signal Process.*, vol. 23, 2015.

[147] H. Lin, M. Gharba, and P. Siohan, "Impact of time and carrier frequency offsets on the FBMC/OQAM modulation scheme," *Signal Process.*, vol. 102, pp. 151–162, 2014.

[148] Y. Medjahdi, D. Le Ruyet, D. Roviras, H. Shaiek, and R. Zakaria, "On the impact of the prototype filter on FBMC sensitivity to time asynchronism," in *Proc. ISWCS*, 2012, pp. 939–943.

[149] D. Na and K. Choi, "Low papr fbmc," *IEEE Transactions on Wireless Communications*, vol. 17, no. 1, pp. 182–193, 2018.

[150] N. Ohkubo and T. Ohtsuki, "A peak to average power ratio reduction of multicarrier cdma using selected mapping," in *Proceedings IEEE 56th Vehicular Technology Conference*, vol. 4, 2002, pp. 2086–2090 vol.4.

[151] Y. Cui, F. Liu, X. Jing, and J. Mu, "Integrating Sensing and Communications for Ubiquitous IoT: Applications, Trends, and Challenges," *IEEE Netw.*, vol. 35, no. 5, pp. 158–167, 2021.

[152] F. Liu, Y. Cui, C. Masouros, J. Xu, T. X. Han, Y. C. Eldar, and S. Buzzi, "Integrated sensing and communications: Toward dual-functional wireless networks for 6g and beyond," *IEEE J. Sel. Areas Commun.*, vol. 40, no. 6, pp. 1728–1767, 2022.

[153] Z. Wei, F. Liu, C. Masouros, N. Su, and A. P. Petropulu, "Toward Multi-Functional 6G Wireless Networks: Integrating Sensing, Communication, and Security," *IEEE Commun. Mag.*, vol. 60, no. 4, pp. 65–71, 2022.

[154] K. Ammar, O. B. Hai Belkacem, and R. Bouallegue, "OQAM-FBMC Based Radar Sensing and Wireless Communication in V2V Context," in *Proc. ISCC*, 2021, pp. 1–6.

COLLEGES BRETAGNE LOIRE SCIENCES POUR L'INGENIEUR ET LE NUMERIQUE

IMT Atlantique
Bretagne-Pays de la Loire
École Mines-Télécom

Titre : Étude de nouvelles formes d'ondes multiporteuses filtrées dans le contexte des systèmes MIMO massifs

Mots clés : Beyond 5G, formes d'ondes multi-porteuses filtrées, FBMC/OQAM, OFDM, mMIMO, efficacité spectrale, estimation de canal.

Résumé : Les applications et les services envisagés pour les systèmes de communication sans fil de la 6G imposeront des contraintes diverses à la conception du système. La forme d'onde actuelle de la 5G, OFDM, souffre d'une liste d'inconvénients qui remettent en question son adéquation et sa capacité à remplir ces exigences. Les formes d'onde multiporteuses filtrées, telles que FBMC/OQAM, constituent des alternatives prometteuses pour les futurs réseaux mobiles. Malgré les progrès réalisés ces dernières années concernant cette forme d'onde au niveau de l'émetteur et du récepteur, il reste encore des défis importants à relever. Le premier défi consiste à assurer la compatibilité avec la technologie MIMO massive, qui est essentielle pour la prochaine génération de réseaux de données sans fil. Le deuxième est lié à l'amélioration de l'efficacité spectrale, et le dernier défi concerne la garantie d'une technique d'estimation de canal robuste en dépit de diverses perturbations. L'objectif principal de cette thèse est de proposer des solutions à ces défis. Les travaux réalisés ont abouti aux contributions suivantes : (1) Proposition d'une nouvelle technique de transmission ayant pour objectif l'amélioration de l'efficacité spectrale pour les systèmes à une antenne de transmission. La technique proposée offre un gain en efficacité spectrale plus élevé lorsqu'elle est combinée à la FBMC qu'à l'OFDM. S'ajoute à cela, son efficacité prouvée avec la FBMC en présence de décalages temporels. (2) Pour améliorer encore l'efficacité spectrale, certaines avancées récentes liées à la forme d'onde FBMC/OQAM ont été étendues au contexte des systèmes multi-utilisateurs massifs mMIMO, notamment en prenant en charge les communications asynchrones et en surpassant les solutions actuelles. (3) L'efficacité des propositions précitées dépend fortement de la précision de l'estimation du canal, par conséquent, une nouvelle conception de la structure des pilotes a été proposée. L'estimation qui en résulte surpasse les performances des techniques actuelles tout en réduisant la part de la signalisation et en permettant l'utilisation de techniques conventionnelles d'estimation du canal.

Title: Investigation of novel filtered multi-carrier waveforms in the context of massive MIMO systems

Keywords: Beyond 5G, Filtered multi-carrier waveforms, FBMC/OQAM, OFDM, mMIMO, Spectral efficiency, Channel estimation.

Abstract: The applications and services envisioned for the 6G wireless communication systems will place different requirements on the system design. The current 5G waveform, OFDM, suffers from a list of drawbacks that question its ability to fulfill these prerequisites. Filtered multi-carrier waveforms, such as FBMC/OQAM, provide viable alternatives for future mobile networks. While recent years have seen some advancements in FBMC/OQAM waveform technology at the transmitter and receiver sides, there are still critical challenges to consider. The first challenge involves ensuring compatibility with massive Multiple-Input Multiple-Output (mMIMO) technology, which is essential for the next generation of wireless data networks. The second is related to improving spectral efficiency (SE), and the last challenge pertains to ensuring a robust channel estimation technique despite various impairments. The main goal of this thesis is to address these challenges. The work carried out has resulted in the following contributions: (1) Proposal of a novel transmission technique targeting SE enhancement for multi-carrier single-input-single output transmissions. It showed higher SE gain when augmented with FBMC than that with OFDM, added to its proven efficiency even in the presence of timing offset impairments. (2) To further enhance the SE, some recent advances related to the FBMC/OQAM waveform has been extended to the context of MU-mMIMO systems notably supporting asynchronous communications and outperforming state of the art solutions. (3) The efficiency of the aforementioned proposals highly relies on the accuracy of channel estimation, therefore, a novel pilot structure design has been proposed targeting the FBMC/OQAM waveform. It outperforms state of the art techniques while enhancing SE and enabling conventional channel estimation techniques.